CHALMERS

Modeling of Load Interfaces for a Drive Train of a Wind Turbine

Master's Thesis in the Master programme Applied Mechanics

FABIO BALDO

Department of Applied Mechanics

Division of Dynamics

Swedish Wind Power Technology Center

Chalmers University of Technology

Gothenburg, Sweden 2012

Master's Thesis 2012:10

Modeling of Load Interfaces for a Drive Train of a Wind Turbine
FABIO BALDO

Master's Thesis 2012:10

ISSN 1652-8557
Department of Applied Mechanics
Division of Dynamic
Swedish Wind Power Technology (SWPT)
Chalmers University of Technology
SE-412 96 Gteborg
Sweden
Telephone: + 46 (0)31-772 1000

Cover: A wind farm in eastern Oregon
Chalmers reproservice
Gteborg, Sweden 2012

"Vola solo chi osa farlo"

Luis Sepulveda

Abstract

The increasing problems of environmental pollution and the urgent government requests to reduce the CO_2 emissions have motivated energy companies to focus their attention on Green Power technologies. Wind turbine starts to assume a significant role in terms of amount of green energy production. Hence companies decided to design larger wind turbines in order to harvest more power from wind, building multi-MW wind turbines; these turbines are subjected to high loads and, since the components are more flexible, they present significant deformations. As the multi-MW wind turbine requires high investment, energy companies are leading strong researches in order to have a deeper comprehension of their behavior and as a consequence reduce as much as possible the downtime due to failure causes and guarantee the payback of the initial cost. Large part of research work is focused on the simulation of wind turbine components in order to define the loads and deformations that occur during different operational scenarios and using the data for designing them instead of using field measurements that requires higher cost. Hence several models of wind turbine with different level of complexity can be found in literature.

This Master project aims to model the load acting on the interface of the drivetrain system which are respectively: rotor, generator and tower interface. A Multi body system is proposed for the Rotor Load Interface model (RLI), which includes also the gyroscopic effect caused by yaw moment. Two techniques for calculating the aerodynamic forces are proposed, specifically Uniform Forces Distribution (UFD) method and Real Forces Distribution (RDF) method. A series of simulations under different wind conditions, according to IEC standard, are presented and the results discussed. A sensitivity analysis of RDF method is performed in order to obtain a good compromise between load blade calculation accuracy and computational time. Furthermore the RLI model is validated against field measurements.

The Generator Load Interface (GLI) model proposed to evaluate the loads coming from the electrical components for both an induction machine and for a PM machine which are based on third-order differential equations generator model. Various simulations are performed, in particular different mechanical torques are implemented in order to analyze the response of electromagnetic torque, additionally, network fault conditions are simulated as well.

The Tower Load Interface (TLI) model is a multi-body system, designed with mass

lumped-parameter technique, and it can evaluate the load of the drivetrain system supports when the tower is subjected to vibrations. The off-shore tower is also implemented in TLI model. Simulations of on-shore wind turbine tower under constant wind condition are performed. Furthermore the effects of periodic waves on the drivetrain system of an off-shore wind turbine are investigated.

Key words: Wind turbine, Modeling, Drive train system, Generator model, Tower model, Rotor model.

Acknowledgements

To increase the knowledge within the field of wind power, Chalmers University of Technology has been an active partner when the Swedish Wind Power Technology Canter was created (http://www.chalmers.se/ee/swptc-en).The department of Applied Mechanics at Chalmers is one of the important actors in the center.

This Master thesis project is developed for the Master programme in Applied Mechanics, at Chalmers University of Technology, Gothenburg, Sweden. The examiner is Professor Viktor Berbyuk and the supervisor Stephan Struggl.
Firstly I would thank Viktor Berbyuk and Stephan Struggl for the constant support they gave me during the project. Then I would thank all friends that I met during my exchange experience in Sweden, in particular Mattieu Jacques, Caroline, Eva, Nick, Mattieu Big friends of a lot of adventures, and to my thesis neighbors Senad and Alexey for all the chilling time spent together.

Special thanks to my parents and Giulia for always supporting me specially during discouragement time and helping me to believe in myself.
Last, but not least, I would thank my Italian friends Bobo, Poalo Pozzi, Marsupanna, Lorenzo, Mattia, Pelmo for the unforgettable moments, that I will preserve forever in my heart.

Fabio Baldo, Sweden 11/06/12

Contents

List of Figures **iv**

List of Tables **vii**

1 Introduction **1**

1.1 Thesis background 1

1.2 Thesis objective 2

1.3 Thesis overview 4

2 Wind Turbines State of the Art **5**

2.1 Introduction 5

2.2 HAWT 6

2.3 Rotor 6

2.4 Drivetrain 7

2.5 Generator 8

2.6 Tower 10

3 Rotor Interface **11**

3.1 Introduction 11

3.2 Rotor load 12

3.3 Modeling Techniques 16

3.4 RLI model 17

3.4.1 Wind conditions library 19

3.4.2 Blade loads library 20

3.4.3 Rotor Library 24

3.4.4 Generator . . . 25
3.5 2 MW Siemens ® Wind Turbine . . . 27
3.5.1 Constant wind condition . . . 29
3.5.2 Normal turbulence wind condition . . . 33
3.6 Sensitivity analysis . . . 35
3.7 Validation of RLI model . . . 37
3.8 Further effects . . . 39
3.9 Future works . . . 41

4 Generator interface **42**
4.1 Introduction . . . 42
4.2 Generator models . . . 44
4.3 GLI model . . . 46
4.3.1 ABC to DQ0 conversion . . . 47
4.3.2 Induction and PM generator . . . 48
4.3.3 Drivetrain . . . 50
4.4 Simulations . . . 51
4.4.1 Induction generator . . . 52
4.4.2 PM generator . . . 62
4.5 Cogging torque . . . 64
4.6 Future works . . . 65

5 Tower interface **66**
5.1 Introduction . . . 66
5.2 Tower load . . . 66
5.3 TLI . . . 69
5.4 Simulations . . . 72
5.4.1 On-shore Wind Turbine . . . 73
5.4.2 Off-shore Wind Turbine . . . 75
5.5 Future works . . . 77

6 Conclusions **78**

Bibliography **81**

A Wind Turbines parameters and IEC:2005 standard **85**

B Wave Loads Derivation **91**

C Simulink models **92**

C.1 MatWorks ® Wind Turbine 92

C.2 MatWorks ® GBE 93

D List of Symbols and Abbreviations **94**

List of Figures

1.1 *Distribution of downtime for failure in Finland 2000-2004 [22].* 2
1.2 *Drivetrain interfaces illustration - modified from [39].* 3

2.1 *Example of wind turbine blades [25].* 7
2.2 *2P 2.9 GE Gearbox, two stage planetary with one stage parallel shaft - Indirect drive system [24].* 8
2.3 *Different type of generators for Wind Turbine technology [16].* 9
2.4 *Different tower structures [5].* 10

3.1 *Forces and velocities acting on a blades, axial wind direction frame system.* 12
3.2 *Frame system from Simscape, Matlab ® [36].* 14
3.3 *Rotor Load Interface Simulink model.* 18
3.4 *Normal turbulence model example - wind average speed of 15 m/s.* . . . 20
3.5 *NACA 0015 airfoil - Lift and Drag coefficient VS angle of attack.* . . . 21
3.6 *Lift force distribution comparison.* 22
3.7 *RLI model - Uniform Forces Distribution (UFD) block.* 23
3.8 *RLI model - Real Forces Distribution (RFD) block.* 24
3.9 *Rigid body parameters specification.* 25
3.10 *RLI model - Generator block.* 25
3.11 *Wind Turbine input parameters - mask interface.* 27
3.12 *2MW Siemens wind turbine Post-processing, Pitch angle=20[deg], Wind speed=15[m/s], Constant wind condition.* 29
3.13 *2MW Siemens wind turbine Rotor Power, Pitch angle=20[deg], Wind speed=15[m/s], Constant wind condition.* 30

3.14 *Yaw Motion Law* 31
3.15 *2MW Siemens wind turbine Gyroscopic Moment, Pitch angle=20[deg], Wind speed=15[m/s], Constant wind condition.* 31
3.16 *2MW Siemens wind turbine Post-processing, Pitch angle=20[deg], Wind speed=15[m/s], Normal turbulence wind condition.* 33
3.17 *2MW Siemens wind turbine Rotor Power, Pitch angle=20[deg], Wind speed=15[m/s], Normal turbulence wind condition.* 34
3.18 *2MW Siemens wind turbine Gyroscopic Moment, Pitch angle=20[deg], Wind speed=15[m/s], Normal turbulence wind condition.* 35
3.19 *2MW Siemens wind turbine Sensitivity analysis, Pitch angle=20[deg] Wind speed=15[m/s], Constant wind condition.* 36
3.20 *Output power comparison between Hönö and RLI model.* 38
3.21 *Tower shadow effect.* 39
3.22 *Wind shear effect - Height Vs Wind speed.* a=0.2 40

4.1 *Different wind turbine configurations [17].* 43
4.2 *Equivalent circuit of a induction generator - Fifth order model [20].* . . 44
4.3 *Equivalent circuit of a induction generator - First order model [14].* . . 46
4.4 *Generator Load Interface model, Induction generator - Simulink block set.* 47
4.5 GLI model - ABC to DQ0 conversion block set. 47
4.6 *Chalmers model - Induction Generator Machine.* 48
4.7 *Risø National Laboratory model - PM Generator Machine.* 49
4.8 *GLI model - One Mass Drive train.* 50
4.9 *GLI model - two-mass Drive train [4].* 50
4.10 *180 kW Induction Generator - Generator characteristic, Voltage, Electrical torque, Rotor speed; Mechanical Torque constant and One-mass drivetrain* 52
4.11 *180 kW Induction Generator - Electrical and Mechanical power, Power Losses; Mechanical Torque constant and One-mass drivetrain.* 53
4.12 *180 kW Induction Generator - Generator characteristic, Voltage, Electrical torque, Rotor speed; Mechanical Torque constant and Two-mass drivetrain.* 54
4.13 *180 kW Induction Generator - Electrical and Mechanical power, Power Losses; Mechanical Torque constant and Two-mass drivetrain.* 55

4.14 *180 kW Induction Generator - Generator characteristic, Voltage, Electrical torque, Rotor speed; Mechanical Torque drop and Two-mass drivetrain.* 56
4.15 *180 kW Induction Generator - Generator characteristic, Voltage, Electrical torque, Rotor speed; Network fault 250 ms and One-mass drivetrain.* 57
4.16 *180 kW Induction Generator - Electrical and Mechanical power, Power Losses; Network fault 250 ms and One-mass drivetrain.* 58
4.17 *180 kW Induction Generator - Generator characteristic, Voltage, Electrical torque, Rotor speed; Network fault 250 ms and Two-mass drivetrain.* 59
4.18 *180 kW Induction Generator - Electrical and Mechanical power, Power Losses; Network fault 250 ms and Two-mass drivetrain.* 60
4.19 *180 kW Generator Network fault 250 ms - Comparison of the rotor speed with One-mass and Two-mass drivetrain.* 61
4.20 *4.5 MW PM Generator; Mechanical Torque drop - Two-mass drivetrain.* 62
4.21 *4.5 MW PM Generator - Network fault 250 ms and Two-mass drivetrain.* 63
4.22 *Cogging torque of a 4.5 MW direct-driven PMSG, time domain and FFT analysis [21].* 64

5.1 *Loads of an off-shore wind turbine tower.* 67
5.2 *Representation of tower model.* 70
5.3 *Tower Load Interface Simulink block set - On-shore tower.* 71
5.4 *Deflection and FFT analysis of 100 m - On-shore tubular steel tower, thrust force of* 10^6 *N.* 73
5.5 *Moment of deflection, Reaction force of Drivetrain supports, Reaction force of generator supports - On-shore tubular steel tower, thrust force of* 10^6 *N.* 74
5.6 *Wave Force, deflection and FFT analysis of 65 m - Off-shore tubular steel tower, thrust force of* 10^6 *N and Wave load.* 75
5.7 *Moment of deflection, Reaction force of drivetrain supports, Reaction force of generator supports - Off-shore tubular steel tower, thrust force of* 10^6 *and Wave load.* 76

C.1 *MatWorks wind turbine by Steve Miller.* 92
C.2 *MatWorks GBE by Dallas Kennedy.* 93

List of Tables

3.1 List of Rotor Loads 16
3.2 Validation of RLI model, comparison with Hönö measurements. 37

5.1 List of Tower Loads. 69

A.1 *Wind Turbine SWT-2.3-82 parameters [26].* 86
A.2 *Wind Turbine Hönö parameters [38].* 86
A.3 *180 kW Induction Generator [38].* 87
A.4 *4.5 MW PM Generator [21].* 87
A.5 *Data of on-shore wind turbine tower [34].* 88
A.6 *Data of on-shore wind turbine nacelle.* 88
A.7 *Data of off-shore wind turbine tower [33].* 89
A.8 *Data of off-shore wind turbine nacelle.* 89
A.9 *Data of off-shore wind turbine foundation [33].* 90

Chapter 1

Introduction

1.1 Thesis background

The increasing problem of global warming, combined with the reduction of fossil fuel sources, contributes to make wind turbine an establish renewable technology for the future energetic scenario. Wind turbines have been subjected of an intense research programme in the last decades and actually wind power technology presents an annual growing rate of 23.6 %, with a total worldwide power installed capacity of 196 630 Megawatt and 2,5% of the global electricity consumption [23]. The increasing demand of wind power production led several energy companies (GE, Siemens, Vestas) and the reaserch centers to start a severe development work, with the attempt to improve the performances and at the same time to reduce both maintenance and investment costs. This task can be achieved through the employment of simulation tools and wind turbine models.

Particular attention is paid on the drivetrain system that represents the set of components necessary to transmit the power from the rotor to the generator, specifically shafts, bearings, gearbox, coupling and gearbox, if presents.

The new generation of wind turbines becomes bigger and heavier, therefore the components are consequently more flexible and deformable, and this necessarily leads to significant vibrations that put the wind turbine system under high variational stresses. In fact, the wind is for definition highly random which implies that loads transferred from the blades to the transmission system are also random, so the drivetrain system is subjected to high variable loads determining high fatigue loads and consequently to a reduction of lifetime.

Recent researches [22] show that statistically the drivetrain system represents one of the main causes of downtime for failure. Hereinafter a statistical distribution of the downtime for failure of all wind turbines operating Finland from 2000 to 2004 is reported

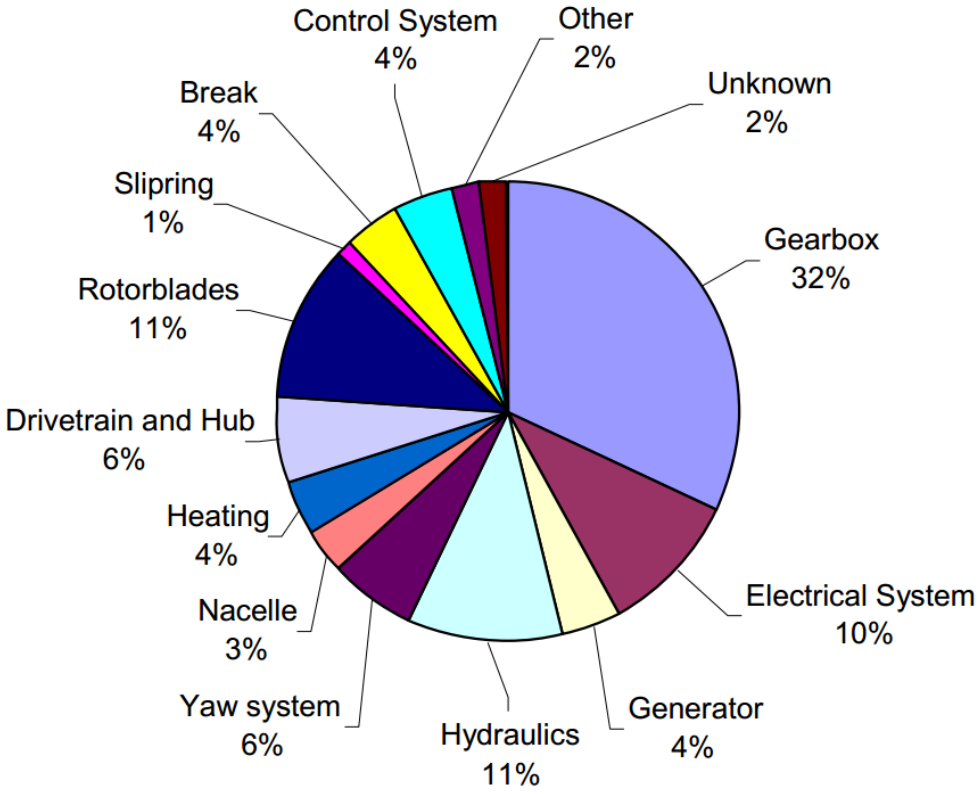

Figure 1.1: *Distribution of downtime for failure in Finland 2000-2004 [22].*

From the pie chart it can be observed that about 6% of the downtime is caused by drivetrain and hub system failures, but if the gearbox failures are included on drivetrain downtime for failure the percentege becomes the 38% yielding, therefore, the drivetrain system to be the main cause of downtime.

1.2 Thesis objective

The main target of this Master thesis project is to cover the lack of knowledge about the loads on wind turbine drivetrain systems interfaces. Nowadays it is possible to find in literature a large number of advanced drivetrain models with different level of complexity, that enable to evaluate loads, displacements and deformations with high

level of accuracy. The results obtained with such models had yielded to a significant improvements of the wind turbine performance and reliability, nevertheless cases of drivetrain failure are still often experienced.

Hence the aim of this project is to model and evaluate the loads interface in order to provide realistic input data for advanced drivetrain simulations. The interfaces under consideration are respectively: rotor, tower and generator interface. For a better understanding what the interfaces consist of and where are positioned on drivetrain system, a representative scheme is reported in the figure below:

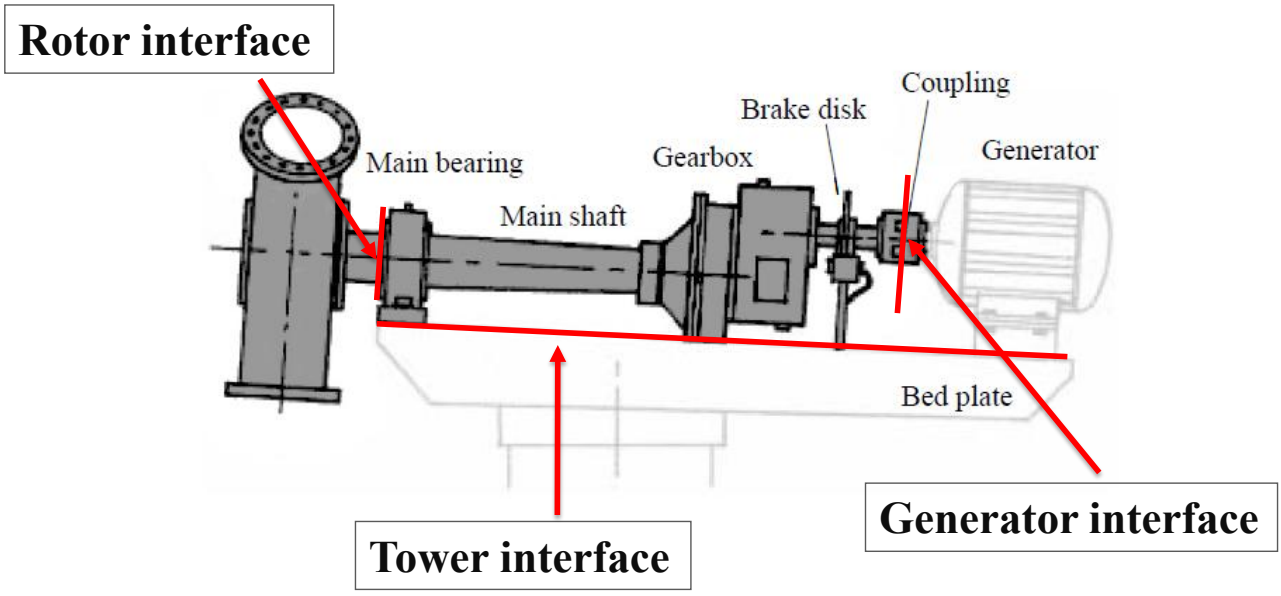

Figure 1.2: *Drivetrain interfaces illustration - modified from [39].*

In reality such interfaces can be imagined as a cross section of the components that connect the drivetrain system to the other parts of the wind turbine. In more detail, the rotor interface is a cross section of the low speed shaft, the generator interface is represented by the coupling system that connect the rotor generator to the high speed shaft while the tower interface are the constraints components that fix the drivetrain to the nacelle, e.g. bearings.

Moreover the interfaces models developed in this project want to provide a new tool that evaluate the interface load data for different set of operational scenarios with a good level of accuracy but in a fast way. In fact the commercial software such as FAST ®, Vidyn ®can provide interface load with high accuracy but they require high computational time as well as high time for setting the model.

1.3 Thesis overview

- **Chapter 1 - Introduction and Background**
  This chapter shows briefly the background of the project and illustrates the task of the work.

- **Chapter 2 - Wind Turbine State of the Art**
  The most recent wind power technologies are presented and a global overview of the wind turbine main components is presented.

- **Chapter 3 - Rotor Interface**
  The definition of the rotor loads from theoretical point of view is presented. Briefly description of the most wide speared techniques for rotor model is also reported. The Rotor Load Interface (RLI) Simulink model is presented and each constitutive blocks are detailed described. Different simulations with various wind conditions are shown and the results analyzed. Additionally, a sensitivity analysis of RFD method has been conducted. Lastly the validation of the RLI model against measurement field is presented.

- **Chapter 4 - Generator Interface**
  Description the different generator models is presented. The Generator Load Interface (GLI) Simulink model is illustrated, describing all blocks. Simulations with different mechanical torque have been conducted in order to analyze the response of the generator as well as simulations of network fault for studying the variations of the loads due to electrical issues. Furthermore the issue of the cogging torque is also presented and illustrated with an example.

- **Chapter 5 - Tower Interface**
  The set of mathematical equations of tower loads are presented. The Tower Load Interfaces (TLI) model is presented and the simulations of an on-shore tower as well as off-shore tower under constant wind speed are shown.

- **Chapter 6 - Conclusion**
  An overview of the project work and briefly illustration the main features of each interface model developed are presented. General conclusions on Msc project work and the contribution to the modeling of wind turbine drivretrain systems are stated.

Chapter 2

Wind Turbines State of the Art

This chapter is an introduction to the state of the art of wind turbine technology. A classification and description of the most widespread solutions for the components of modern wind turbine are presented.

2.1 Introduction

In the actual scenario of wind power technology it is possible to identify a large quantity of solutions to extract energy from wind. The main classification of wind turbines is based on rotor spatial orientation and basically it can be distinguished two categories: horizontal axis wind turbine (HAWT) and vertical axis wind turbine (VAWT). The latter solution was substantially neglected in the past due to a low efficiency available of about 30% estimated, nevertheless, nowadays this technology begins to widespred again thanks to its low capital cost and less mantainance compared to HAWT technology. Hence energy industries strarts to increase the reasearches of this wind turbine technology in order to improve the amount power extracted from the wind as well as the efficiency.
Considering the worldwide installed wind turbines it can be observed that the dominant technology of wind power market is the horizontal axis. HAWT technology is the product of more than four decays of research and production, particularly during the last years, from big manufactures such as GE, Siemens and Vestas, just to mention some . The level of technology reached in fields of material, electronic and mechanics allows to build wind turbine capable of generate 6 MW with dimensions of e.g. 60 meters for the rotor blades length and around 100 meters for tower height.

2.2 HAWT

Modern HAWTs are a complex electro-mechanical systems that involves several engineering disciplines, starting from aerodynamics, mechanical engineering coming to electrical and control engineering. An efficient operation of wind turbines need a strong integration of all constitutive components in order to harvest the maximum energy possible from wind, and this can be achieved combining different solutions.
In the following sections the main components and solutions of modern horizontal HAWT are presented and discussed.

2.3 Rotor

The rotor represents one of the main component of a wind turbine because it is the system responsible for extracting the power from the wind. It can be divided into two different parts: the rotor blades and the rotor hub.
When the wind strikes on rotor blades, they generate respectively lift force and drag force. Basically the lift force is responsible of the rotation of the blades instead the drag force causes bending of the blades. Modern blades exploit the experience gained in the aerospace field and are manufactured with complex shapes in order to generate high lift force and reduces significantly the turbulence phenomenas occurring on tip of the blade.
Multi MW wind turbine blades should be designed as a compromise between stiffness and lightness because they can avoid large deformations during high turbulence wind conditions and possible catastrophic impact with the tower and they must have low inertia for rapidly adapting to the variations of the wind speed. Commonly the material engaged in wind turbine, which can satisfy such properties, is fiberglass. Recently for multi-MW wind turbine the carbon fiber starts also to be used.
Concerning the rotor hub, this component represents the connection device between the blades and low speed shaft. For stall control wind turbines the blades are rigid connected to the rotor hub while, for pitch control wind turbines, the pitch actuators are situated into the rotor hub allowing to regulate the rotor angular position.

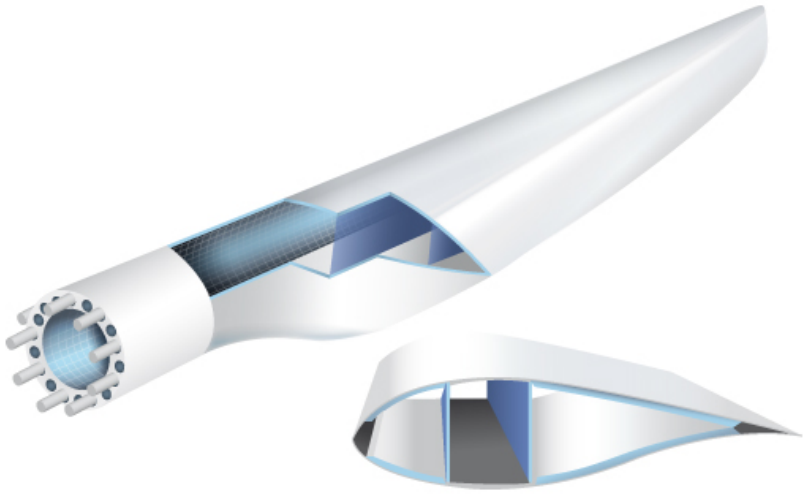

Figure 2.1: *Example of wind turbine blades [25].*

2.4 Drivetrain

A drivetrain system can be identified with all transmission components that connect the rotor system with the generator. The most widespread technology is indirect drive system that is composed of a low speed shaft supported by bearings, a gearbox system necessary for multiplying the rotational speed and a coupling system that connect the high speed shaft to the generator. Recently thanks to the development of the electronic, the modern generators can support a large number of poles pairs that allow them to rotate at speed close to rotor one; for this reason energy companies starts to develop different drivetrain system configurations. Nowadays the drivetrain configurations can be classified into three main categories:

- Indirect drive system
- Hybrid drive system
- Direct drive system

The first two concepts are characterized by the presence of a gearbox which transfers the power from low speed shaft to the high speed shaft. The main difference that distinguishes these solutions is the transmission ratio value; the indirect drive system is typically designed with a three stages gearbox with a coupling system which connects the generator to the high speed shaft, and for instance it can perform a transmission ratio of 1:136 [24]. Hybrid drive system consists of two stages gearbox and the generator

can be integrated to the last stage and the transmission ratio is normally around 1:20. The third technology, direct drive system, is the simplest from the mechanical point of view since it consists of a single shaft the directly connects the rotor to the generator without any intermediate gearbox stage; that means that the rotation of rotor blades exactly corresponds to the generator one.
An example of three stage gearbox engaged in indirect drive system is illustrated in the figure below

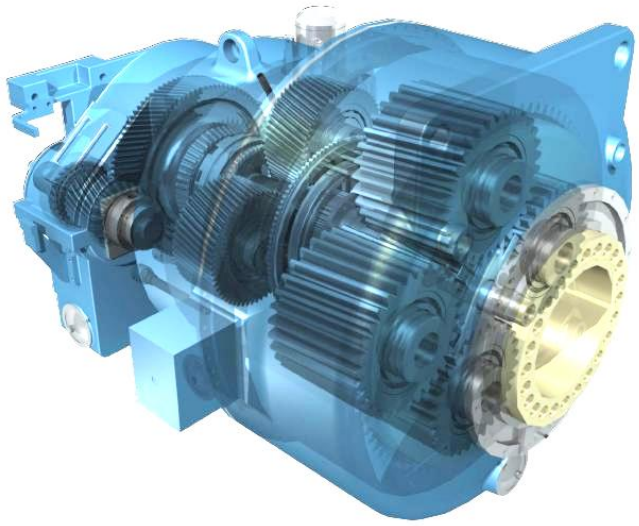

Figure 2.2: *2P 2.9 GE Gearbox, two stage planetary with one stage parallel shaft - Indirect drive system [24].*

The indirect drive technology is the most developed compared to the other two technologies; on the other hand direct drive and hybrid drive train system are getting more importance and started to widespread since they have less mechanical components which implies less maintenance and less possibilities of failure. On contrary, these systems required more electrical and power electronic components that could lead to a major probability of electrical failure and also to lower efficiency.

2.5 Generator

The generator represents the technical device that allows to convert the mechanical energy extracted from the wind to electrical energy. Modern wind turbines are usually

equipped with either an induction generator or a synchronous generator according to the drivetrain system installed. Hereinafter the types of generator commonly engaged in wind turbines technology are listed

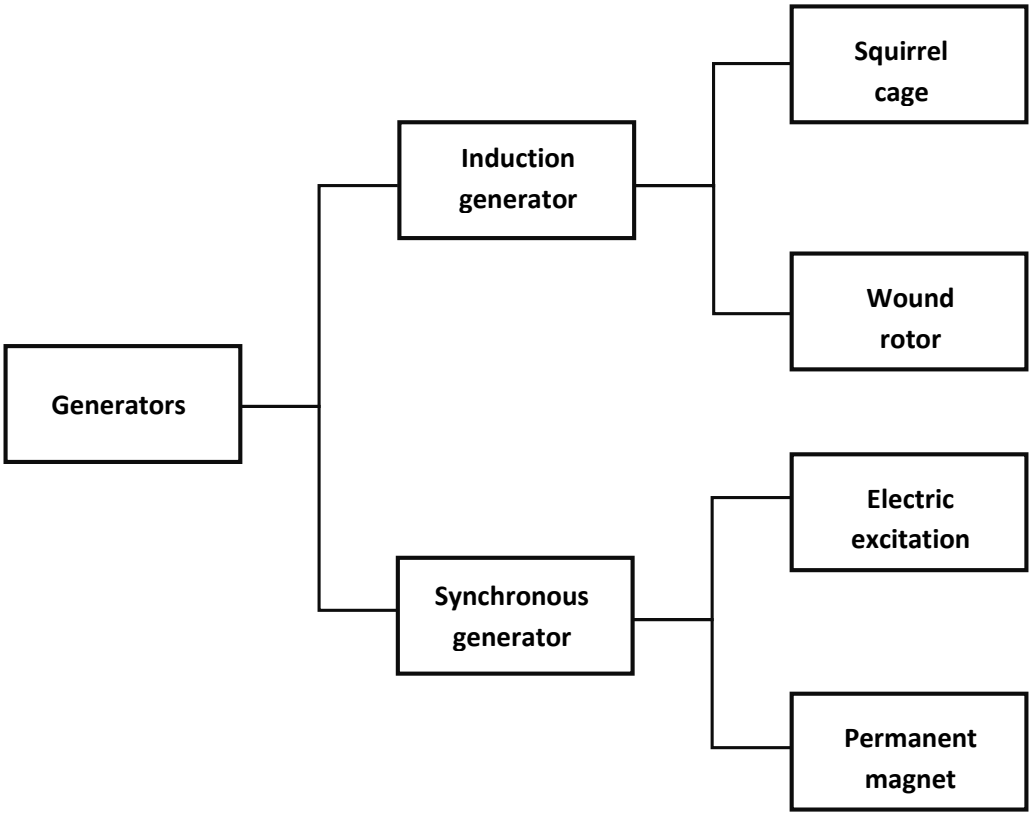

Figure 2.3: *Different type of generators for Wind Turbine technology [16].*

The induction generator is an asynchronous machine which means that rotates asynchronously respect to the magnetic field. With this type of machine the rotor speed varies according to the load applied on the shaft, more is the load higher is the rotor speed, and if any load is applied the generator rounds at synchronous speed. As shown in the figure above, the induction generators can be classified into two categories, respectively: wound rotor and squirrel cage. Both generator types are commonly used for indirect drive wind turbine, therefore they require limited space inside nacelle as well as limited power electronic.

On the contrary, for synchronous generators, the rotor speed is unique and it is the magnetic field, namely the synchronous speed. In wind turbine industry, two configurations are commonly used, specifically electric excitation and permanent magnet (PM).

The first model is basically installed in small turbines, instead permanent magnet is mostly designed for direct drive wind turbines. PM generators, for direct drive technology, present large sizes because they needs a several numbers of pair pole in order to round at same speed of the rotor blade (e.g. max 15 rpm), so they require large space inside nacelle and also additional space for the cooling system of the power electronic. More details on generators properties can be found in literature reference, for instance on paper [20].

2.6 Tower

The tower is the component responsible of lifting up the turbine system in the air. The design of this part required a particular attention from the structural point of view since this support undergoes turbine loads, such as thrust force or gyroscopic force, and from the wind pressure which is distributed along the entire height. Moreover off-shore wind turbine towers also have to resist to wave forces. The tower is designed in order to have a limited bending, under critical wind conditions, and avoid large potential catastrophic crashes with blades during operation.
The most of modern wind turbines have tubular structure which is made of a series of steel modules, reinforced with concrete, and welded each other. This structure guarantee a high stiffness and at same time a good damping of the vibrations. For small size wind turbine, old fashion lattice towers are often used since they are economic and easy to transport, on the other hand they need that required periodically maintenance due to the number of bolted connections and they can be dangerous for people if they climb them up. In the following figure the different tower structure are shown.

Figure 2.4: *Different tower structures [5].*

Chapter 3

Rotor Interface

The definition of rotor load from a theoretical point of view is presented. Different modeling techniques for rotor are discussed. The Rotor Load Interface (RLI) model is presented and described in details. A series of simulation examples of 2 MW wind turbine are illustrated and examined. The sensitivity analysis of the RFD aerodynamic loads calculation block is also shown. Moreover the validation of the RLI model against field measurements is presented.

3.1 Introduction

The rotor is characterized by rotor blades and rotor hub, which is the connection device between blades and shaft, and it is responsible of harvesting power from the wind. When an airflow impacts on the blades surface, a pressure distribution is generated on them so that the rotor starts to round, producing torque. The interaction between wind and blades has further effects that must be carefully take under consideration since they can significantly affect the life-time of the wind turbine components. For instance the drag force on the blades results in high variable thrust force along the shaft that subject the drive train supports to high variable fatigue load cycles.
The magnitude of the loads strongly depends on the size of the wind turbine, for instance the gyroscopic moment which occurs with yaw controlled wind turbines can be normally considered negligible for small wind turbine but, for multi MW wind turbines, become significant and they can considerably affect the durability of drivetrain components e.g. bearings.
Hence it is clearly important to define the rotor loads that are transmitted to the

drivetrain. The rotor interface can be identified and for indirect drive wind turbine is located on the low speed shaft,instead for direct drive wind turbine, main shaft that directly connects the rotor to the generator.

3.2 Rotor load

When an airflow strikes the blades of wind turbine, it starts to rotate thanks to the aerodynamic forces generated along the blades. The revolution speed highly depends on the aerodynamic profile of the rotor blades. From the basics of the aerodynamic a wind turbine blade can be imagined as an airfoil which passes through an airflow with a constant speed. The contact between the air and the airfoil creates a pressure distribution on blade surface that consequently generate the lift and the drag forces. Considering a frame system where the plane of rotation of the rotor is perpendicular to the axial wind direction, the system of forces and the system of speeds of a wind turbine blade can be represented with the following scheme

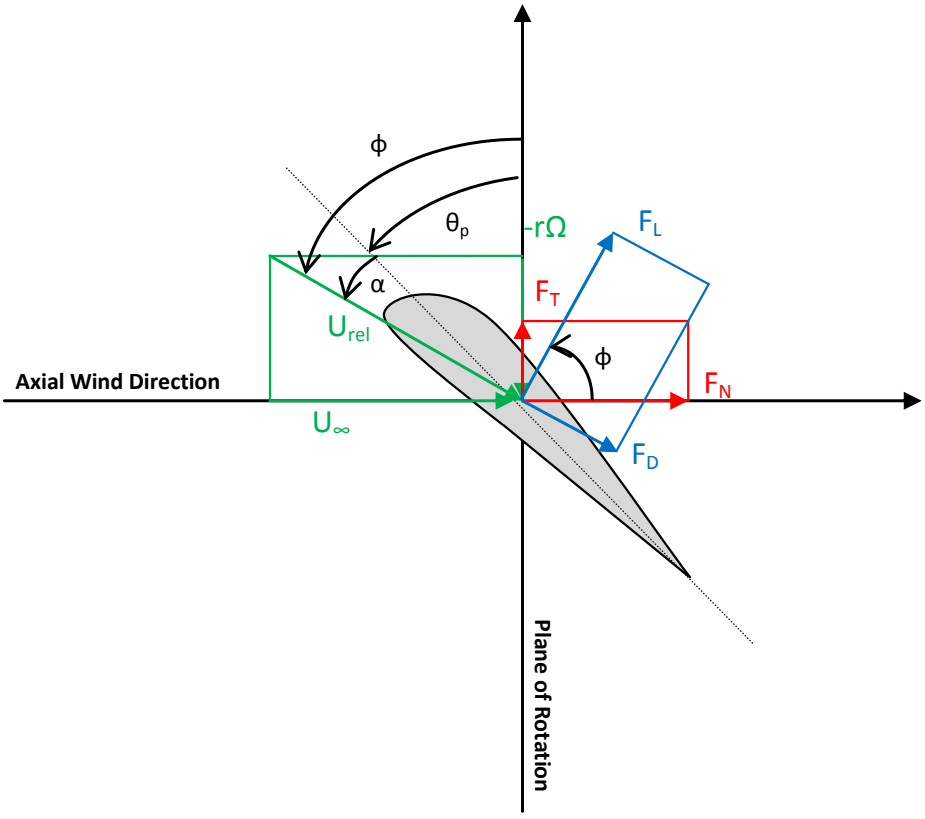

Figure 3.1: *Forces and velocities acting on a blades, axial wind direction frame system.*

As can be observed from the scheme above, the relative wind speed U_{rel} is defined as a vectorial combination of two orthogonal velocities. The axial component is the free stream velocity U_∞ and orthogonal component is the angular contribution of the peripheral speed of the rotor $r\Omega$. The relative speed vector forms an angle with rotation plane that is called inflow angle (φ). As it can be seen from the figure this angle can be also expressed as the sum of the two angles, respectively: pitch angle (θ_P) and the angle of attack (α). The pitch angle is, on active control wind turbines, a variable angle controlled by a hydraulic or electric system that varies the inflow angle in order to arrange the highest lift force available and reducing the drag force component, instead on stall control wind turbines this angle is fixed and the blades are designed to reach the stall conditions at a specific wind speed. The angle of attack is the angle between the airfoil chord and the relative wind speed direction.
Looking at the system of forces, it can be stated that the airflow generated on a blade the lift (F_L) and the drag (F_D) forces, as already mentioned, but since the blades are constrained to rotate on the plane of rotation these forces are projected respectively along this plane and along the plane where the axial wind direction lies.
Hence according to this new frame system the F_T force, which is responsible of torque production, and F_N force, which determines the thrust force, can be defined using simple trigonometric calculation with the following equations

$$\begin{aligned} F_T &= F_L sin(\varphi) - F_D cos(\varphi) \\ F_N &= F_L cos(\varphi) + F_D sin(\varphi) \end{aligned} \tag{3.1}$$

As known from theory [5], the drag force generates the thrust force but, as stated in equation 3.1, it also contribute to reduce the F_T force, responsible of energy production. Therefore in order to improve the efficiency of a wind turbine and increase the power production a pitch control system should be installed, so that the drag component is limited as much as possible. A deeper analysis of definition of lift and drag forces will be presented in section 3.4.
In order to describe all the rotor loads it is necessary modifying again the frame system, setting the X-axes along the main shaft and the Y-axes and Z-axes on fixed to the plane of rotation of the rotor.

The new frame system is reported in the figure below

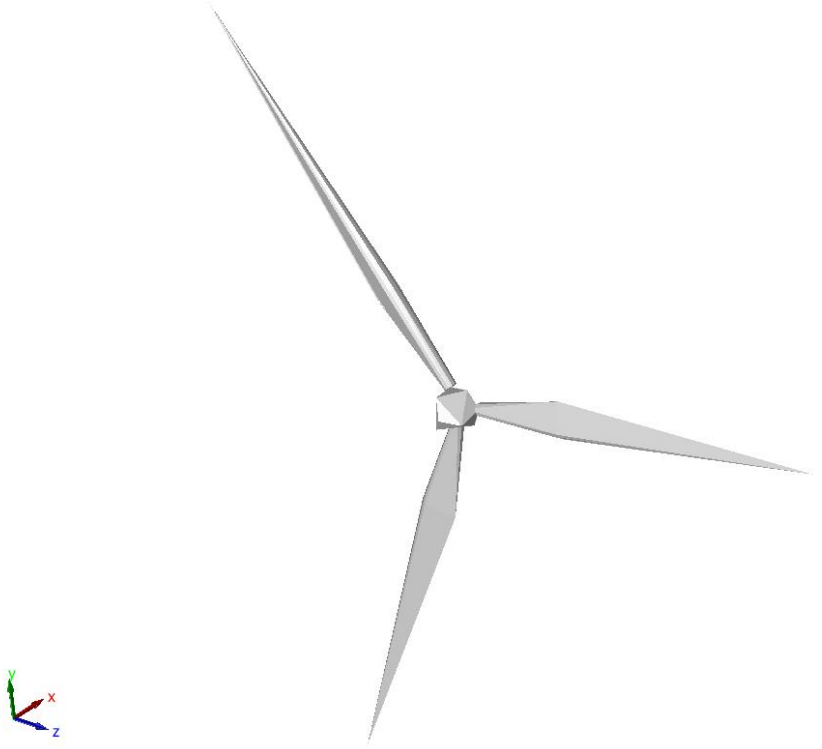

Figure 3.2: *Frame system from Simscape, Matlab ® [36].*

According to this system it is possible to define a vector of generalized forces as follow

$$\mathbf{Q} = \begin{bmatrix} F_x \\ F_y \\ F_z \\ M_x \\ M_y \\ M_z \end{bmatrix} \tag{3.2}$$

This vector expresses respectively the force and the moments along the three directions of the frame system. The F_x force is the thrust force, defined with equation 3.1. The F_y force represents the total weight force of the rotor system which consists of the weight of the three blades plus the rotor hub weight. The force on Z direction, F_z, can be set equal to zero since this force arises only if an eccentricity between the center of mass of the rotor and the shaft axis occurs; for instance this issues arises when there are misalignment errors during assembly phase. This force causes a periodical load

which depends on the rotor speed as well as on the value of the eccentricity. F_z can be expressed with the following equation

$$F_Z = m\epsilon\omega^2 sin\omega t \tag{3.3}$$

where ϵ is the eccentricity, and ω is the rotor speed.

In general for the modern wind turbines the F_z force can be considered negligible since they are assembled with advanced techniques and the rotor is designed in order to guarantee the correct balance both in static and dynamic conditions.

Concerning the three moment components, the moment along X-axes simply represents the torque transmitted to the drivetrain system, calculated as the product between the spinning force and the distance of the its point of application to the center of rotation. The moments M_y and M_z should be considered only for the wind turbines equipped with a yaw system. When such a device is present, according to the frame system M_y is defined as yaw moment. This moment comes from the energy necessary to overcome the frictions between the surface of motion of the yaw mechanism and under dynamic condition depends on the inertia of the entire nacelle. The yaw moment can be expressed with the following expression

$$M_y = c\dot{\theta} + I\ddot{\theta} \tag{3.4}$$

Where c represents the friction coefficient that must be estimated either theoretically or empirically while the I is the nacelle inertia. The formula 3.4 does not include the aerodynamic resistance of blades because it is a second order effect as the yaw motion is small.

The moment along the Z-axes M_z represents the gyroscopic moment arising from the presence of a yaw motion. The gyroscopic effect occurs when external torque is perpendicularly applied to the axis of rotation of a spinning system with a torque applied, giving rise to a moment orthogonal to both torque directions, the gyroscopic moment. According to [5] the gyroscopic moment for a three blades wind turbine can be analytically described with the following equation

$$M_z = 3\omega_k\omega\sum_{i=1}^{n} m_i r_i^2 \tag{3.5}$$

Where ω_k is the angular yaw speed, ω the rotor speed, m_i the ith discrete mass of the rotor blade discretization and r_i is the distance from the rotor center to middle point

of the respective discrete mass.
If the wind turbine has two blades the expression for moment along Z-axes is the following

$$M_z = 4(\omega_k \omega \sum_{i=1}^{n} m_i r_i^2) cos^2(\omega t) \tag{3.6}$$

The rotor loads defined above are summarized in the following table

Loads	**Symbols**	**Formula**
Thrust force	F_x	$F_L cos(\varphi) + F_D sin(\varphi)$
Weight force	F_y	$3m_{blades} + m_{rotorhub}$
Eccentricity force	F_z	$m\epsilon\omega^2 sin\omega t$
Torque	M_x	$F_T \cdot (2/3) \cdot R$
Yaw moment	M_y	$c\dot{\theta} + I\ddot{\theta}$
Gyroscopic moment	M_z	$3\omega_k \omega \sum_{i=1}^{n} m_i r_i^2$

Table 3.1: List of Rotor Loads

3.3 Modeling Techniques

Before setting the simulation environment it is necessary to define the method for modeling the rotor. Nowadays three different techniques are widely used in modeling field, namely: rigid multi body (RMB), the flexible multi body (FMB) and the finite element (FE) technique.
The RMB technique defines the bodies of the system as rigid, in this way the number of the degrees of freedom (DOFs) are limited to motion of the bodies. The joints that connect the different bodies are modeled as spring, damper, backlash depending on the connection or surface of contact that has to be modeled. In general RMB model is used to study the overall motion and loads response of the system, rather than analyzing its deformations under dynamic conditions.
On the contrary the FE technique is preferable when it is required to have a detailed analysis of the internal deformation and stress distribution of a critical component which is highly subjected to failure, for instance bearings of the drivetrain system. Generally speaking, FE analysis discretized a component into large number of nodes

that represent the DOFs; such number essentially depends on the accuracy of the results desired, and usually starts from 5000 up to millions. On the other hand higher is the number of DOFs higher is the computational time needed.
The FMB technique can be seen as a combination of MBS and FE method. FMB method defines the system RMB in the same way of the RMB technique, setting the DOFs of the bodies motions but each component is replaced with a flexible body instead of a rigid body. The flexible body is reduced to its modal representation, including the dynamic and static response properties. The FMB method requires lower computational time than FE technique and allows to analyze the influence of the flexibility on the interfaces of the components.
The RMB technique suits perfectly the task of the project and for simulation of the Rotor Load Interface, however the FE and FMB approaches can provide a deeper analysis of the rotor loads and they can be proposed for future outlooks.
The entire project, included the other two sections GLI and TLI, is developed with Simulink software, from Matworks ®. The choice of the software is based on the large possibilities of modeling which it offers as well as the possibility of interfacing with other softwares.
Additionally Simulink offers a large number of libraries dedicated to different fields such as aerospace, hydraulic and, in particular, the Simscape library provides specific tools for RMB modeling.

3.4 RLI model

The starting point of Rotor Load Interface model is the Wind Turbine model developed by Steve Miller from MatWorks ® [35], reported in Appendix C. This model provides a complete wind turbine system including for instance tower model, advanced hydraulic yaw system and so on. The intention of RLI model is to define a tool the evaluate the rotor loads, therefore the level of complexity of the MatWorks model has been reduced removing the extra blocks that are not necessary to achieve the task.
The RLI model maintains two concepts of MatWorks model: Rigid Multi Body system of rotor blades and rotor hub and technique used for calculating the aerodynamic forces, in particular the method defined as Uniform Force Distribution. The rest of the blocks has been removed or substituted by others that fit for the RLI model.

Therefore, after revising the MatWorks model, the RLI model is essentially divided into four parts; the first part includes different wind condition models, the second one is dedicated to aerodynamic loads calculation, the third part comprises the blade model and the last one is the generator block sets in order to provide a counter torque. Moreover an extra block, defined *Rotor loads scope*, includes different instruments for detecting in real-time a series of variables such as rotor speed, spinning moment, etc. Each of four parts is defined as library where different options can be selected. These libraries allow to maintain a single block set of the RLI model but, at the same time, setting different simulation conditions, for instance setting different wind conditions or selecting the number of blades, etc. ; moreover it is possible to add new options maintaining the previous ones. The RLI blocks set is shown in the following figure

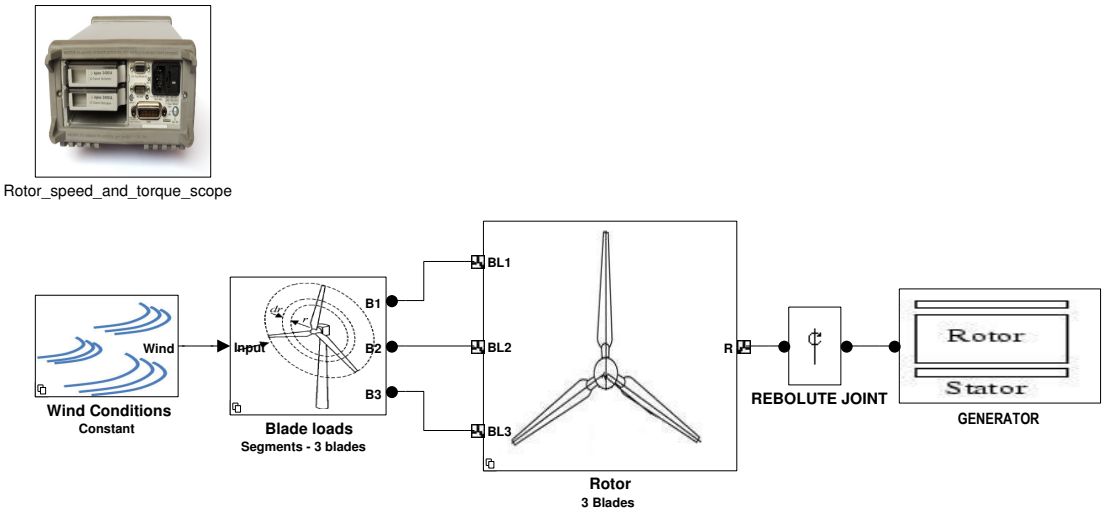

Figure 3.3: *Rotor Load Interface Simulink model.*

By observing figure 3.3 it is possible to describe the operative logic of the RLI model. Starting from the left, the wind conditions block generates the wind signal further used as input for the Blade Loads block. Within this block the aerodynamic loads of the blades, specifically the spinning moment and bending moment, are calculated and then, subsequently, an ideal mechanical actuator applies these loads to the blade bodies at a predefined point. Later on the rotor hub body is directly connected to a revolute joint, which represents the DOF of rotation, and allows the entire rotor system to round. Lastly the generator block is a simple torque actuator that produces a counter torque in order to balance the rotor torque.

The additional scope block includes the output interfaces of the different sensors for

the measurement of the variables under investigation.

3.4.1 Wind conditions library

The Wind conditions library includes four wind conditions that define the wind signal in time-domain, necessary to calculate the aerodynamic forces of the blades. The definition of the wind conditions is based on IEC:2005 standard. These standard provide different wind models that are taken into account by setting different factors, for instance the wind direction. For RLI model, the four wind conditions implemented are: normal turbulence model, extreme wind speed model, extreme operating gust model and extreme turbulence model; furthermore a empty and a constant blocks are set in order to allow future implementations of the wind condition model developed at Chalmers and to define a constant wind signal, respectively.
According to IEC:2005 standard, before defining of the four wind signals it is required to specify the environment characteristics. The IEC:2005 standards ranks the environment conditions into three categories depending on the level of turbulence intensity [28]. For RLI model the environment category chosen is the one with low turbulence characteristics.
The definition of the signal of the four wind conditions is given by the following equation

$$W_{input} = W_{average} + random(\sigma_1) \tag{3.7}$$

Where W_{input} is the input signal of the aerodynamic loads block, $W_{average}$ is the average speed value of the wind that usually is experienced on the site where the wind turbine is located, and σ_1 represents the standard deviation that is defined with a specific formula for each the wind conditions listed above; the equations are reported in Appendix A. Hence, since the nature of the wind is not deterministic, in order to define a realistic wind model, the wind signal is defined as random function within the interval of speed is defined by upper and lower limits established with deviation standard value σ_1.
In the following page an example of normal turbulence wind condition signal, set with an average speed of 15 m/s, is reported

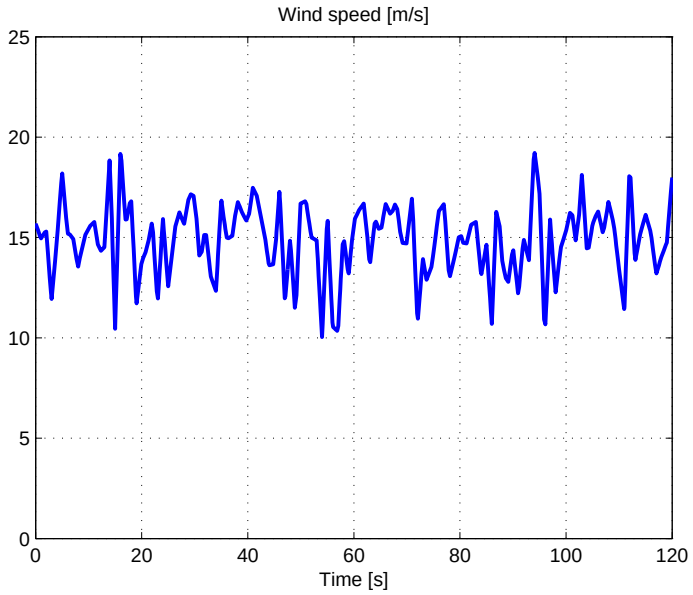

Figure 3.4: *Normal turbulence model example - wind average speed of 15 m/s.*

3.4.2 Blade loads library

The second block of the RLI block set in figure 3.3, starting from the left, is the Blade loads library. This library contains two different techniques for calculating of the aerodynamic forces, namely uniform force distribution (UFD) and real force distribution (RFD). Both methods are based on the aerodynamic theory explained in §3.2, but the UFD technique calculates one single value of the lift and drag forces in a way that the lift and drag coefficients remain constant along the blade length, while the RFD block divides the blades into different segments and for each of them the lift and drag forces are calculated, later on they are summed up obtaining the total spinning and bending torques.

As already stated in §3.2 the a lift and drag forces are a function of aerodynamic coefficients, and the equations that express this relation are given as

$$\begin{aligned} F_{Lift} &= \tfrac{1}{2} C_L \rho A v_{rel}^2 \\ F_{Drag} &= \tfrac{1}{2} C_D \rho A v_{rel}^2 \end{aligned} \tag{3.8}$$

Where ρ is the air density, A is the area swept by rotor blades, v_{rel} the relative wind speed and C_L and C_D that are respectively the drag and lift coefficients. These two parameters strongly depend on the airfoil shape as well as the angle of attack, resulting in a non-linear coefficients. In order to understand the influence of these parameters

on the aerodynamic forces, a diagram of NACA 0015 airfoil of lift and drag coefficient as a function of the angle of attack is reported below

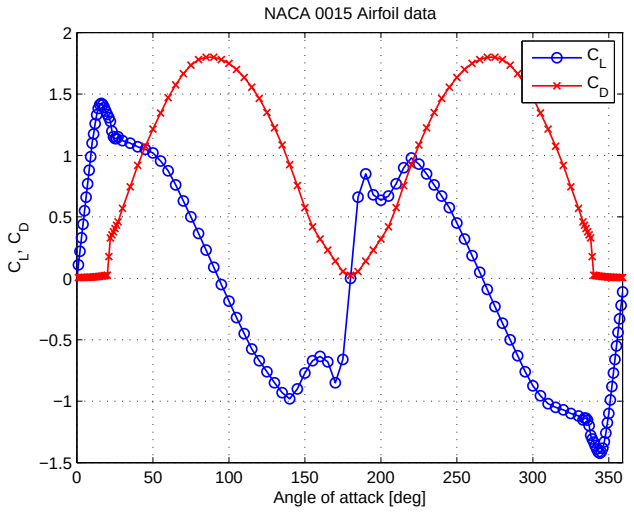

Figure 3.5: *NACA 0015 airfoil - Lift and Drag coefficient VS angle of attack.*

As it can be noticed, for small angle of attack, the lift coefficient starts from zero and rapidly reaches the maximum value whilst drag coefficient remains approximately equal to zero. When a specific angle of attack, which varies accordingly to aerodynamic characteristics of the airfoil, is reached the stall condition occurs and the lift coefficient value has a relevant drop, whereas, at the same time, the drag coefficient starts to increase considerably. After 90 degrees the lift and drag coefficients have an opposite trend although for wind turbine applications such angles of attack are never swept. In general the interval of the angle of attack for wind turbine blades defined between 0 and 30 degrees.

From this considerations it can be affirmed that the lift and drag forces along the blade length are highly non-linear, moreover in reality the turbulence at rotor hub zone as well as at tip of the blades affect significantly the aerodynamic of the rotor.

With these observations, it becomes important defining models that can simulate the force distribution along the blade as realistic as possible. UFD and RFD methods provides different shape of the force distribution. A comparison of lift force distribution among the two techniques and a real blade force distribution is reported.

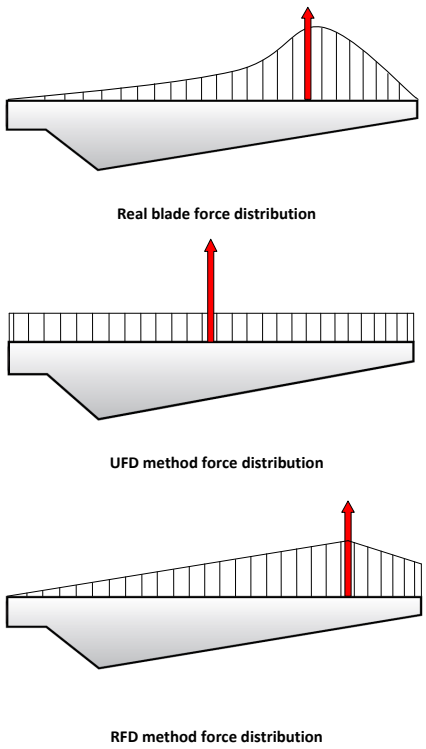

Figure 3.6: *Lift force distribution comparison.*

Starting from the top of the figure, the lift distribution of a real wind turbine blade is shown; the area close to the rotor hub has a low lift force value because of two effects: first the peripheral speed of the blade is particularly low if compared to the free airflow speed determining a small angle of attack, approximately close to zero that according to 3.5, gives a small lift coefficient; the second effect is the turbulence, caused by the interaction between the rotor hub and airflow, which generates wakes that upset the the air passing through the blade and reduce the value of the wind speed. Observing the central part of lift distribution it can be noticed that, with increasing the distance from the center of rotation, the lift force rapidly increases. This is due to increase of the radius the peripheral speed and later of the relative wind speed value and to the increase of C_L and C_D coefficients. On the tip of the blade, as any airfoil invested by a air flow, the wingtip vortices significantly reduce the lift force and, without any winglet, it can drop until zero value.
Concerning the UFD lift distribution, a single value of lift force is considered for the entire blade length, therefore an uniform distribution is obtained. With this technique the point of application of the total aerodynamic force is at the middle point of the blade length. Moreover with UFD method it also is possible to set the point of application of

the total force at 2/3 of the blade length in order to have more realistic lift distribution. On contrary RFD technique presents a distribution that can be assumed as quasi-linear. In fact when the blade is divided into different segments the values of the angle of attack and consequently of C_L and C_D change from one segment to another, so that the effect of the lift reduction on the rotor hub zone is considered.

Uniform forces distribution block

The block set of the UFD method implemented, taken from MatWork and modified for RLI model, is reported in the following figure

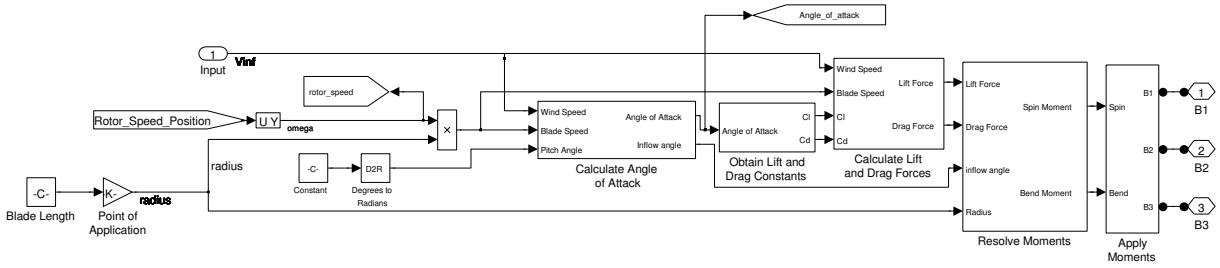

Figure 3.7: *RLI model - Uniform Forces Distribution (UFD) block.*

The block receives as input: the pitch angle, the wind speed signal from the Wind Conditions block and the rotor speed, which comes from a speed sensor located at the revolute joint. The speed values are updated at each iteration and used for calculating the relative wind speed as well as for the inflow angle. The angle of attack is the difference between the inflow angle and the pitch angle. Subsequently, this value is used as an input for a look-up table where the airfoil drag C_D and lift C_L coefficients data are stored. Once the two parameters are defined, they are multiplied respectively with the density and the swept area of rotor in order to determine equation 3.5. Lastly the lift and drag forces are multiplied with the distance between the center of rotation and the point of application in order to obtain the spinning and bending moments.

Real distribution block

For the implementation of RFD technique a Embedded Matlab file is employed. In fact a Mex file with a code that calculate in loop the aerodynamic forces for each segment allows to freely set the number of segments and compact the block set that otherwise could result too complex. The RFD block set is shown in the following figure

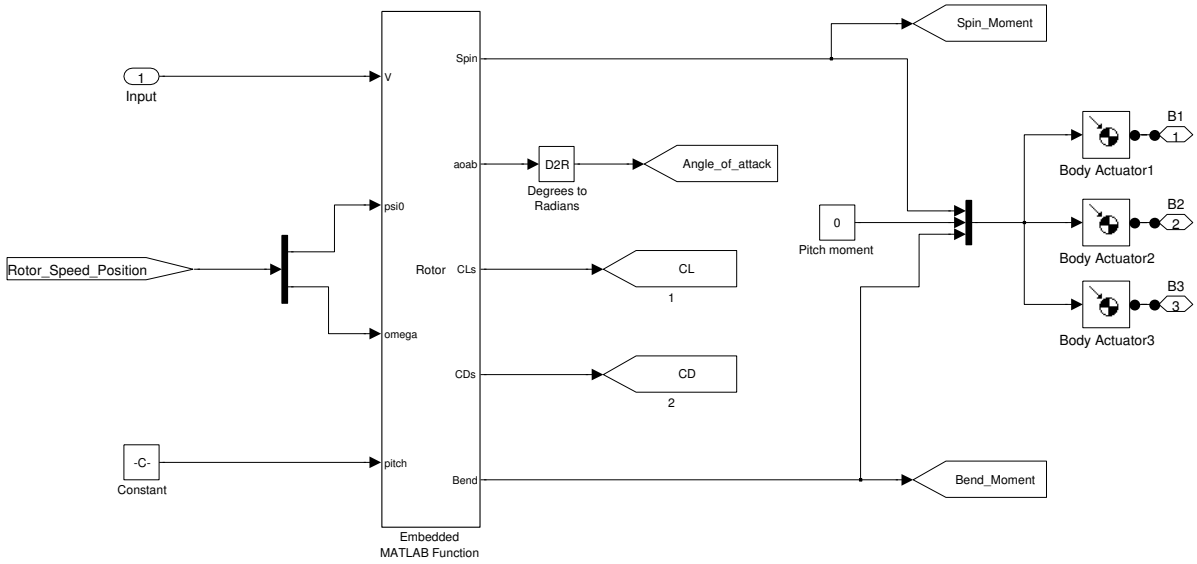

Figure 3.8: *RLI model - Real Forces Distribution (RFD) block.*

As it can be seen the input data are the same of UFD block set. The Embedded Matlab file block contains the code purposely dedicated to calculate the spinning and bending moments. Basically the code calculates, in the same way as UFD, the aerodynamic forces but this operation is repeated for each segments which the blade is divided into. The code also receives as input the C_L and C_D coefficients values as vectors and automatically interpolates the values the coefficients if the input data are furnished with interval of values larger than one degree.
Later on the forces of each single segment are multiplied with the distance between the center of rotation and the respective middle point, obtaining the single spinning and the bending moments contribution, which are then summed up in order to calculate the total spinning and bending moment of the blades.

3.4.3 Rotor Library

The Rotor library includes the RMB system of the rotor, in particular the blades body and the rotor hub body. The rotor system is designed by using the tools of *Simscape* MatWorks library. In particular blades are rigid body with specific mass and geometric characteristics, which are connected the rigid body of the hub with a weld joint. When a rigid body is inserted in the model the specification of the data has to

be done using the following mask interface

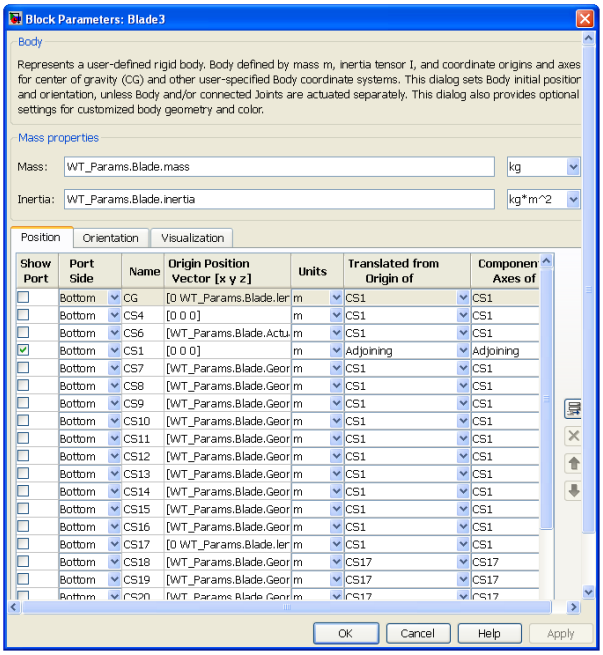

Figure 3.9: *Rigid body parameters specification.*

The interface allows to specify three parameters, respectively: geometry, mass and inertia.

3.4.4 Generator

The main purpose of the generator block is to create a constant counter torque that balances the rotor torque. The generator block set is reported in the figure below

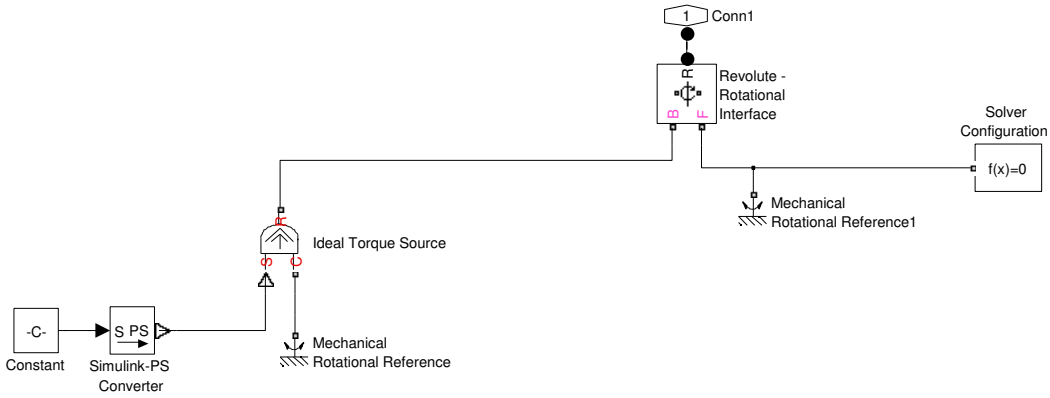

Figure 3.10: *RLI model - Generator block.*

In general, a wind turbine generator behaves as a counter torque in order to balance the torque coming from the drive train system. The modern generator can adapt the electromagnetic torque according to the load conditions, but in RLI model the generator is set as a constant counter torque. To set the counter torque value it can also be taken into account the power losses of the rotor as well as the drivetrain system, for instance dissipations due to friction or lubrication, therefore the counter torque can be set with higher value according to estimation of the power losses. For instance from a power balance of the system it is possible to estimate approximately the power losses and lately define the resistance torque.
On the contrary for small wind turbine the counter torque can be set equal to the one of the generator as the friction losses do not affect significantly the output power.

3.5 2 MW Siemens ® Wind Turbine

In this section the rotor 2 MW Siemens wind turbine is used to perform a different simulations. The choice of the 2 MW Siemens wind turbine is based on the large number of data that are available on Siemens website [26] and that are required to set the RLI model parameters.
When the RLI code is compiled a mask interface appears offering the possibility of typing different parameters of the wind turbine under investigation. In particular the mask interface requires to set the geometric and the mass properties of the rotor, respectively: blade mass, blade length, blade inertia, respectively in x, y, and z directions and the pitch angle. Moreover, the generator counter torque as well as the average wind speed have to be set. The wind turbine input parameters mask interface is reported in the following figure

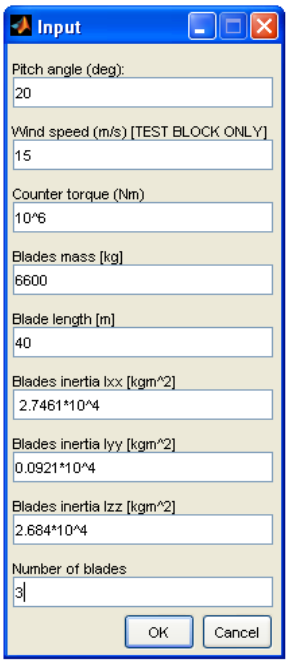

Figure 3.11: *Wind Turbine input parameters - mask interface.*

It can be observed that the simulation parameters can be directly inserted in the interface without modifying any block of the model. Subsequently, through a selection menu, the wind conditions, described in Appendix A and section §3.2, can be specified. After defining the input parameters the simulation can be started and a 3d virtual machine displays a movie of rotor model motions, that allow to observe the rotor re-

sponses under different set of operational scenarios.
When the simulation ends, the spinning moment, the bending moment, the rotor speed, the electrical torque, the angle of attack and power are automatically post-precessed and outputs are reported in time domain. Moreover using the RLI model is also possible to simulate the gyroscopic loads, defined with equations 3.5 and 4.1, occurring with wind turbines equipped with yaw motion system.
In the following sections a set of simulations of 2.0 MW Siemens wind turbine are presented. All the simulation are performed using both aerodynamic loads calculation techniques, specifically UFD and RFD, and the RFD is set with a number of segments of 20.
Although in reality a pure constant wind speed condition rarely occurs, the first simulation is performed with a constant wind speed signal. In this manner it is possible to observe the main differences of rotor responses with the two aerodynamic loads calculation methods that otherwise, with complex signal (e.g. turbulence signal), it could be difficult to recognize.

3.5.1 Constant wind condition

The settings for the first simulation are: constant wind speed signal of 15 m/s, pitch angle of 20 degrees and counter torque of 10^6 Nm whereas the technical specification of the rotor are reported in Appendix A. The time-simulation is set on 120 seconds which is considered a sufficient time for reaching the steady state condition. The results of the simulation are reported in the figure below

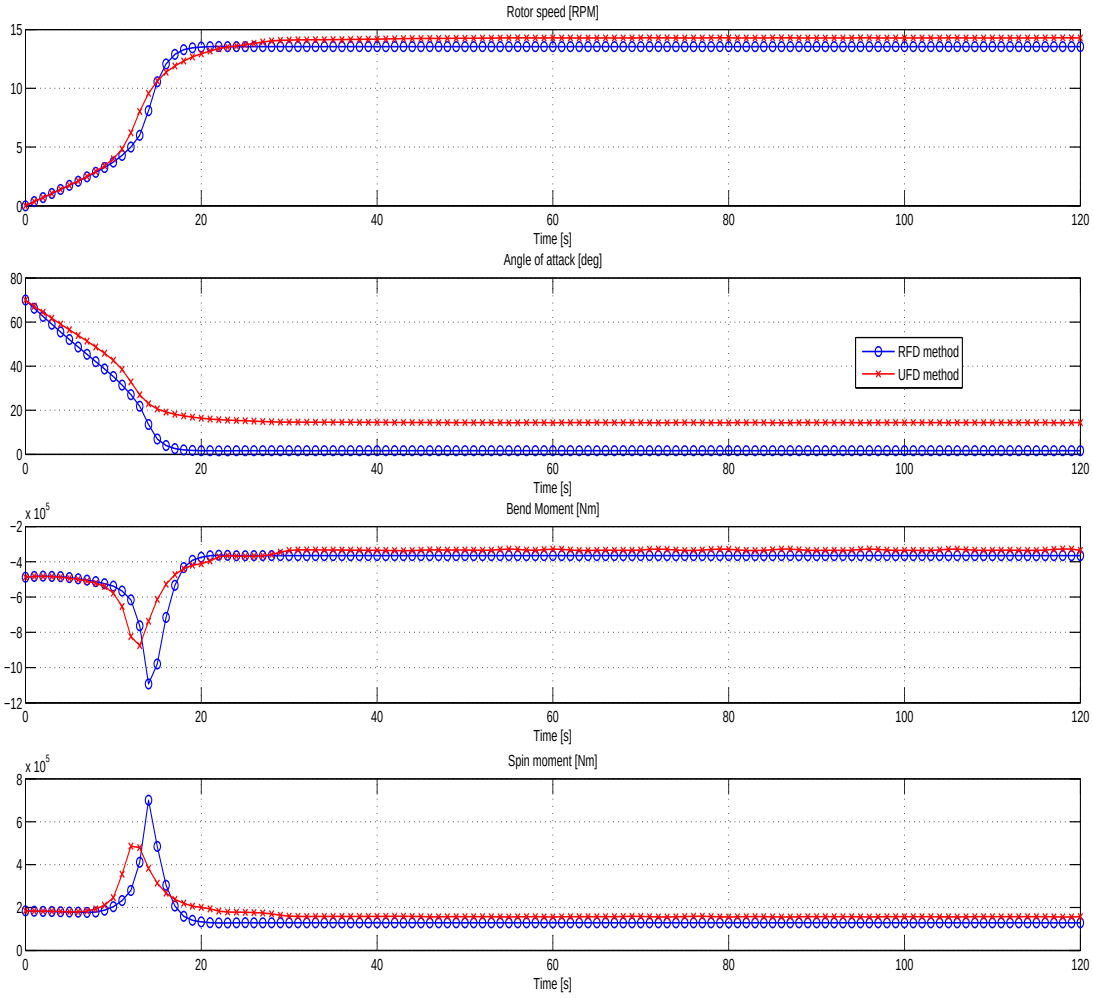

Figure 3.12: *2MW Siemens wind turbine Post-processing, Pitch angle=20[deg], Wind speed=15[m/s], Constant wind condition.*

Observing the figure it can be affirmed that UFD and RFD have a different response.

Starting from rotor speed, the UFD model presents higher values than RFD. The same observation can be done for the angle of attack and the spinning moment while the bending moment has a lower value overall the simulation time. The reason of these results is that RFD presents lower aerodynamic load on blades since the effect of the low rotor speeds in rotor hub area is taken into account while with UFD technique the same load is applied along the entire blade and this leads to higher spinning moment and consequently higher rotor speed as well as angle of attack. Moreover with the RFD technique also the output power results lower than UFD method because of the lower loads on the blades, as shown in plot below.

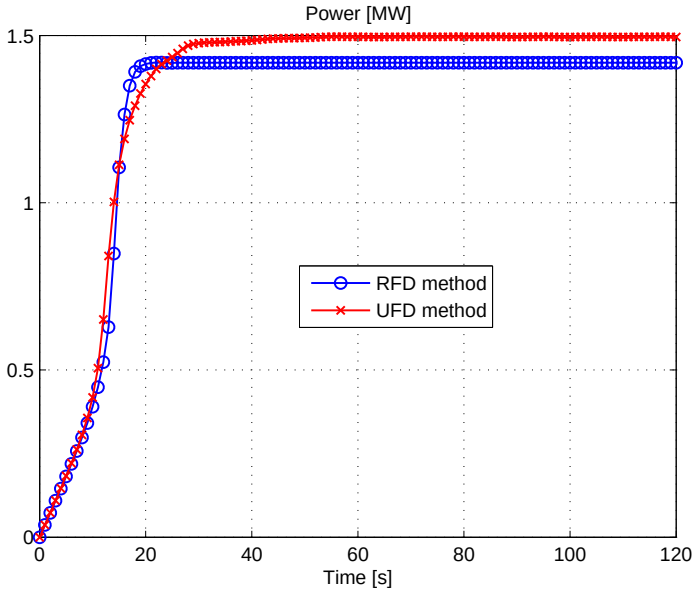

Figure 3.13: *2MW Siemens wind turbine Rotor Power, Pitch angle=20[deg], Wind speed=15[m/s], Constant wind condition.*

Looking at initial transient phase, in particular from the starting point, the response of both techniques is approximately the same because, at low wind speed, the effect of the rotor hub is not relevant making output power of the two methods comparable.
Furthermore the gyroscopic moment is also investigated under constant wind condition, therefore a yaw motion of the nacelle is implemented. Specifically the yaw motion is set with a constant angular speed of 1 degrees per second at steady state speed condition and a ramp-up and ramp-down for the starting phase and final phase respectively. The yaw motion law and the gyroscopic loads, in time domain, are reported in the following figure.

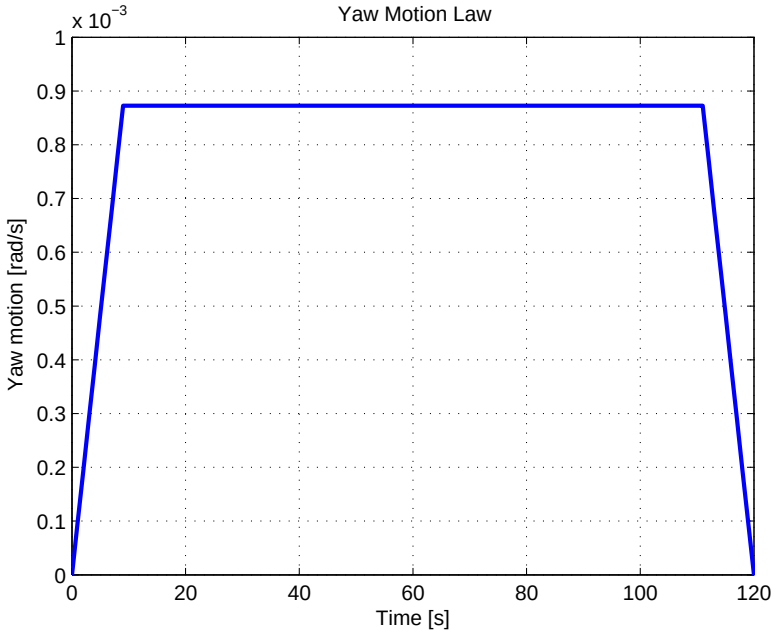

Figure 3.14: *Yaw Motion Law*

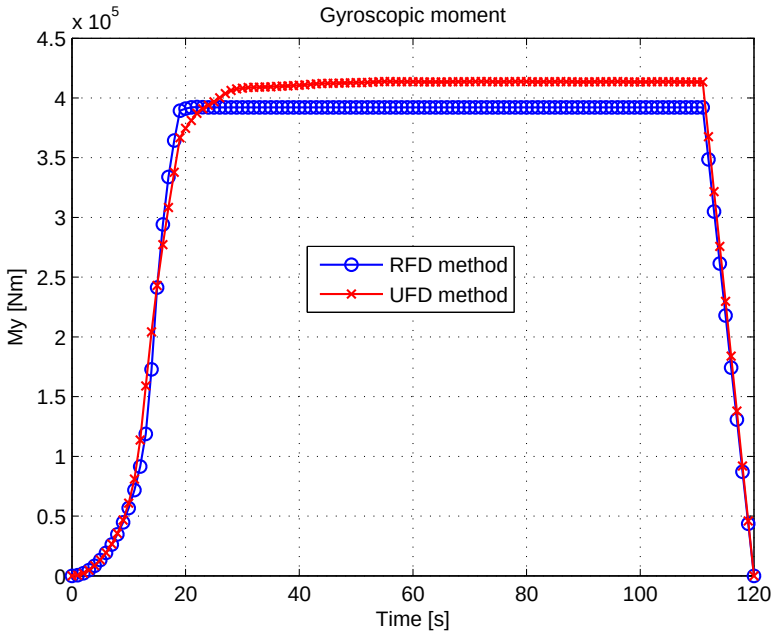

Figure 3.15: *2MW Siemens wind turbine Gyroscopic Moment, Pitch angle=20[deg], Wind speed=15[m/s], Constant wind condition.*

From the figure above it can be immediately observed that the gyroscopic loads are two orders of magnitude lower than the spinning as well as the bending moments and for this reason the gyroscopic moment is not always considered. For small wind turbine this assumption can be accepted but for multi-MW wind turbines the gyroscopic load should be considered during the design phase in order to certificate the durability of the wind turbine of 20 years, especially for bearings.

3.5.2 Normal turbulence wind condition

In this section the normal turbulence wind conditions are simulated. These conditions are particularly common for on-shore wind turbine located in the middle of field where the interaction of the wind with the surrounding vegetation, such as trees, can generates high turbulence. The same conditions can be found in wind farm where wakes of the first line wind turbine strongly affect the airflow of the turbine positioned behind. The representation of this wind conditions is reported in the figure 3.4, §3.4. The simulation is set with a constant pitch angle of 20 degrees, average wind speed of 15 m/s and counter torque 10^6 Nm; the simulation results are reported in the figure below

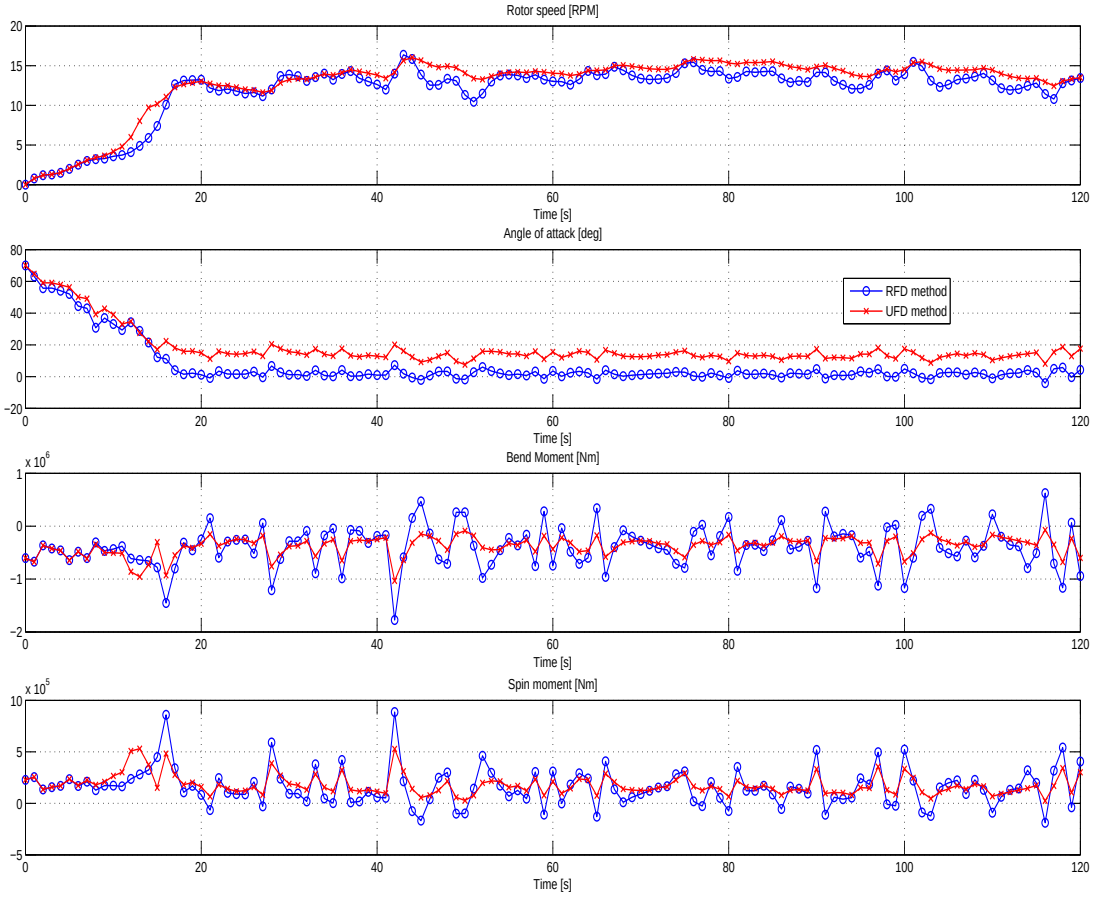

Figure 3.16: *2MW Siemens wind turbine Post-processing, Pitch angle=20[deg], Wind speed=15[m/s], Normal turbulence wind condition.*

As it can be noticed the variables of RFD method globally have lower values compared to the UFD method since it generates lower values of lift and drag forces according to what already stated for constant wind speed simulation. Furthermore looking at the shape of the response obtained with RFD, it seems that with this technique the rotor reacts faster to the variations of the wind conditions. This trend can be rationally explained thinking that RFD model provides a lift distribution closer to reality since the drag and lift coefficient vary along the blade length while for UFD method the coefficient are unique resulting in less sensitivity to rapid variations of the wind speed. Therefore it can be affirmed that UFD method filter the output value with a consequence of less accuracy. The same observation can be made for the output power that is shown below

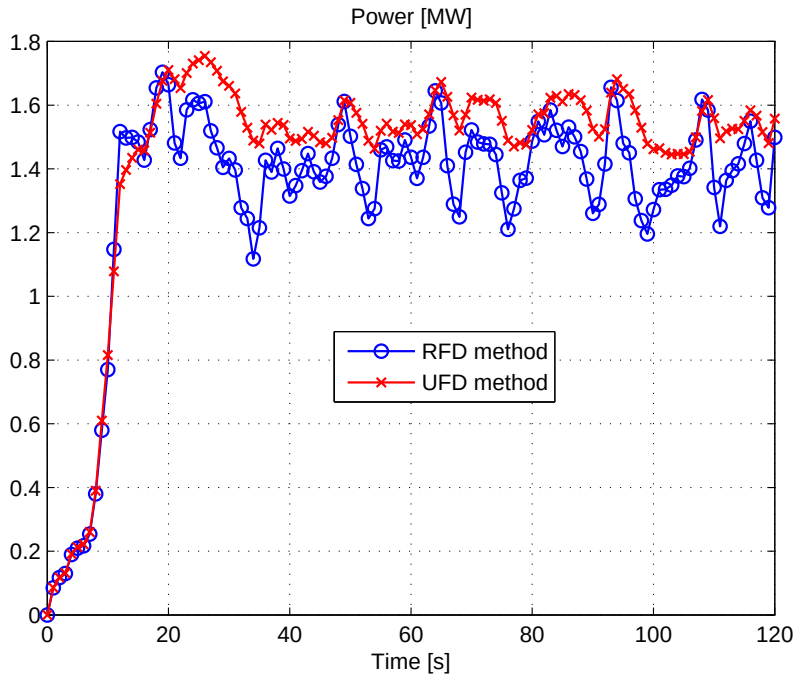

Figure 3.17: *2MW Siemens wind turbine Rotor Power, Pitch angle=20[deg], Wind speed=15[m/s], Normal turbulence wind condition.*

In fact, the output power of RFD method presents lower value than UFD technique and, as occurs in the constant wind simulation, in the initial transient phase the response is nearly the same for the reasons stated above.
The analysis of gyroscopic effect is performed also for normal turbulence wind conditions. The yaw motion law of the nacelle used for testing this wind conditions is the

same reported in figure 3.14. The results obtained are reported in the next figure

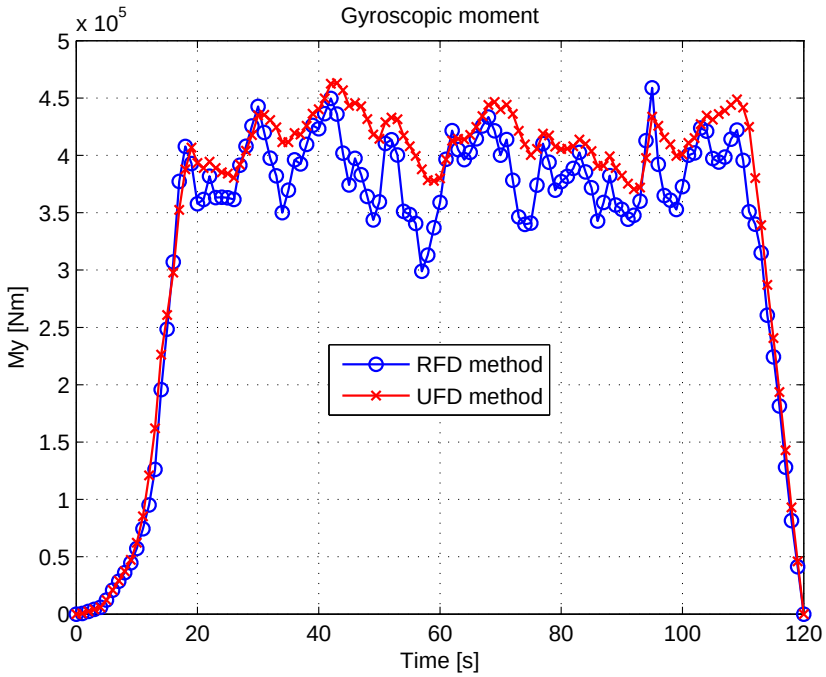

Figure 3.18: *2MW Siemens wind turbine Gyroscopic Moment, Pitch angle=20[deg], Wind speed=15[m/s], Normal turbulence wind condition.*

Looking at the y-axis, the gyroscopic moment values are two order of magnitude less of the spinning and bending moments. In spite of this difference between them is important, as already stated with the previous simulation the loads becomes relevant for the drivetrain components and the high variations that can be subjected to can significantly affect the durability of them.

3.6 Sensitivity analysis

Regarding the RFD method, it can be stated that the accuracy of the aerodynamic loads calculation strongly depends on the number of segments in which the blade is divided. Therefore it is interesting make a sensitivity analysis in order to understand in which manner the number of segments can affect the aerodynamic loads calculation. Moreover the aim of this analysis is also to obtain a reasonable trade off of between the computational time and the accuracy of the results.
The analysis consists of making different simulations of 2 MW Siemens wind turbine

[26] under the same initial conditions but varying the number of segments which the blades are divided into; therefore such analysis is performed for four variables, respectively: rotor speed, thrust force, output power and CPU time. In order to guarantee that the data of each iteration are under stationary conditions, the last value of the simulation is used since it is assumed that the transient phase has been ended. The sensitivity analysis leads to the following results

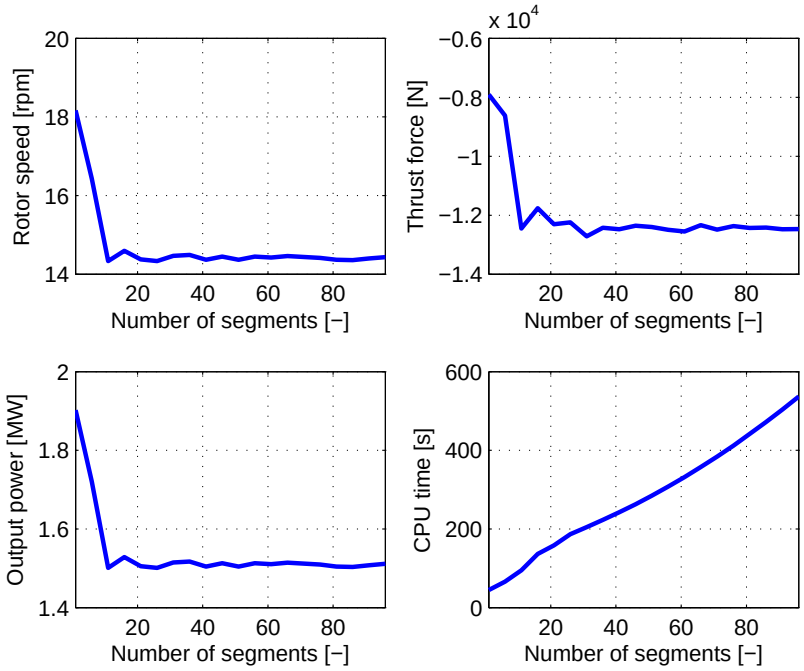

Figure 3.19: *2MW Siemens wind turbine Sensitivity analysis, Pitch angle=20[deg] Wind speed=15[m/s], Constant wind condition.*

It can be noticed that for a small number of segments the RFD technique shows overestimated values of the three variables under investigation. This behavior is originated from the fact that aerodynamic loads are highly non-linear because of the C_L and C_D coefficients therefore, for a low segmentation the addition or the reduction number of segments can modify the angle of attack of single segments and, observing the fig. 3.5, this small variations leads to C_L and C_D significantly different values. This phenomena decreases with the increase of the number of segments and, looking at the figure above, the output variables after 20 segments are stabilized around a define values. Such number of segments is indicated as the best number as a compromise for computational time and reliability of the results; in fact with 20 segments the CPU time required is

180 seconds and increasing the number of segments can simply lead to higher computational time without generating more accurate results.
Hence it can be concluded from the sensitivity analysis that the most reasonable value for segmentation of the blades is 20.

3.7 Validation of RLI model

In this section, the RLI model is validated against Hönö wind turbine measurement data [38]. The variables under consideration are, respectively: output power, thrust force, rotor speed and torque, that are provided for different wind speed values and different angles of attack.
The validation of RLI consists of comparing different working points at different wind speeds and at different pitch angles. The comparison can be done following this procedure; first the RLI model has to be set up with Hönö parameters, then, after having defined the wind average speed and the pitch angle of the blades, on the torque graph of Hönö datasheet it can be identify the value of the counter torque that must be set as input data on the mask interface. Subsequently, after running the simulation the output results, for instance power and thrust force at the steady state condition are used to compare the values obtained against Hönö measurement data.
This procedure is performed for wind speed values that swept from 5 m/s to 20 m/s, obtaining the comparison different working points as settle in the following table

Working points	**Power [kW]**		
	RLI	Hönö	Difference [%]
W= 5 m/s T= 750 Nm	6.3	5	8.9
W= 7.5 m/s T= 2000 Nm	16.4	15	8.6
W= 10 m/s T= 3200 Nm	23.0	22.5	2.3
W= 12.5 m/s T= 3800 Nm	23.5	23	2.2
W= 15 m/s T= 2900 Nm	20.8	20	3.8
W= 17.5 m/s T= 2400 Nm	18.3	17.5	6.0
W= 20 m/s T= 2200 Nm	16.4	15	9.5

Table 3.2: Validation of RLI model, comparison with Hönö measurements.

From the table it can be stated that RLI model presents a good level of accuracy par-

ticularly in the wind speed range between 10 m/s to 17,5 m/s, where the maximum difference is 6%. This gap is essentially due to choice of setting the RLI model paramenters using a NACA 63-200 airfoil while the Hönö airfoil is manually shaped in order to be a mix of NACA 63-200 and FFA-W3-xxx, therefore the C_L and C_D coefficients are different and can affect the values of aerdoynamic forces. Concerning low and high wind speed, the RLI data and from Hönö measurement data differ of more than 7%; the values power obtained with the simulation and the Hönö data are reported in the following plot which shows the gap that lag between the two data series overall the wind speed range

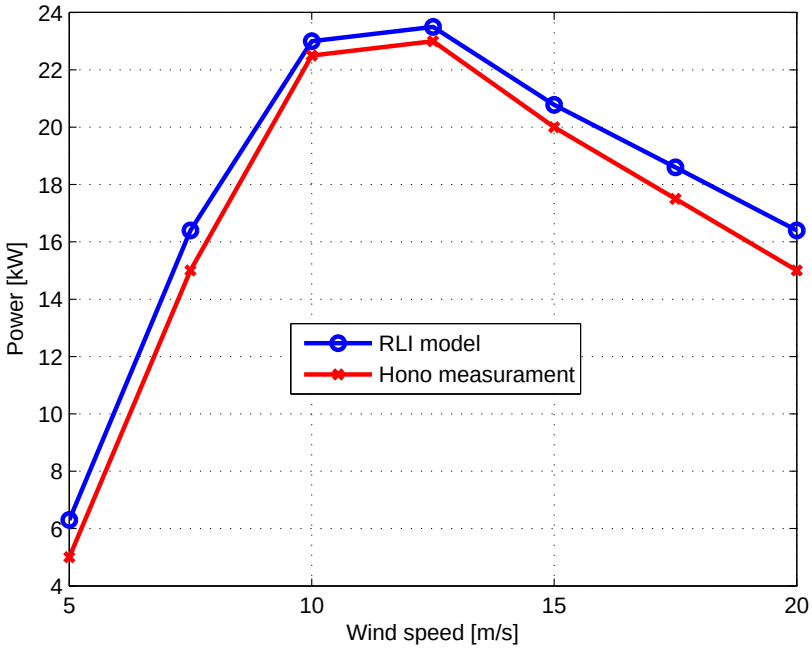

Figure 3.20: *Output power comparison between Hönö and RLI model.*

besides the different airofil shape implemented, for low wind speed, the different between Hönö data and RLI response is also due to the friction of components that usually is a non-linear function of speed, and in RLI model in not considered. This observation can be also extended for high wind speed since with at high rotor speed the losses on rotational components such as bearing increase and higher is the friction higher are the losses. For this reason the RLI model shows higher output power compared to Hönö data.

As conclusion RLI model globally presents a good accuracy of the results and good

level of reliability, nevertheless it can be suggested, for future improvements, to define the friction among the mechanical components with a more realistic model, for instance implementing the blade flexibility.

3.8 Further effects

Besides wind turbulence there are other effects that influence the output torque and one of these is the tower shadow effect. This phenomenon consists of a reduction of the incident flow caused by tower blockage which alters the wind distribution. When a blade is aligned the wind striking the blade drops, determining a ripple effect on torque as it can be observed from the picture below [14].

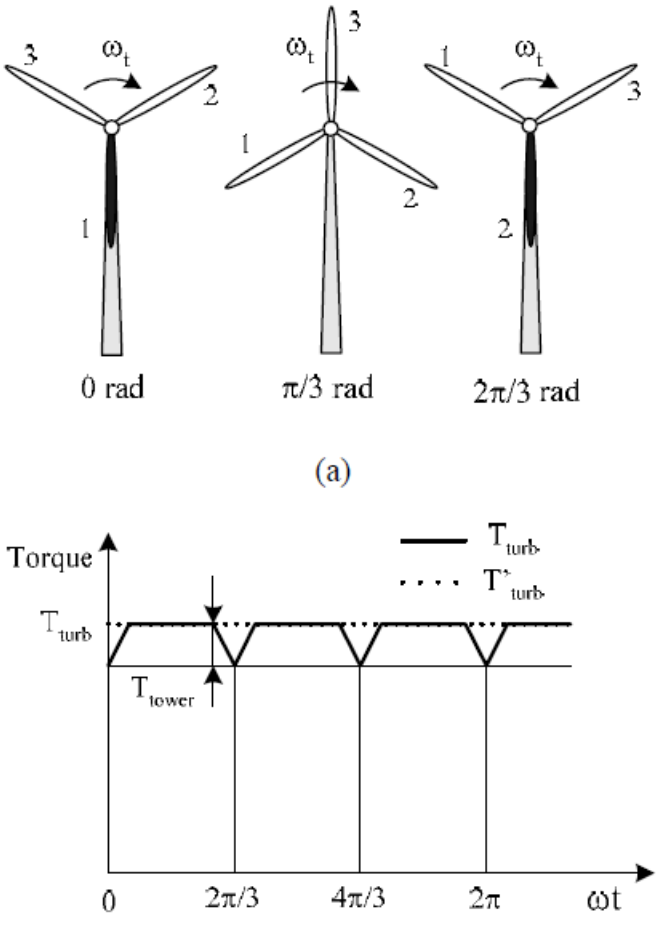

Figure 3.21: *Tower shadow effect.*

The order of magnitude and the shape of the rippled torque depend on the characteristic

of the structure.

Another effect is the wind shear that it is particularly important for the multi-MW wind turbine due to the height of the tower that can be reached around 120 meters. The wind shear profile can be expressed by the formula [29]

$$\left(\frac{W}{W_0}\right) = \left(\frac{z}{z_0}\right)^a \tag{3.9}$$

where a is the wind shear exponent and W and W_0 are the wind speeds at the heights above the ground Z and Z_0. In order to understand how the wind speed varies with height, the wind shear function, with $a = 0.2$ and a wind average speed of 6 m/s, is plotted below

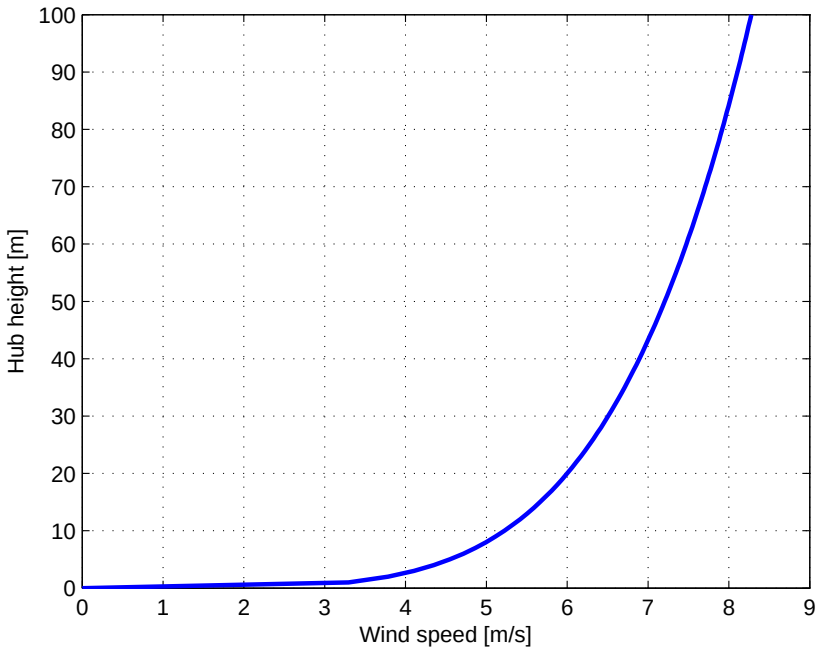

Figure 3.22: *Wind shear effect - Height Vs Wind speed.* a=0.2

At ground level the wind speed is practically absent due to the friction between airflow and the ground. With the increase of the height, the wind speed increases significantly and becomes exploitable for wind energy application over 40 meters from the ground level [6].

3.9 Future works

The RLI model represents a starting point of the Rotor Load Interface calculation, therefore the RLI model can be improved from different points of view. Hereinafter two suggestions are discussed:

1. The blades are modeled as rigid body without considering any flexibility. This assumption can be made if one wants to have an indicative the amount of loads on rotor interface and can also provide quite accurate results, in particular for small size with turbines. Considering a multi MW wind turbine, the blade length can reach 40 m of length, so it becomes relevant modeling the blades as a flexible body.
   The flexibility of blades can be modeled on RLI model using two methods, namely: mass lumped-parameter and FE. The first approach consists of a discretization of the blade into different masses and connect each of them with spring and damper, while the FE method provides to import the nodes from an FE model of the model generated with an external software (e.g. Abacus).

2. The RLI model presents different wind conditions that define the wind signal along axial direction of the wind turbine. In order to dispose a more realistic and more accurate wind model, the turbulent components along the orthogonal direction with respect to the axial one must be taken into account. Thereby if the axial wind direction lies on a X-axis the other two components on the wind lies respectively on Y and Z axis.
   The IEC:2005 standard provides a set of equations for defining analytically three dimensions wind model or alternatively it is possible to implement the wind model developed by Applied Mechanics department at Chalmers.

Furthermore the RLI model needs to be validated also against the data from complete wind turbine commercial software such as Vydin, FAST, AdamsWT in order to guarantee that the rotor load interface data are reliable and quite accurate.

Chapter 4

Generator interface

The main wind turbine configurations from the electrical point of view are briefly introduced. Different modeling techniques of wind turbine generators are discussed. The Generator Load Interface model is presented and different operational scenarios are simulated, including network fault. The issue of cogging torque is introduced and explained with an example.

4.1 Introduction

The Generator, together with the rotor and drivetrain, represents the core of a wind turbine. As already mentioned on *Wind Turbines State of the Art* chapter the generator is the device that converts the mechanical power extract from the wind into electrical power. Nowadays the generators of modern wind turbine, especially for multi-MW application are equipped with sophisticated power electronic which can control the electrical torque and rapidly change it if some problem occurs during normal operational time.
The generator and power electronic can be combined together forming different configurations, but in general the most widespread are, respectively: fixed-speed wind turbines with a squirrel cage induction generator, double fed induction generator (DFIG) and full power converter (FCWT). The fixed-speed wind turbine configuration is one of the first technology developed and is still used for small size wind turbines, on the other hand large size wind turbines are commonly built with DFIG and FCWT concepts. Hereinafter the functional scheme of each configuration is reported in the figure.

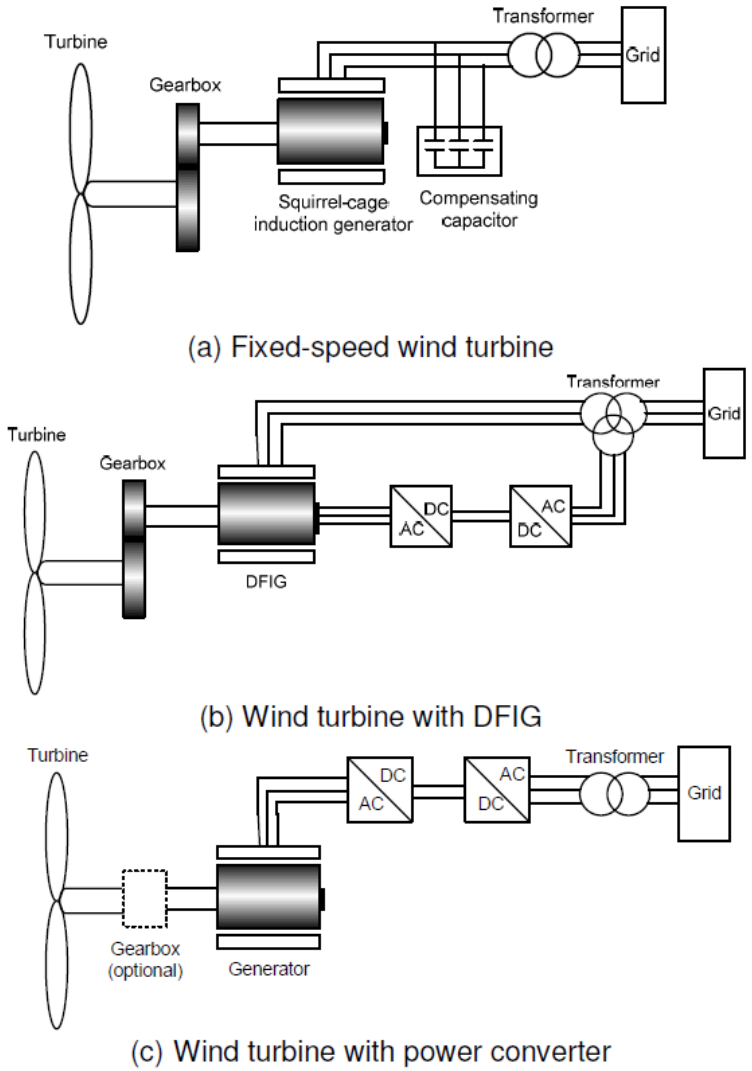

Figure 4.1: *Different wind turbine configurations [17].*

From the figure above the fixed-speed configuration consists of a squirrel cage induction machine and a capacitor bank, necessary to reduce the demand of reactive power, and a soft-stater which limits the in-rush current of the generator during the starting-phase. The fixed-speed solution is widely used to small size wind turbines that are controlled by either stall or active stall control [16] without requiring power electronic devices.

The DFIG configuration is equipped with a variable speed generator and a converter which is directly connected to the stator stage while the rotor stage is connected to the grid. This configuration is commonly used for indirect-drives wind turbines and has high efficiency thanks to a limited size of electronic components but usually it needs a

mechanical brake in order to avoid possible failure. In fact if a longer lasting network fault occurs, the generator starts to accelerate without control because the mechanical torque of the rotor is not counter balanced by any electromagnetic torque.
The FCWT configuration is normally used for direct drive wind turbines, equipped with a PM generators. The FCWT can resit to any network problems because the entire power pass trough a converter but on the other hand a large amount of electronic components and large cooling system are required, leading inevitably to a lower efficiency of the wind turbine.

4.2 Generator models

According to figure 2.3 of §2.5, the types of generator can be divided in synchronous and asynchronous. Both generators are defined with a set of the electromagnetic equations that describe its operation in dynamic as well as steady state conditions.
Referring to [7] the classification of generator models is based on the number of differential equations involved, in particular it is possible to define three models: first order model, third order model and fifth order model [7].
The fifth order model represents the most detailed since both rotor and stator flux dynamic are taken under consideration. The fifth order model consists of four electromagnetic equations and one mechanical equation. The definition of the equations is done using the a equivalent circuit of the generator, which is reported in the figure below

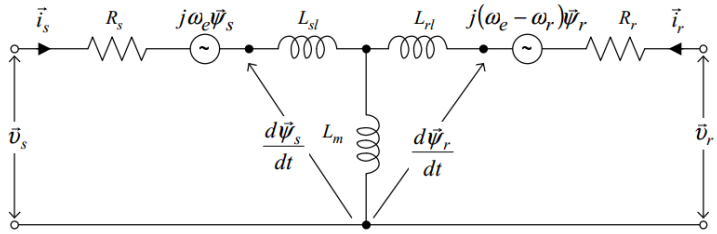

Figure 4.2: *Equivalent circuit of a induction generator - Fifth order model [20].*

The equations that governs the stator and rotor can be stated as

$$\vec{v_s} = \vec{i_s}R_s + j\omega_e\vec{\psi_s} + \frac{d\vec{\psi_s}}{dt} \tag{4.1}$$

$$\vec{v_r} = 0 = \vec{i_r} R_r + j(\omega_e - \omega_r)\vec{\psi_r} + \frac{d\vec{\psi_r}}{dt} \tag{4.2}$$

where ω stands for rotational speed while $\vec{v}$, $\vec{i}$ and $\vec{\psi}$ are the voltage, the current and the flux, respectively, and r and s subscript refers to rotor and stator variables. Currents and flux can be related by the following expression

$$\begin{aligned} \vec{\psi_s} &= \vec{i_s} L_s + \vec{i_r} L_m \\ \vec{\psi_r} &= \vec{i_r} L_r + \vec{i_s} L_m \end{aligned} \tag{4.3}$$

where L_s an L_r are the stator and rotor inductances and L_m represents the mutual inductance.

In order to obtain an mechanical equation that describe the dynamic of the rotor generator, the wind turbine system can be represented as simplified mechanical system that consists of a single rotating disk which includes the rotor generator and blades rotor system. This relation of the model is given as

$$(J_g + J_r)\frac{d\vec{\omega_r}}{dt} = T_e - T_m \tag{4.4}$$

J_g is the rotor generator inertia, J_r the rotor blades inertia, while T_e and T_m are the electrical and mechanical torques respectively, and combining those equations the fifth order model is defined.

The third order model of an induction generator can be defined by excluding the stator flux. Essentially this model can be described using the same equations of fifth oder model but neglecting the differential equations of the stator flux, remaining two electromagnetic equations and one mechanical.

In order to analyze the steady state condition of an induction generator the first order model can be involved. This model provides the same equations of the previous models without taking into account the electrical dynamic due to rotor and stator flux. Hence the first order model of induction generator can be represents with the following equivalent circuit

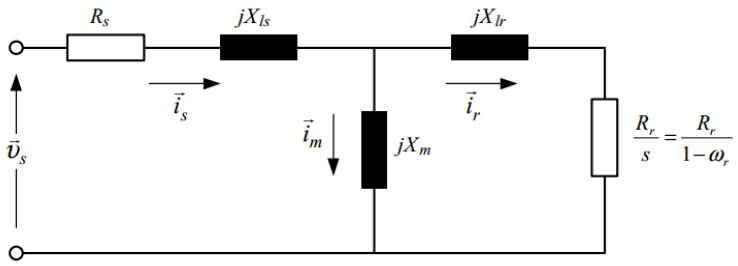

Figure 4.3: *Equivalent circuit of a induction generator - First order model [14].*

From the figure above the rotor current can be easily obtained and as consequence calculate the electrical torque.

4.3 GLI model

For GLI model a third order model is adopted to simulate a generator both under dynamic conditions and under steady state conditions. Such model requires the introduction of reference frame in order to define the dynamic equations stated in the section before. According to [16] it is possible to define two different reference frame respectively: ABC, natural frame system, and DQ0, arbitrary reference system. The natural frame system defines an induction generator using phase variables as coupled stator and rotor three-phase circuits, for example the currents are defined as 6-element vector, namely three rotor and three stator currents; on the other hand the DQ0 frame system sets the variables, for instance voltages, as space vectors of two dimensions [16]. In particular, GLI model provides a block specifically designed to convert the voltage value from the grid to DQ0 reference frame system; the voltage value obtained on this reference system are later send to the generator block, where the electromagnetic equations are implemented. Moreover the generator requires the rotor speed as input, and this variables is obtained with a model of the drive train system, which receives the electrical torque and the mechanical torque as input and calculate the angular speed of the rotor. This model configuration is adopted for both induction generator and PM generator.

The GLI Simulink block set of the induction generator is reported in the figure below

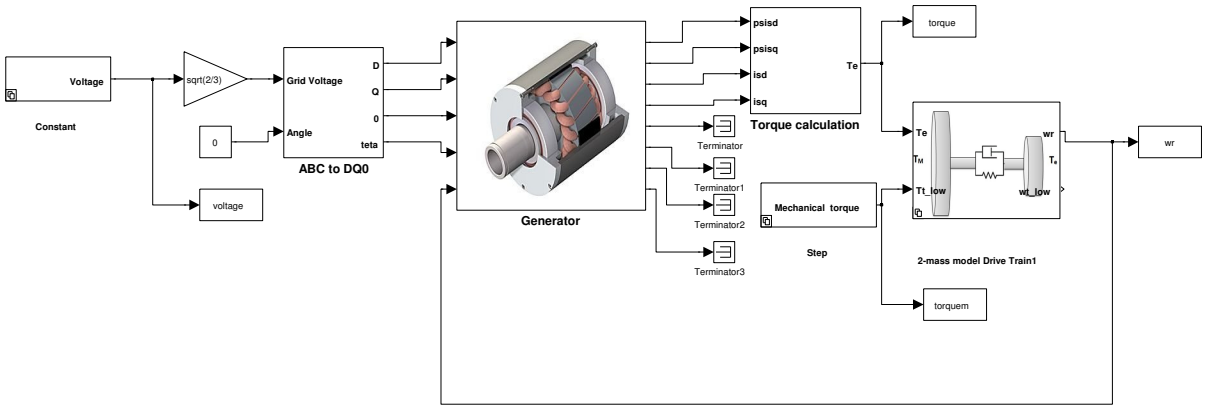

Figure 4.4: *Generator Load Interface model, Induction generator - Simulink block set.*

In order to have a better comprehension of the GLI model operation the main block, ABC to DQ0, Generator and one mass Drive train are presented in more detailed.

4.3.1 ABC to DQ0 conversion

The voltage grid signal needs to be defined in a three phases reference system. For GLI model the signal is first converted to the natural frame system and, later on, to DQ0 system. This conversion is executed through the following Simulink block set.

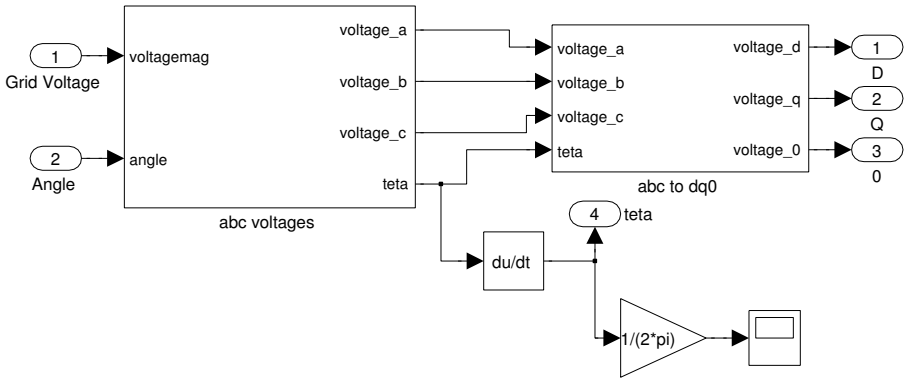

Figure 4.5: GLI model - ABC to DQ0 conversion block set.

As it can be observed the *abc voltage* block takes the voltage grid specified as input and through trigonometric equations, defines the shape of the three phases voltage into the

natural frame system. Later on the voltage values obtained are converted into machine frame system by the *abc to dq0* block and they become the input for the the Induction machine.

4.3.2 Induction and PM generator

In this section the Induction and PM generator Simulink model are presented and illustrated. The Induction generator block defines the electromagnetic equations specified in the introductory part, specifically 4.1,4.2 and 4.3. The input for the model are respectively the voltage in dq0 reference system and the rotor speed, the three voltage as stated before are provided by the *abc to dq0* block instead the rotor speed is provided by the drivetrain model. On the other hand the output of the block are the rotor and stator fluxes as well as the rotor and stator current that are subsequently combined together in order to obtain the electromagnetic torque. For the induction generator, the model used is the induction generator model developed by Electric department at Chalmers. The model is based on three order of differential equations model and is implemented in Simulink. In the following figure the Chalmers Induction Generator Simulink block set is reported

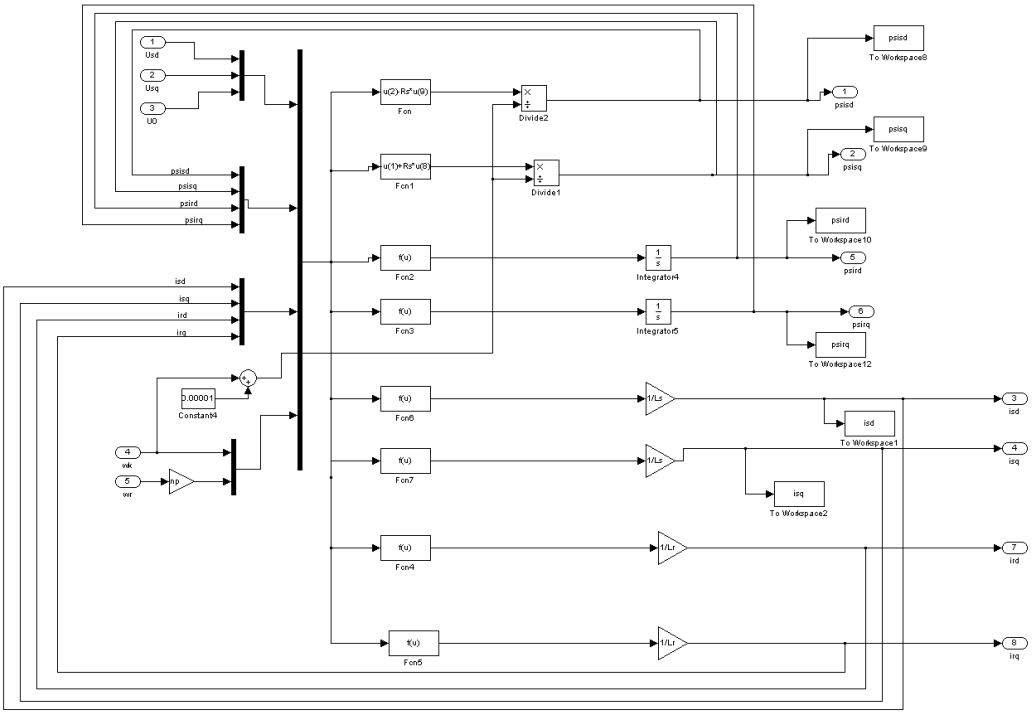

Figure 4.6: *Chalmers model - Induction Generator Machine.*

Concerning the PM generator, a similar model is proposed. The starting point is the Simulink PM generator model developed by Risø National Laboratory [36]. The model provides a third order PM generator which is described by 4.2 equations but without considering the slip on voltage rotor equation. As for the induction generator the input of Risø model are respectively, the rotor speed and the three voltage, while the output data are stator fluxes, the rotor and stator currents and the electromagnetic torque. Hereinafter the Risø PM generator Simulink block set is presented.

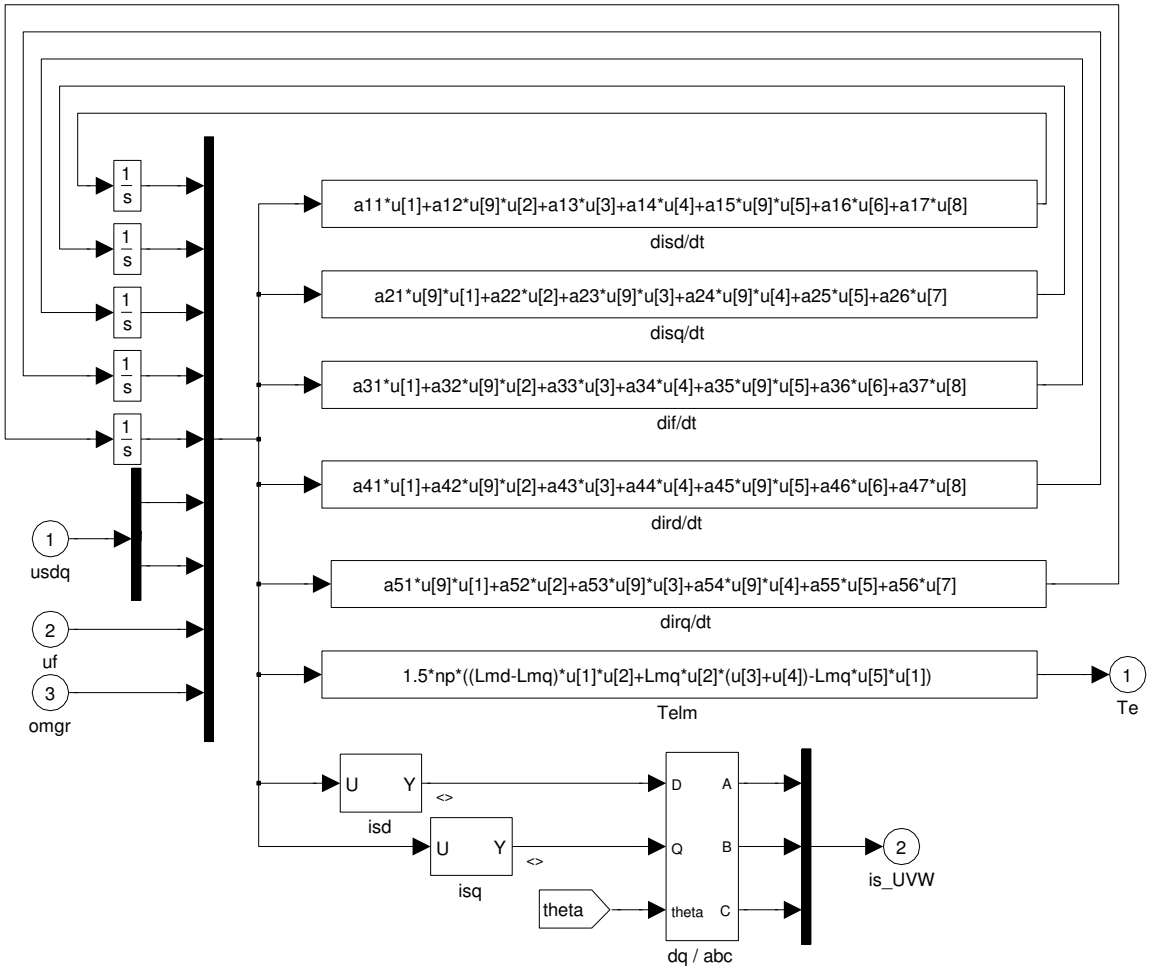

Figure 4.7: *Risø National Laboratory model - PM Generator Machine.*

4.3.3 Drivetrain

As stated in the introductory section, the third order generator required a mechanical equation in order to determine the rotor speed that represents the input of the Induction and the PM Simulink generator models. The rotor speed varies according to the dynamic response of the dirvetrain system, therefore the rotor speed is a function of generator, rotor and gearbox inertias as well as the electromagnetic torque and rotor mechanical torque. With GLI model two different drivetrain models are implemented, namely one-mass and two-mass drivetrain model. The first model is essentially one rotating mass including both rotor and generator inertia, on which a mechanical torque and electromagnetic torque are applied with opposite direction and the balance equation is the 4.3 relation. Hereinafter the Simulink model of one mass dirvetrain is reported

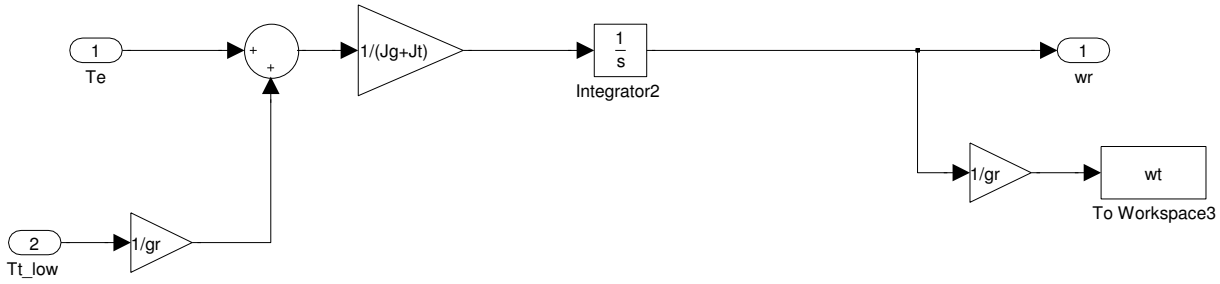

Figure 4.8: *GLI model - One Mass Drive train.*

On the contrary the Two-mass drivetrain model is a unique shaft with a torsion spring and damper which connected the rotating mass of the rotor with the generator one and the model can be represented with the following scheme.

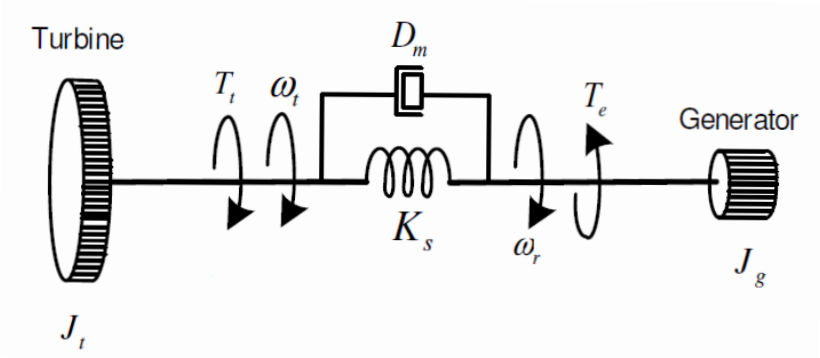

Figure 4.9: *GLI model - two-mass Drive train [4].*

According to the notations of the picture above the mathematical equations of a two-mass drivetrain model are given as [4]

$$J_t \frac{d\omega_t}{dt} = T_t - K_s(\theta_r - \theta_t) - D_m(\omega_r - \omega_t) \tag{4.5}$$

$$J_g \frac{d\omega_r}{dt} = -T_e - K_s(\theta_r - \theta_t) - D_m(\omega_r - \omega_t) \tag{4.6}$$

$$\frac{d\theta_t}{dt} = \omega_t \tag{4.7}$$

$$\frac{d\theta_r}{dt} = \omega_r \tag{4.8}$$

4.4 Simulations

In this section different simulations of an induction and PM generator are presented. The induction generator under consideration is a 180 kW power and the PM generator is a 4.5 MW power and for both, the construction characteristic are reported on Appendix A, respectively on table A.3 and A.4. Basically with these simulations, the response of the generator under different scenarios are investigated; specifically the electromagnetic torque response subject to a constant mechanical torque as well as to a drop, furthermore the influence of network emergency is also simulated, in particular a network fault.

The set of variables under investigation for both types of generator are: generator characteristic, the grid voltage, electromagnetic torque and rotor speed. All the variables are detected in time domain. Additionally the electrical and mechanical power and the power losses are investigated as well.

4.4.1 Induction generator

Set of Mechanical Torques

In the first simulation a constant mechanical torque and one-mass drivetrain model are set, and the generator starting rotor speed is 0 rpm. In the following figure the response of the generator is illustrated

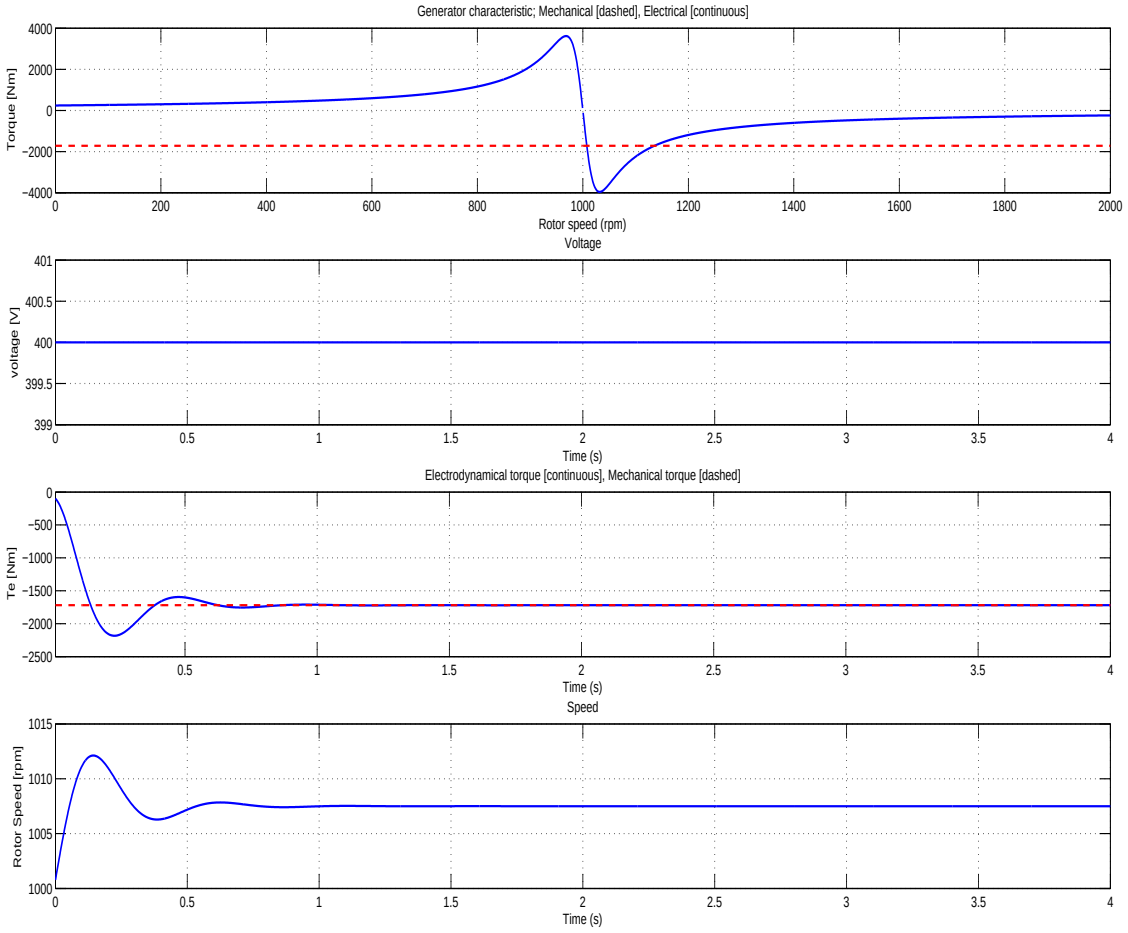

Figure 4.10: *180 kW Induction Generator - Generator characteristic, Voltage, Electrical torque, Rotor speed; Mechanical Torque constant and One-mass drivetrain*

From the figure the voltage curve remains constant for the overall time simulation. Looking at the generator characteristic it can be noticed that the line of the mechanical torque crosses the line of the generator in the stability zone and at the corresponding

rotor speed of 1010 rpm which represents the steady state condition. From paper [29], the induction generator can vary the rotational speed depending on the amount of load applied, generating a difference with synchronous speed and what is defined as slip. Observing the torque curve, during the starting phase, the electromagnetic curve is lower than the mechanical one so the rotor starts to accelerate and when the rotor speed is approaching to the steady state speed value, it starts to decrease but, due to inertia of the drive train system, it continues to raise, forcing the generator to produce a higher electromagnetic torque compared to the mechanical torque. In this condition the electromagnetic toque that works in opposite direction of mechanical torque force the rotor to decelerate until the steady state conditions are recovered again. In this way an oscillation of the torque and of the rotor speed around the respective steady state values occurs as shown on the previous figure. The steady state condition can be reached because the generator working point is located on the stability zone. Moreover the output power and power losses in time domain are illustrated in the figure below

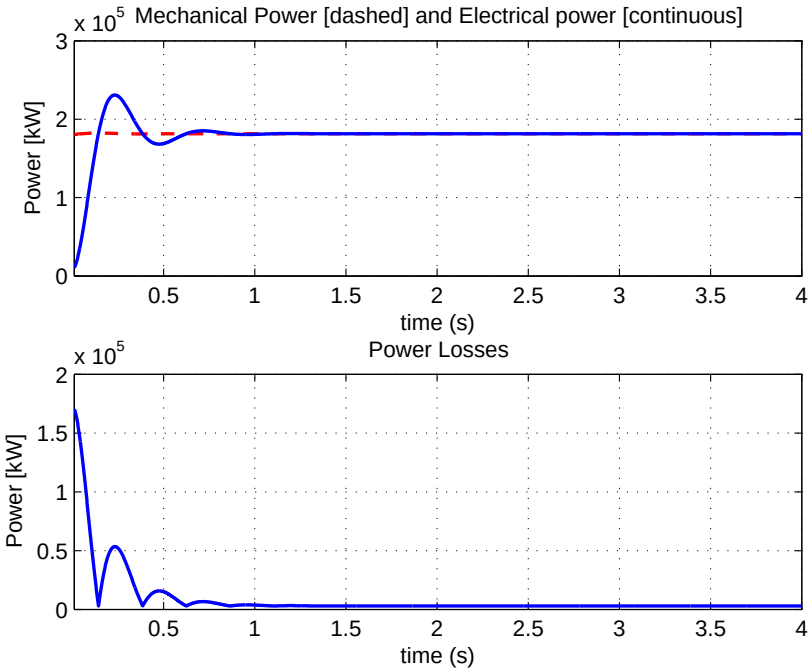

Figure 4.11: *180 kW Induction Generator - Electrical and Mechanical power, Power Losses; Mechanical Torque constant and One-mass drivetrain.*

Basically the power losses observed during steady state condition are caused by the Joule effect of stator and rotor resistances. Under dynamic conditions further power

losses occur, in particular the magnetizing power of inductances and capacitors that are not considered a contribution to electric power as well as the power absorbed from the grid when the electromagnetic torque is higher than the mechanical one. From the figure 4.11, the losses on the starting phase correspond to the energy requires to magnetize the circuits, while on the following peaks are the effect of the power absorbed from the grid.

Maintaining the same scenario and value of the mechanical torque as well as the same generator parameters, a simulation of the induction generator with the two-mass drivetrain model is performed. The simulation results obtained are shown below

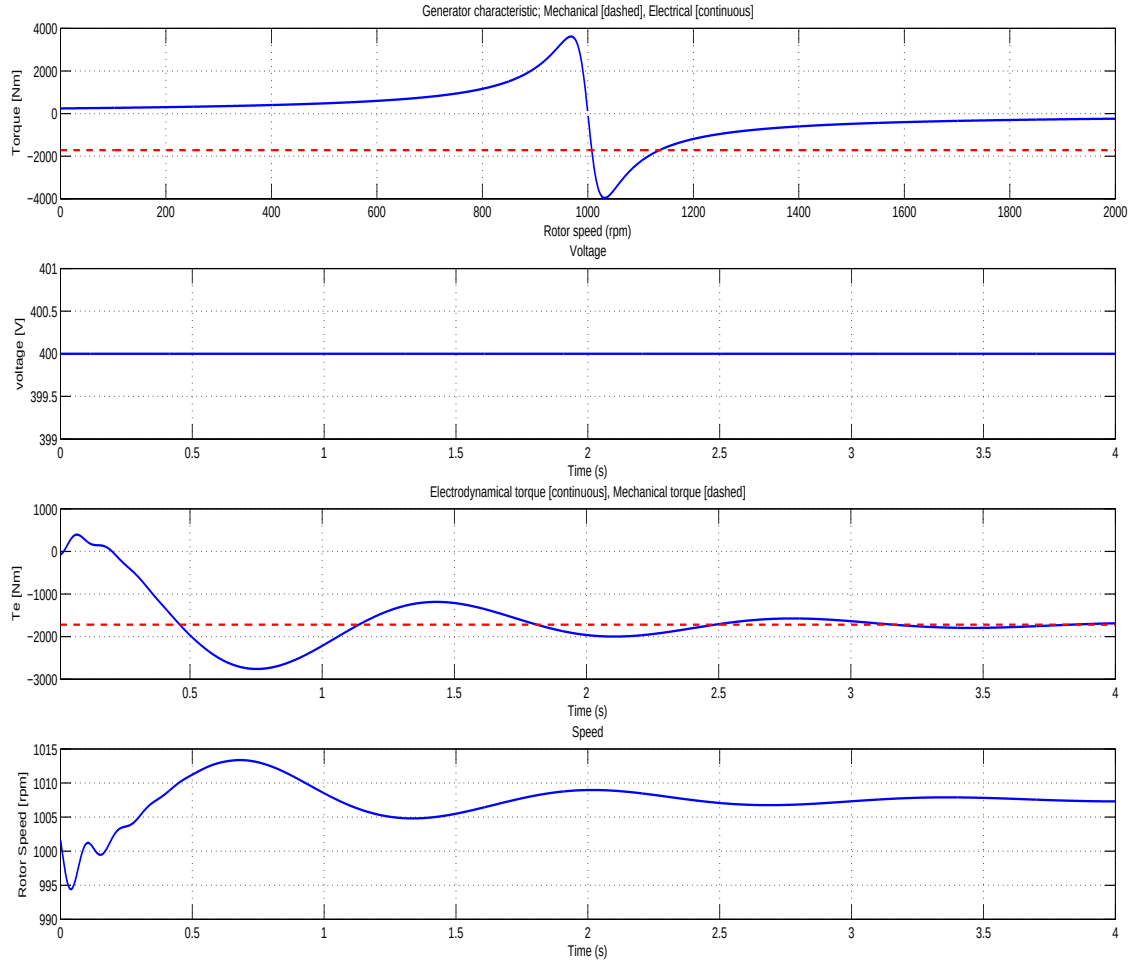

Figure 4.12: *180 kW Induction Generator - Generator characteristic, Voltage, Electrical torque, Rotor speed; Mechanical Torque constant and Two-mass drivetrain.*

The generator characteristic and voltage curve are the same as the previous simulation, the main differences are the responses of rotor speed and of the electromagnetic curve. In fact one can observe that both variables are subject to larger variations which also last longer compared to the case with one-mass drivetrain model. The cause of these oscillations is the shaft flexibility which establishes torsion vibrations along the drive-train system. This oscillations influence also the power response as it can be observed on figure below

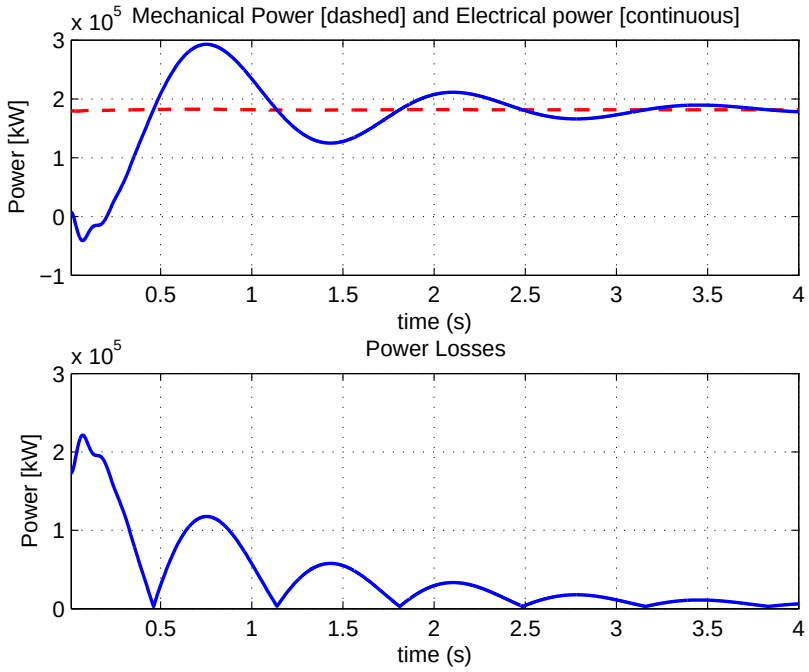

Figure 4.13: *180 kW Induction Generator - Electrical and Mechanical power, Power Losses; Mechanical Torque constant and Two-mass drivetrain.*

Comparing the results with the one-mass drivetrain model simulation of figure 4.11, it can be noticed that the simulation with the Two-mass drivetrain model leads to higher losses because the oscillations, that occur on the shaft, force the generator to produce an electromagnetic torque higher than mechanical one, by taking energy from the grid, necessary to reach the steady state condition.

The second operational scenario investigated is a sudden mechanical step, which in reality, can be caused by a emergency rotor braking. Specifically the step occurs after 20 seconds, when the the steady state condition are reached, and it lasts for 1 second. The magnitude drop is the 80% the rated mechanical torque. Moreover for this simulation the two-mass drivetrain model is adopted. The simulation results are the following

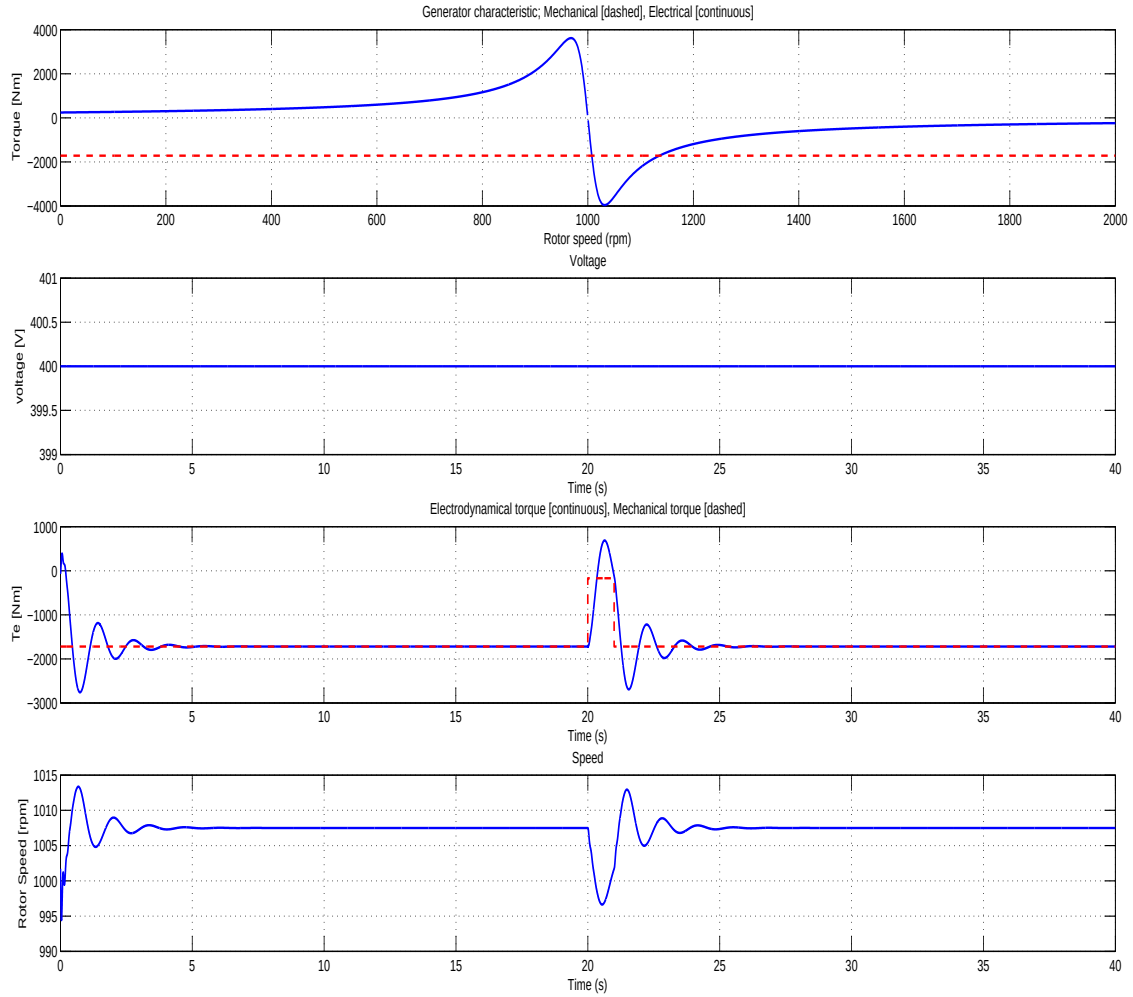

Figure 4.14: *180 kW Induction Generator - Generator characteristic, Voltage, Electrical torque, Rotor speed; Mechanical Torque drop and Two-mass drivetrain.*

When the step occurs the electromagnetic as well as the rotor speed are subjected to a significant change that implies a variation of rotor speed. The rotor speed presents

a drop of 1% going from 1007 rpm to 996 rpm, then when the step of mechanical torque ends the electromagnetic torque is restored and the rotor speed is subjected to a oscillation transimitted to the drivetrain.

Network fault

In this section the response of the induction generator subjected to a network fault is illustrated. Specifically the simulation of the network fault consists of a drop 90% of the grid voltage for a time of 250 ms, that corresponds to the maximum fault time accettable in Sweden [26]. The response of the generator is reported in the figure below

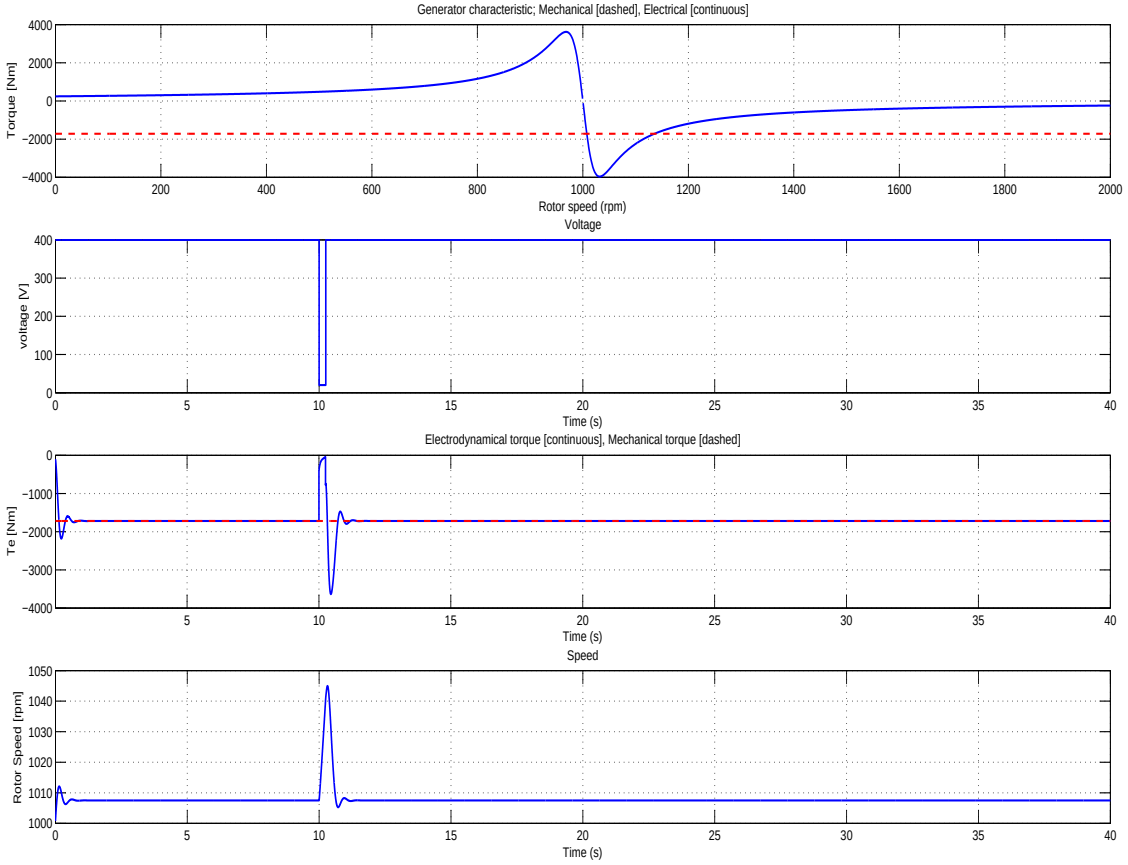

Figure 4.15: *180 kW Induction Generator - Generator characteristic, Voltage, Electrical torque, Rotor speed; Network fault 250 ms and One-mass drivetrain.*

The voltage drop occurs at 10 seconds after the starting point when the generator is under steady state conditions. Looking at the torque curve it can be noticed that when the network fault occurs the electromagnetic curve drops as well. The torque continues to decrease until it reaches the 0 Nm value. When the network fault ends and the voltage is restored, the electromagnetic torque starts to increase again, but due to the drivetrain inertia, the value of the torque exceed the mechanical one up to almost the double. Concerning the rotor speed it can be observed how severe is its variation during the network fault condition, in fact the rotor speed raises to 1040 rpm in just 250 ms. Hence the generator must be equipped with a safety braking system, mechanical or electronic, that can prevent the rotor to run out of control and determine failures and consequent downtime.
In the next figure the output power as well as the power losses are presented

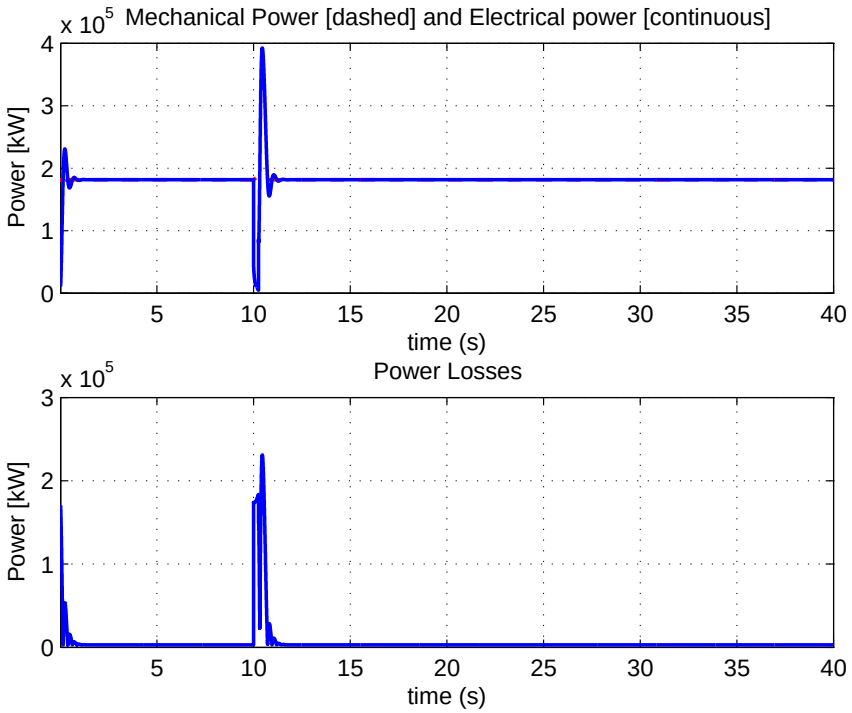

Figure 4.16: *180 kW Induction Generator - Electrical and Mechanical power, Power Losses; Network fault 250 ms and One-mass drivetrain.*

From the figure above, significant power losses can be observed when the network fault occurs. In fact, due to the low voltage of th generator, the mechanical energy is not converted to electrical energy, and this amount of energy is spent for accelerating the

the drivetrain system.

The same simulation is performed with a two-mass drivetrain model in order to investigate the influence of shaft flexibility on the electromagnetic torque as well as on rotor speed. The results obtained are presented in the following figure

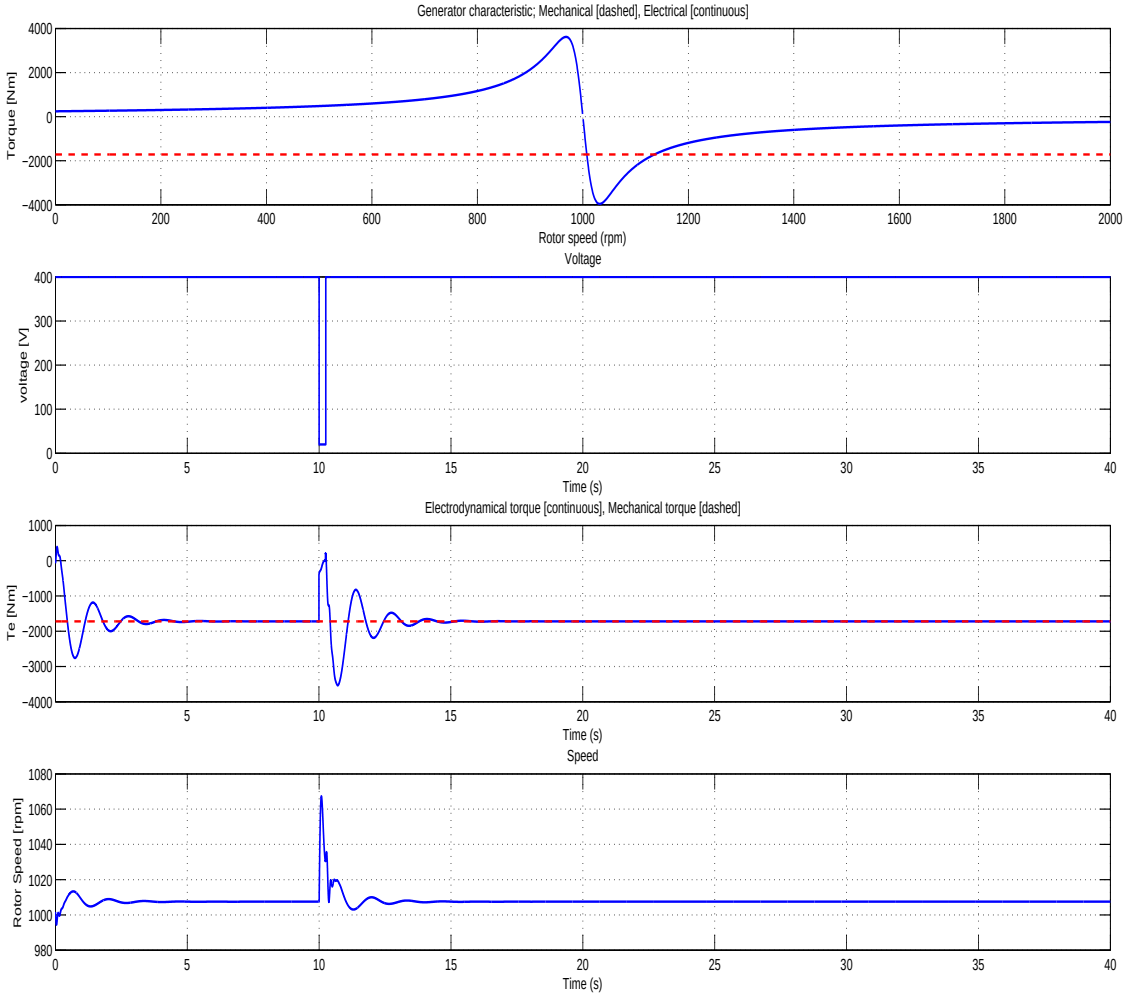

Figure 4.17: *180 kW Induction Generator - Generator characteristic, Voltage, Electrical torque, Rotor speed; Network fault 250 ms and Two-mass drivetrain.*

In this case the voltage drop has been set at 10 seconds because with Two-mass model it takes more time to reach the steady state condition. Immediately one can recognize that the drive train system needs more time to restore the steady state condition after the fault occurs, about 10 seconds, because the shaft flexibility causes oscillation on

the drive train, influencing significantly the generator response and performances.
The output power and efficiency of the induction generator with a two-mass drivetrain model is reported in figure below

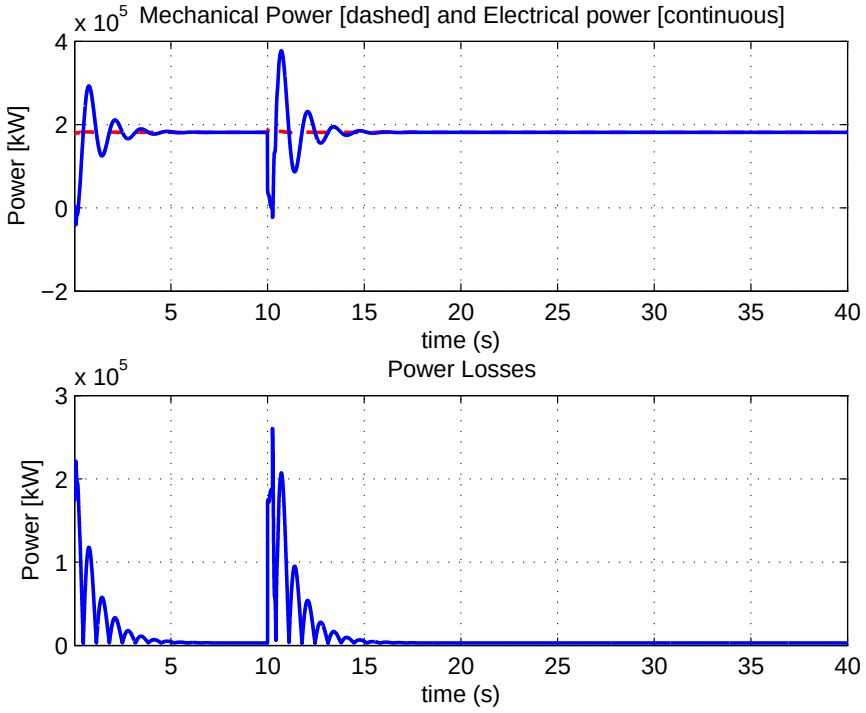

Figure 4.18: *180 kW Induction Generator - Electrical and Mechanical power, Power Losses; Network fault 250 ms and Two-mass drivetrain.*

By observing the power losses curve, it can be noticed that with the two-mass drivetrain model the losses are higher and more protracted on time respect the one-masses model. In fact as already stated, the two-mass drive train model the rotor speed as well as the electromagnetic torque needs more time to recover the rated values.
For this reason a comparison of the generator response with the one-mass drivetrain model and two-mass drivetrain model, under the same setting condition, results interesting. Specifically the simulation consists of evaluating the rotor speed response under a network fault which occurs 10 seconds after the start of the wind turbine, in order to be sure that the drivetrain is on steady state conditions and any residual vibrations of the starting transient phase are present. The network fault lasts for 250 ms as the previous simulations and the results are reported in the plot below

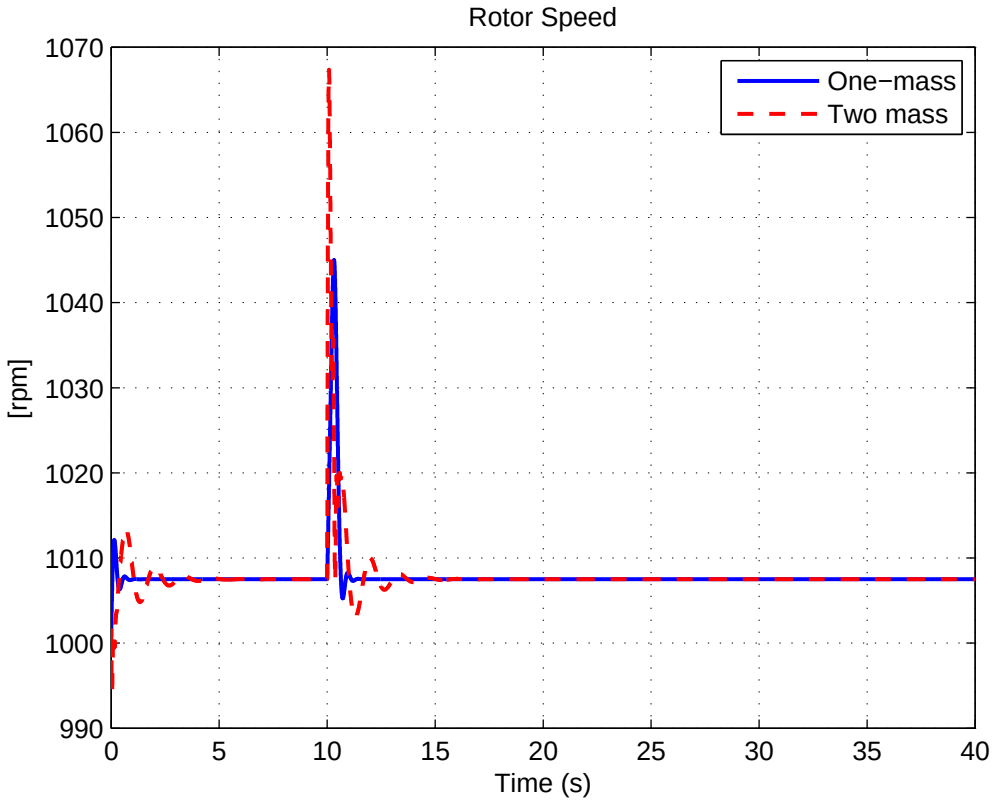

Figure 4.19: *180 kW Generator Network fault 250 ms - Comparison of the rotor speed with One-mass and Two-mass drivetrain.*

The figure shows that the rotor speed for the Induction generator with Two-mass drivetrain model reaches the highest value of 1068 rpm when the network fault occurs. On the contrary the highest rotor speed of Induction generator with One-mass drivetrain model is 1040 rpm. Although the difference between the two rotor speed peaks is 20 %, when a network fault occurs, the generator charcteristic is different and if, after the normal condition are restored, the new working point is situated in the instability zone, the generator could run out of control. So if the shaft is too flexible, under critical conditions, it can avoid the generator to run out of control and causing damages of the electrical componets.

Furthermore as already stated for the previous simulations the Two-mass model establishes more vibrations that need longer time to be extinguished. Hence with the Two-mass drivetrain model the generator, during dynamic conditions, shows a less power production than with one-mass model, concluding that the vibrations of the drivetrain system can affect the power production.

4.4.2 PM generator

Step of Mechanical Torque

The PM generator model under investigation is set with Two-mass drivetrain whose transmission ratio value is equal to one in order to define a direct drive transmission system. The simulation condition is a drop of 90 % of mechanical torque rated vaule which lasts for 2 seconds. The results of the simulation are the following

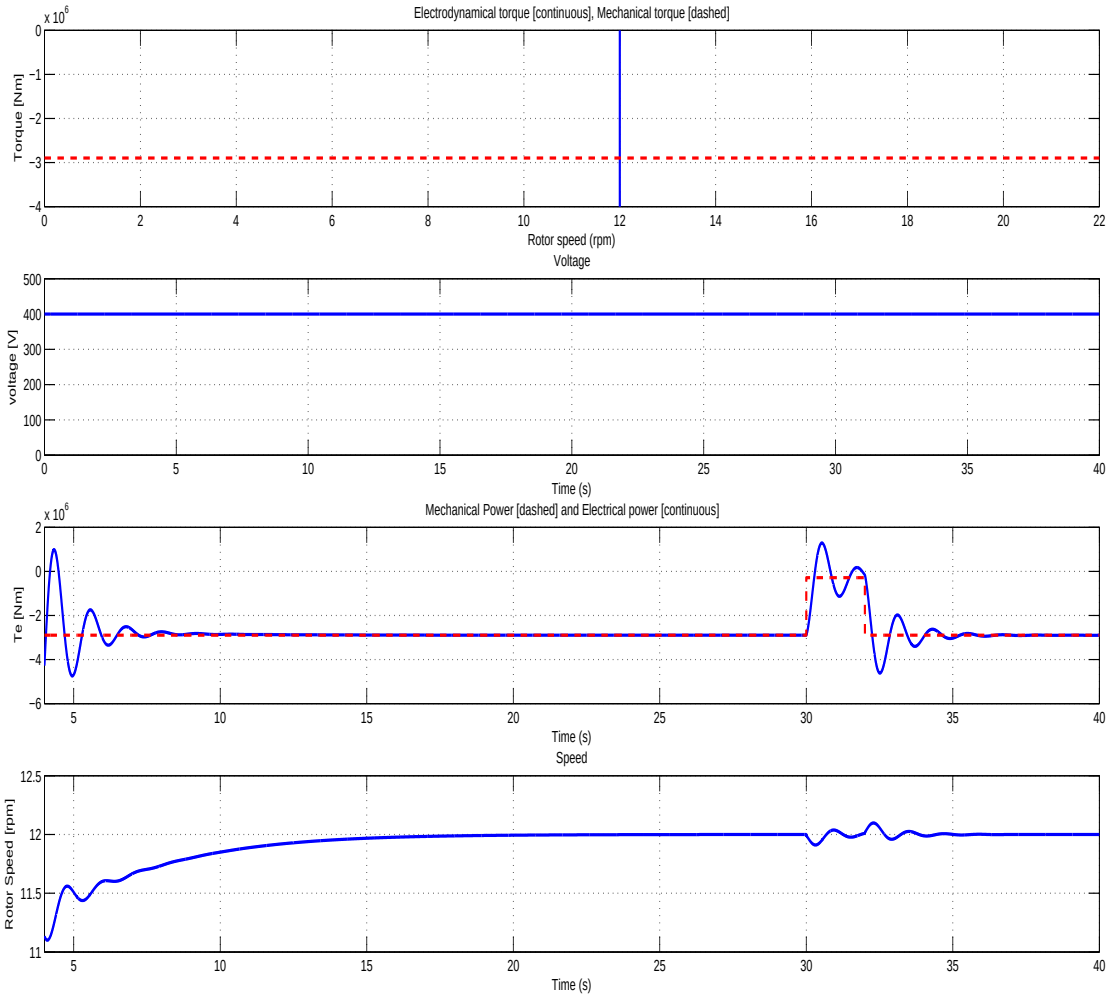

Figure 4.20: *4.5 MW PM Generator; Mechanical Torque drop - Two-mass drivetrain.*

The mechanical drop occurs after 30 seconds from the starting point, allowing the generator to reach the steady state conditions. From the generator characteristic the

synchronous speed of the generator is 12 rpm. This speed remains constant until the mechanical drop occurs, then the generator tries to follow the mechanical torque in order to maintain the synchronous speed. The torque curves show that the response of the electromagnetic curve is characterized by high amplitude oscillations around the mechanical torque while the rotor speed shows small variations of synchronous speed, around 0.08%.

Network fault

As for the induction generator a network fault is simulated for the PM generator. The voltage drop is set after 25 seconds of the starting point and it lasts for 250 ms.

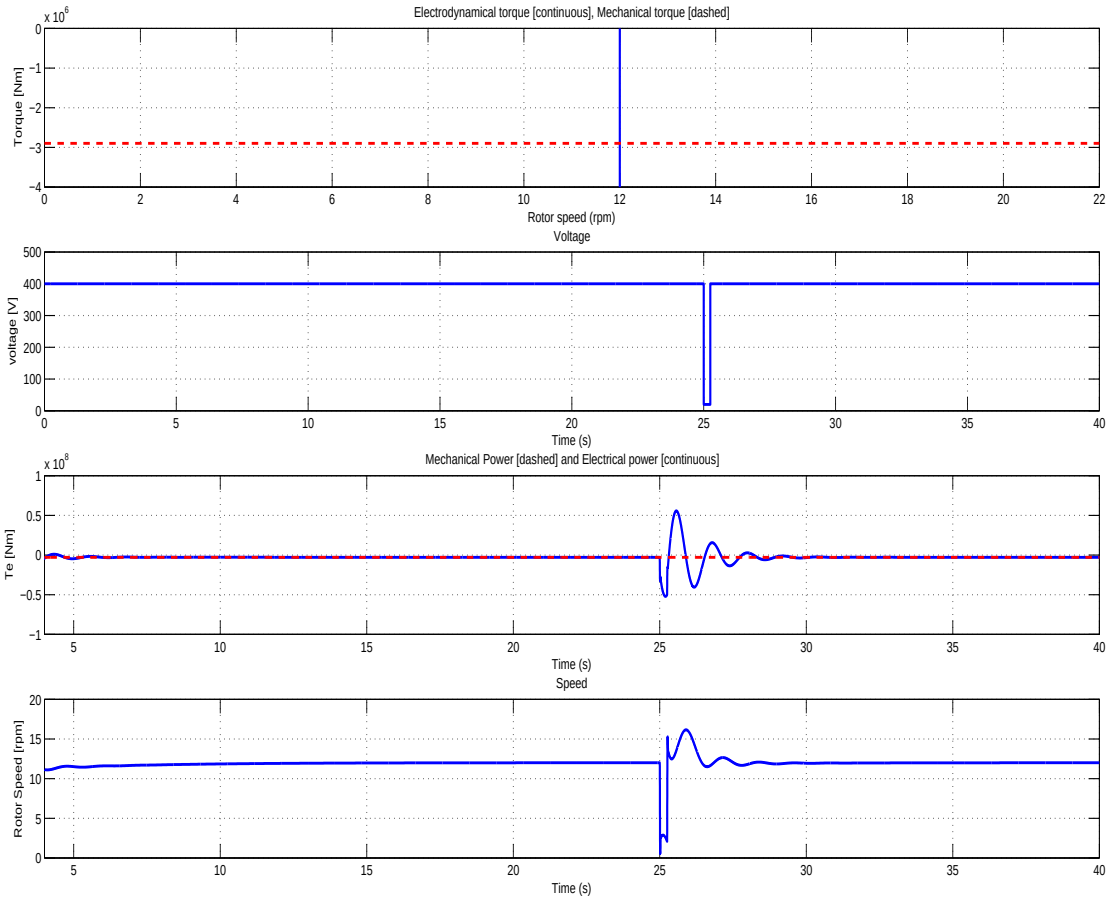

Figure 4.21: *4.5 MW PM Generator - Network fault 250 ms and Two-mass drivetrain.*

According to the torque curves, the electromagnetic torque undergoes to significant

variations showing a value of one order of magnitude higher and lower the rated value. This response heavily affects the rotor speed forcing the generator to rotate at speed considerably different from the synchronous speed. This behavior is caused by the lack of voltage supply that modifies the generator characteristic, changing as a consequence the synchronous speed, and when the voltage is restored the generator needs time to magnetize again the electrical components, causing a delay of reaching the steady state condition

4.5 Cogging torque

In this section the cogging torque effect is briefly presented. This phenomena mostly occurs in PM generator and starts to be taken under consideration specially for large direct drive wind turbines. In fact the cogging torque represents an excitation of the output electromagnetic torque that is due to interaction between the stator and rotor slot magnets, so is a disturbance that always occurs. Hence this oscillation is propagated along the drivetrain with a specific frequency and if the oscillation mode of the drive train is the same that can cause a resonant peak on the drivetrain loads and consequently affect the lifetime of the drivetrain components. Hereinafter the shape of the cogging torque is reported in time domain as well as the FFT of the its signal. The values shown are taken from [21].

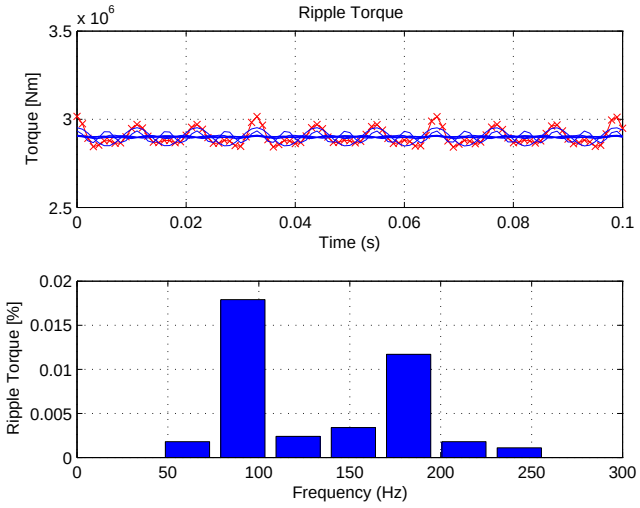

Figure 4.22: *Cogging torque of a 4.5 MW direct-driven PMSG, time domain and FFT analysis [21].*

In time domain signal, blue curves represents the different harmonics while the red one is the total signal. Furthermore the relative amplitude and frequencies of each ripple torque are reported in the bar plot. The percentage of the amplitude is calculated as relative torque value with the respect of the rated torque one.

4.6 Future works

The modern generators are equipped with advanced electronic controls in order to prevent failures as well as to improve the performances and the efficiency. The GLI model is characterized by an induction generator and a synchronous generator without any kind of electronic control. Hence one suggestion for future outlooks is to implement a control of active and reactive powers for both generator types. This modification will affect the response of the generators under different conditons and avoiding potential dangerous conditions that can cause damage of the generator.
Furthermore, concerning the Induction generator, a more advanced model for the drivetrain system can be implemented in order to have a more realistic response of the generator under different operational scenarios. For instance [32] suggests to define a model which takes into account both the inertia of the gears of the gearbox and the efficiency of the entire transmission.
In the end it is recommended to validate the GLI model with measurement data, if available, as well as with the data from commercial software products.

Chapter 5

Tower interface

The set of mathematical equations of the loads acting on an on-shore and an off-shore wind turbine towers are presented. The Tower Load Interface model is presented showing the Simulink block set. The response of an on-shore tower under different constant wind speed conditions is performed. Moreover an off-shore wind turbine tower is tested under constant wind speed conditions and a periodic function representing the interaction between waves and foundations.

5.1 Introduction

The modern wind turbines are subjected to significant loads on tower due to wind pressure but also due to waves in case of off-shore wind turbines. According to the environmental conditions, the interaction between wind and tower as well as waves and foundations generates periodic or random loads that cause vibrations that are directly transmitted to the drivetrain system through connection supports with the tower, e.g. bearings. Moreover for wind turbines equipped with yaw motion system, the gyroscopic effect can establish vibrations that, combined with the ones produced by wind, could yield to critical resonance condition.

5.2 Tower load

The main source of loads for wind turbine tower comes from the wind, from the gravity and, for off-shore application, from the waves. Referring to [33] the loads sustained by tower can be represented as in the following figure

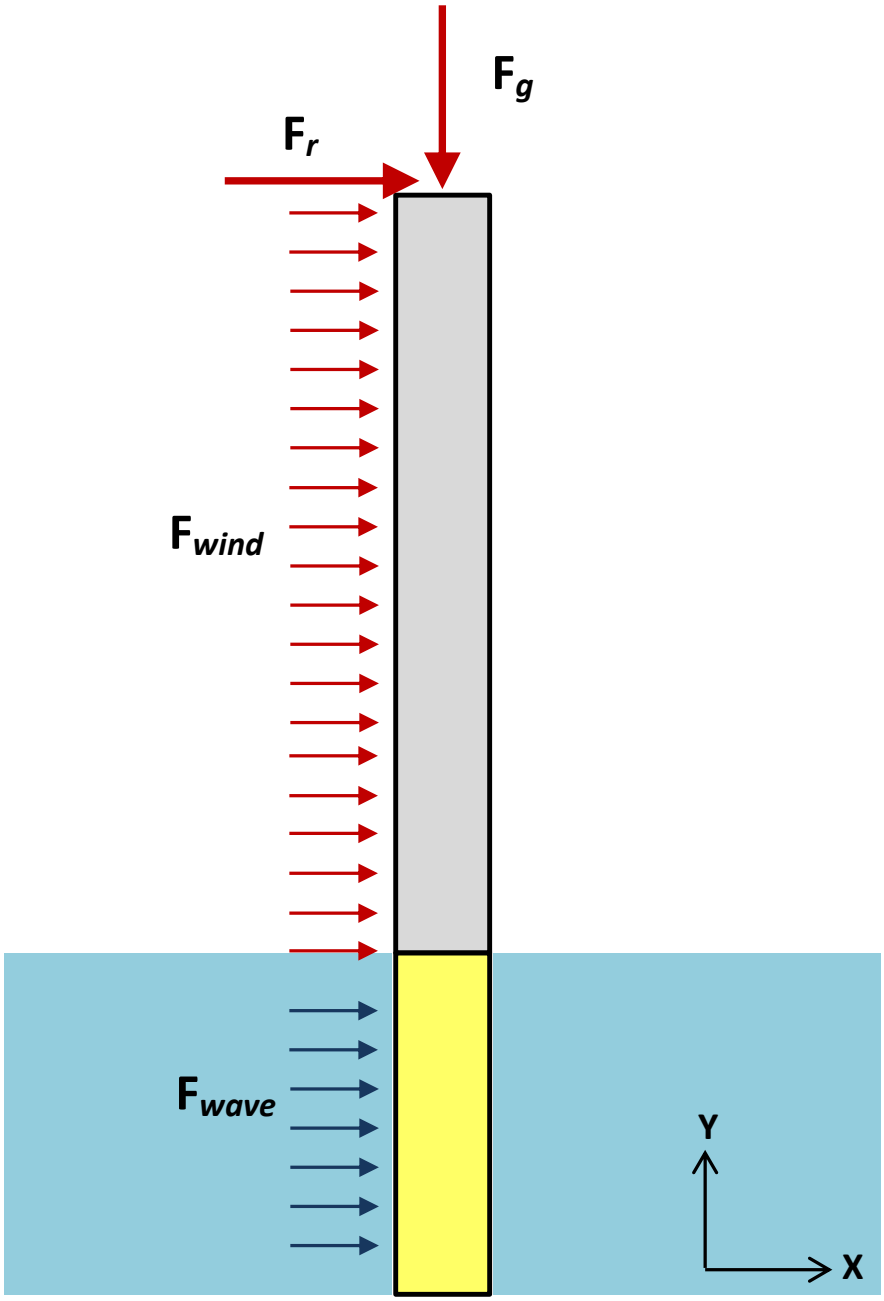

Figure 5.1: *Loads of an off-shore wind turbine tower.*

Specifically the gravity load (F_g) which consists of tower, nacelle and rotor weights, the wave load (F_{wave}) which is the effect of interaction between wave and foundation of the tower, and the wind loads that act on the tower in two different manners. In particular when an air flow invests the wind turbine, the thrust force (F_r) generated on rotor blades is transmitted to the drivetrain and then forwarded to top of the

tower through the supports. Additionally, the interaction between air flow and tower produces a pressure distribution (F_{wind}) along the tower itself which depends on the height according to the wind shear equation 4.5, stated in §3.8.
Each loads are defined with a specific equation, in particular the wind load equation for what concern the thrust force is specified as [33]

$$F_r = \frac{1}{2} C_d \rho_{air} V_S^2 A \cdot B \cdot S \tag{5.1}$$

where C_d is the drag coefficient, ρ_{air} is the air density, V_S is wind speed, A the area swept by the rotor blades, B the number of the blades and S a defined safety factor. Alternatively it is possible to specified the thrust force directly using the RLI model with the possibility to have a time-domain thrust force signal as input for TLI model and not only a single value derivable with 5.1. Regarding the wind force distribution on tower, the resistance force that the tower bears is the formula [33]

$$F_D = pA(C_{DS} + C_{DF} e^{i2wt}) \tag{5.2}$$

Where, A is the area of the interaction between the flow and the tower, p is the dynamic pressure, $p = \rho_{wind} V^2/2$, C_{DS} is the steady resistance coefficient, C_{DF} is vibration resistance coefficient and w is the vortex frequency. The latter factor can be expressed with the Struhal number and is given as $w = 2_s/D$, where D and V_S are the diameter and the wind speed at a specific height.
The gravity force can be simply expressed with the following equation

$$F_g = (m_{tower} + m_{nacelle} + m_{rotorblades})g \tag{5.3}$$

where g is the gravity force that is multiply for the respective mass lifted up by the tower.
The wave load, according to [33], can be estimated using the semi-theoretical Morison equation which expresses the wave force as a combination of inertial force and viscous resistance. The inertial force and viscous forces are related to water particle acceleration and velocity, respectively. Hence the Morison equation is defined as:

$$F_{wave} = C_m \frac{\rho_{sw} \pi D^2}{4} (a_{wave} - a_s) + \rho_{sw} A a_{wave} + C_d + \frac{\rho_{sw} D}{2} (u_{wave} - u_s) \left| u_{wave} - u_s \right| \tag{5.4}$$

Where, C_m is inertia coefficient, C_d is drag coefficient, ρ_{sw} is density of sea water, D is tower diameter, A is area tower, u_{wave} is velocity of water particle, u_s the velocity of

tower, a_{wave} is the accelerations of water particle and a_s the acceleration of tower. The explanation for the calculation of acceleration and speed water particle is reported in Appendix B.
Hereinafter the loads acting on a wind turbine tower are summed up in a table

Loads	**Symbols**	**Formula**
Gravity force	F_g	$(m_{tower} + m_{nacelle} + m_{rotorblades})g$
Wind thrust force	F_r	$pA(C_{DS} + CDFe^{i2wt})$
Wind tower force	F_{wind}	$pA(C_{DS} + CDFe^{i2wt})$
Wave force	F_{wave}	5.4

Table 5.1: List of Tower Loads.

5.3 TLI

The TLI model is essentially divided into two components, the tower and the nacelle. The tower can be figured as a beam subjected to a concentrate load positioned on tip and constrained on the base. The tower is modeled using the lumped parameter technique, in particular this method defines a flexible body as a series of rigid body connected with springs and dampers, which the respective coefficients can be expressed as a function of geometry and material properties of the flexible body under consideration. Referring to [31] a tower of L length can be divided into n elements, called Generalized Beam Elements (GBE), which are a combination of body-joint-body, where the joint is a prismatic joint and each GBEs are welded together in order to obtain the flexible tower.
The second component of TLI model, the nacelle, has been designed simply as two rigid bodies, with a specific mass and inertia, connected each other by two couples of spring-damper in parallel. These two bodies are, namely the bed plate and the drivetrain, which includes the rotor and generator masses. The bed plate is welded to the last rigid body of the tower in order to reproduce exactly the same motion of the tower bending. The two connection elements are used to model the drive train and generator supports, therefore the first couple, spring-damper, represents the drivetrain supports while the second one model the generator support. In order to figure how the model is set, a scheme is reported in the next page

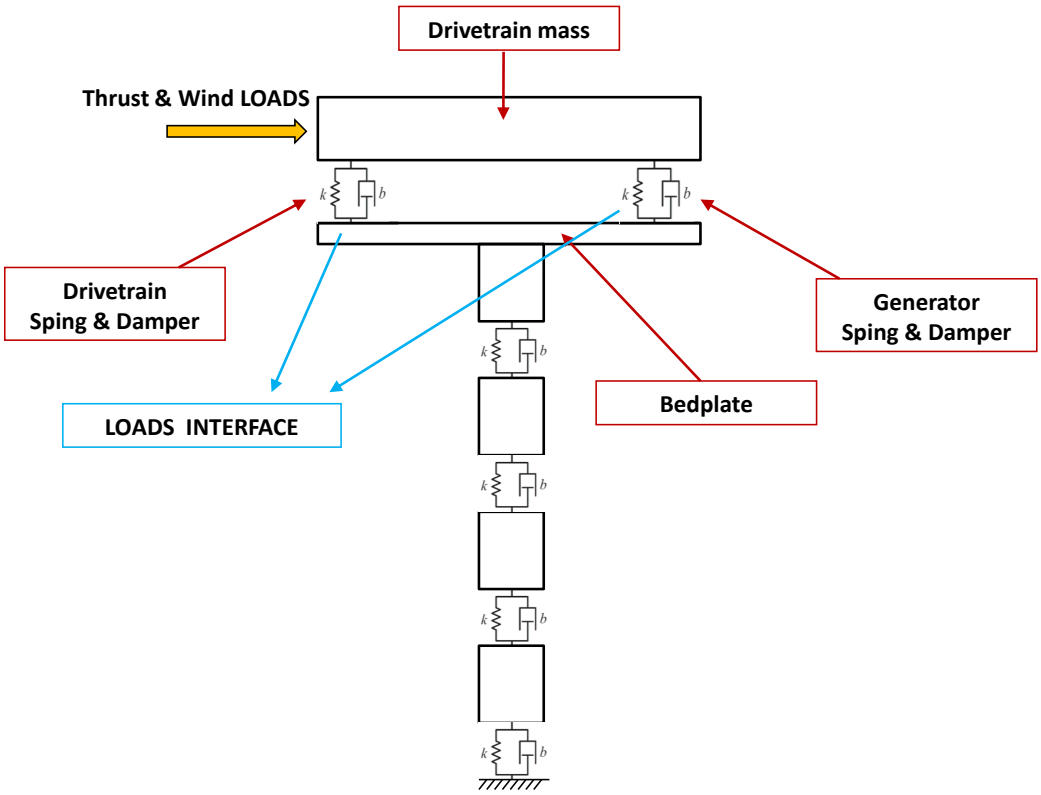

Figure 5.2: *Representation of tower model.*

From the figure, it can be deduced that, if for instance the tower bend to left direction due to thrust force the first interface spring and damper, specifically the drivetrain, is subjected to compression instead the generator spring and damper are stretched. The opposite situation occurs when the tower bend on the opposite side because of the recall force generated by the elasticity of the tower. This behavior established vibrations that are transmitted on the supports and that can affect lifetime of these components.

The TLI model is entirely realized within Simscape environment, where a flexible body can be modeled using the GBE element developed by MatWorks [37], which is reported in Appendix C. The MatWorks GBEs have been designed for simulating a flexible beam. With TLI model, the GBEs are completely redefined in order to obtain a flexible tower, therefore the rigid bodies are set with tower parameters as well as the damping and stiffness coefficients. In the next page the TLI block-set of an On-shore tower model is given

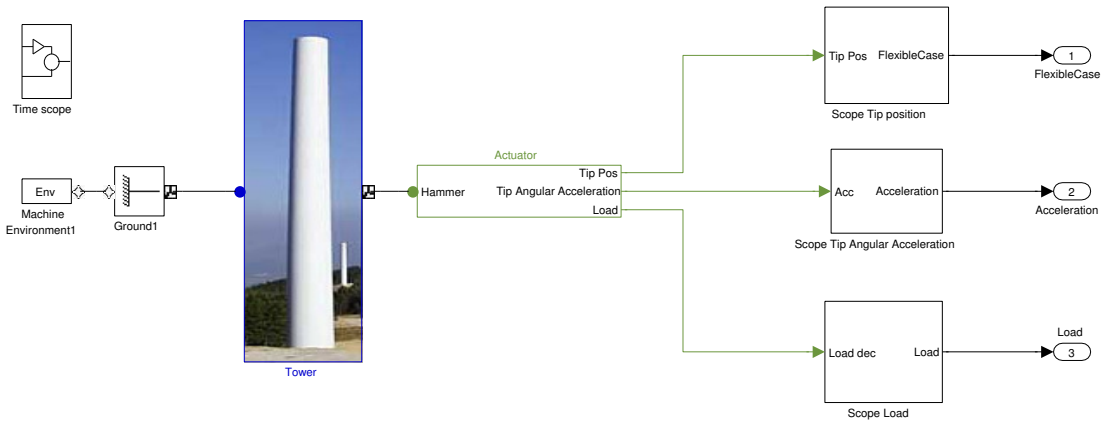

Figure 5.3: *Tower Load Interface Simulink block set - On-shore tower.*

The core of the model is concentrated on the subsystem block set named *Tower*, where the GBEs elements are located. The first GBE element, which represents the tower base, is connected to the ground bound as well as the machine environment block, instead the last element, tower top, is connected the *Actuator* block. Inside this block resides the body actuator which applied the thrust and wind forces specified as well as some sensors for measuring different variables. The Off-shore TLI model is basically the same as the one shown above, except that the Off-shore model includes two GBEs blocks for the foundations which has different material properties. Moreover an additional body actuator is set on top the of the foundation, precisely on second GBE element which is connected to the base of the tower, in order to applied the wave force, formulated according to equation 5.4.

5.4 Simulations

In this section the simulations of an on-shore and an off-shore wind turbine towers under specific wind conditions are presented. The on-shore wind turbine tower under investigation is a 100 m tubular tower built with steel material while the off-shore tower is a 65 m tubular tower with foundation of 20 m depth under sea level. The parameters of the on-shore and off-shore towers are reported on appendix A, respectively on table A.5, A.6 and A.7, A.8, A.9. The constant wind speed conditions are set for both towers. The variables investigated for both models are the deflection of the tower, moment on tip of the tower and the most important interface loads, namely generator support and drivetrain support loads. All the variables are reported in time-domain except for the deflection which is analyzed also in frequency domain.

5.4.1 On-shore Wind Turbine

The simulation conditions of the on-shore wind turbine are: wind speed at 15 m/s and thrust force of 10^6 N with a simulation time of 10 seconds. The tower deflection and the respective FFT analysis is reported in the next page

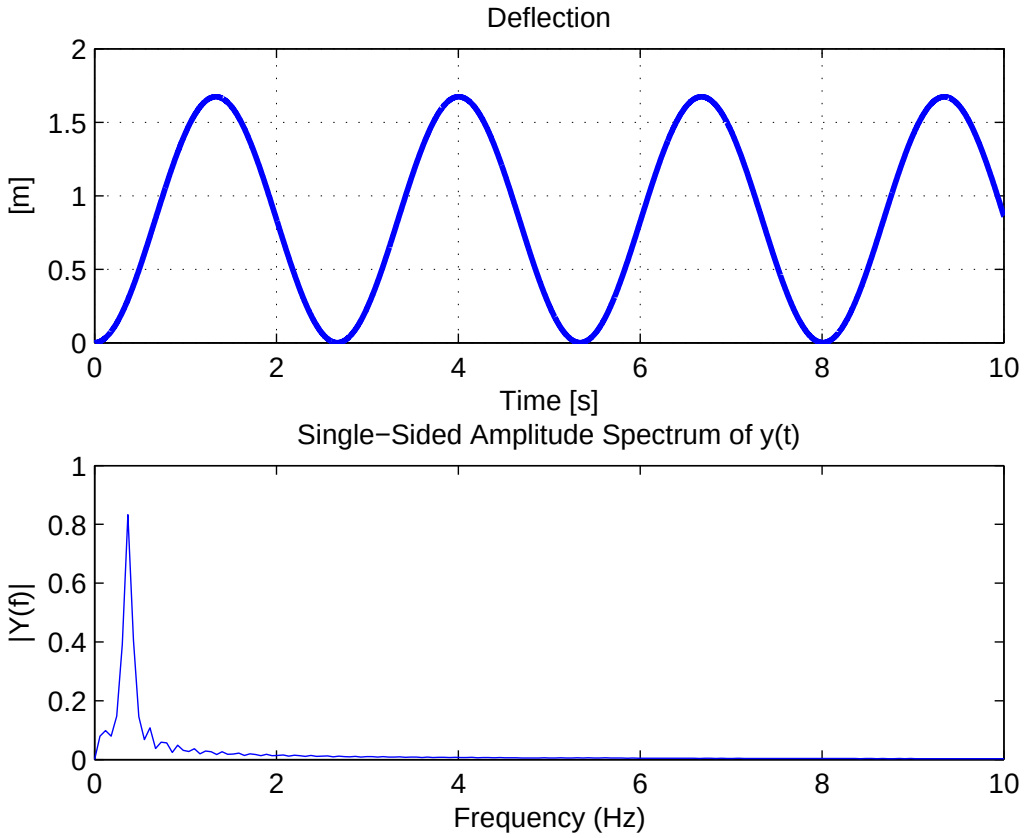

Figure 5.4: *Deflection and FFT analysis of 100 m - On-shore tubular steel tower, thrust force of* 10^6 *N.*

From FFT analysis it can be recognized one main frequency peak, precisely 0.366 Hz, which represents the vibration frequency of the tower. The tower oscillation maintains approximately the same amplitude along the whole simulation time because the damping coefficient is significantly lower than the stiffness coefficients, precisely one order of magnitude, and the oscillation are not enough damped. The moment of deflection and the reaction forces on drive train and generator supports have been detected and the time-domain plot is stated below

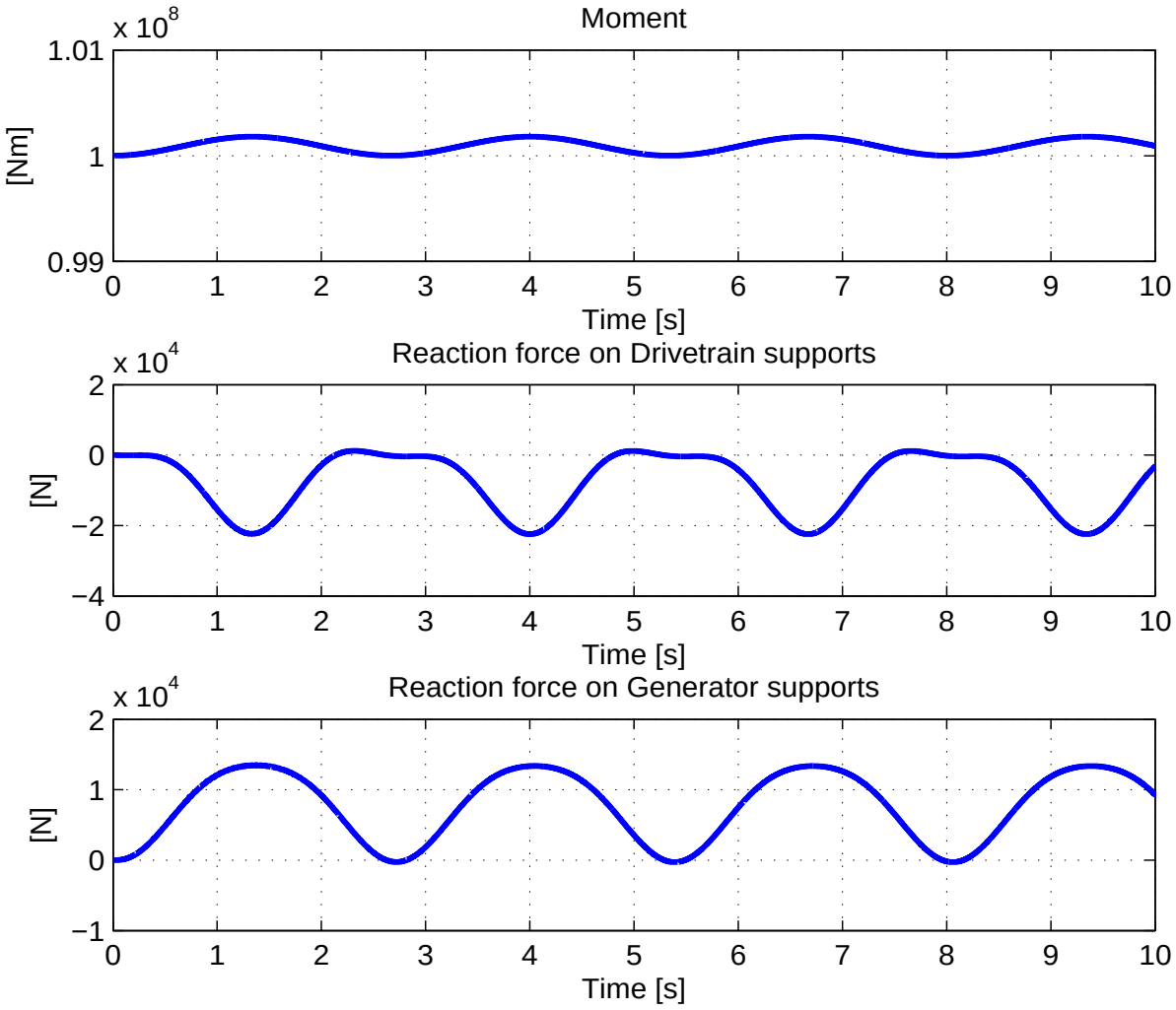

Figure 5.5: *Moment of deflection, Reaction force of Drivetrain supports, Reaction force of generator supports - On-shore tubular steel tower, thrust force of* 10^6 *N.*

The moment of deflection starts from $1.119 \cdot 10^6$ [N], that is moment generated the combination of the thrust force reaction and the wind interaction with the tower. When the tower starts to bend the moment of deflection increases because the weight of the nacelle becomes a contribution on the moment itself. Observing the load on drivetrain support it can be noticed that the load shows two vibrations modes, specifically at 0.5 Hz and 0.8 Hz. The generator support present the same number of vibration modes; the frequency of the first mode is at 0.392 Hz, while the second one is at 5.06 Hz but since magnitude of the force is significantly smaller than the first mode, the vibration

mode becomes hard to recognize on the time domain signal.

5.4.2 Off-shore Wind Turbine

The set of wind condition for the off-shore wind turbine are the same of the on-shore wind turbine simulation, additionally the wave force, expressed by the equation 5.4 in time-domain, is included. The wave force acting on foundation and the tower top deflection with the its FFT analysis are given below

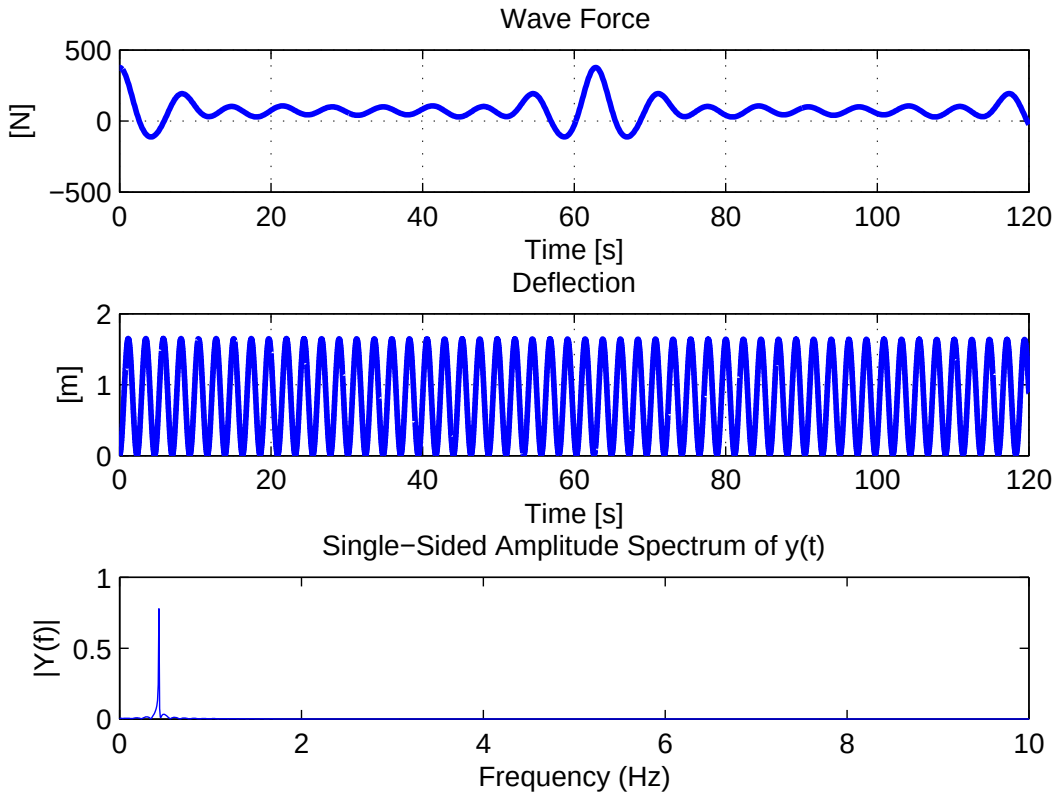

Figure 5.6: *Wave Force, deflection and FFT analysis of 65 m - Off-shore tubular steel tower, thrust force of* 10^6 *N and Wave load.*

The FFT analysis shows a peak at the frequency of 0.432 Hz. The deflection of the tower on X direction reaches a maximum value of 1.6 meters showing a discrete stiffness of the tower. The same observations, stated for the on-shore tower, can be also extended for the off-shore wind tower simulation, hence the deflection response is not significantly influenced by the internal damping of the tower structure, in sense of reducing the

amplitude of the vibrations. The moment of deflection and the reaction forces of the drive train and generator interface are reported in the following figure

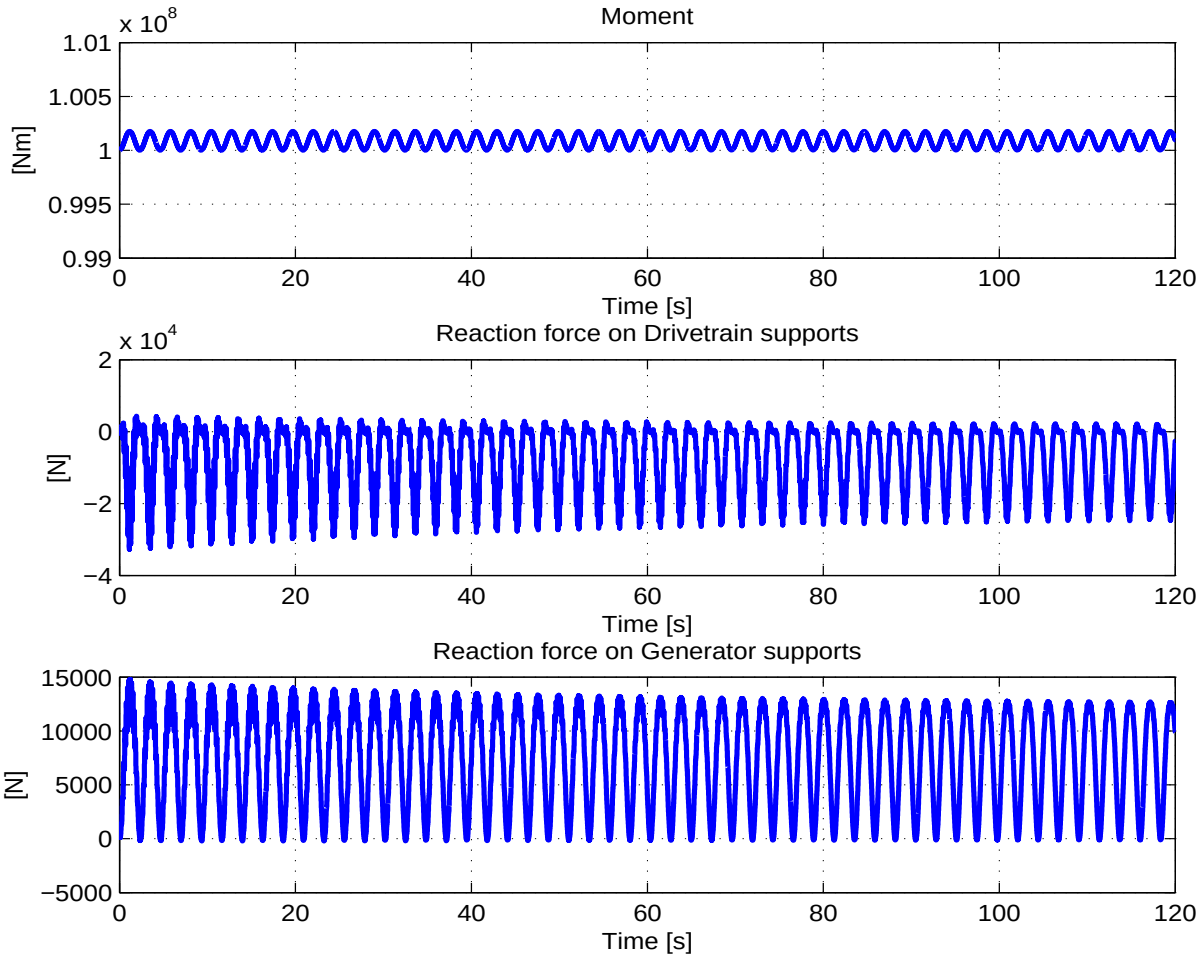

Figure 5.7: *Moment of deflection, Reaction force of drivetrain supports, Reaction force of generator supports - Off-shore tubular steel tower, thrust force of* 10^6 *and Wave load.*

The singal of the reaction forces on the tower interfaces, drive train and generator, show a main vibration mode with other vibration modes characterized by lower amplitude and higher frequencies. The FFT analysis of the generator and drive train reaction force signals had yielded to six vibration modes for each support. The frequencies of the reaction forces of the drivretrain support are: 0.427, 0.674, 0.865 Hz, 2.252 Hz, 6.674 Hz, 7.106 Hz, instead the frequencies of the reaction forces of the generator supports are: 0.452, 2.936 Hz, 5.456 Hz, 6.984 Hz, 8.132 Hz and 9.568 Hz. The signal

of the first two vibration modes of the each reaction forces are characterized by the highest magnitude since they are generated by the wind loads which are significantly greater than wave loads on foundations.
Although the amplitude of the reaction forces has not the same order of magnitude of the main loads coming from the rotor blades, it is advisable to consider them during the design phase in order to avoid any resonance condition on the supports and, therefore, reducing significantly their lifetime.

5.5 Future works

The TLI model represents a initial step for the evaluation of the tower load interface and different improvements can be proposed in order to improve the model and provide more realistic results. The first suggestion is to modify the the connection between the bed plate and the nacelle adding further connection points still using the springs and dampers in parallel in order to have a more realistic representation of the interface. Then setting a proper values for the interface connections, specifically spring and damper. The number of this joints depends of the number of the drivetrain supports, therefore it is possible to have a specific amount of the loads that act on each supports. Moreover a more accurate model of the tower can be implemented using FE theory. Matlab/Simulink allow to use this technique through the procedure developed on [31]. Theoretically this model can provide more accurate results about the deflections of tower.
Moreover the TLI model should be validated against the data coming from FE commercial software for what concerns the tower bending, and the measurement data from what concerns the load on the supports, e.g. bearing loads.

Chapter 6

Conclusions

The main task of this project is to model the loads acting on the drivetrain interfaces of a wind turbine, specifically rotor, generator and tower interfaces. The report begins stating that the large part of downtime of wind turbines is caused by drivetrain failures. This fact have encouraged energy companies to start a strong researches in order to limit this issue. A lack of knowledge about the loads which a wind turbine drivetrain system is subjected to is highlighted. Therefore the investigation of the drivetrain loads of each interface is a meaningful work. The report continues with a chapter for each interface, RLI, GLI and TLI.

After revising the MatWorks wind turbine model [36], the Rotor Load Interface is obtained, which is a multi-body system and is divided into four blocks, respectively: wind conditions, aerodynamic loads, rotor blades and generator. The wind conditions block set defines a set of different wind condition according to EIC standards; the aerodynamic loads block is responsible of calculating the loads that are generated by the interaction between the air flow and blades. The block provides two different methods for the calculation of the aerodynamic loads, namely UFD and RFD. The first method calculates the aerodynamic forces as a single value for the entire blade, instead the RFD technique divides the blades into a different segments and for each of them calculates the respective lift and drag force, then the values are summed up and a more realistic load is obtained. The blades block includes the rigid bodies representing the blades, each of them are defined by inertia and mass properties. Lastly the generator block is set as a counter torque for balancing the rotor torque. Simulations of constant wind speed wind speed conditions underlines that the RFD technique provides in general a

lower output torque and power production. The same conclusion can be extended for normal turbulence wind condition simulations and moreover the RFD technique has a more realistic response under dynamic condition compared to UFD method. The sensitivity analysis of RFD block shows that 20 segments represents a number that gives a good compromise between accuracy and computational time. Furthermore the validation of RLI model against Hönö measurement data shows that the RLI model results has good accuracy with a maximum difference of 9.5 % considering the worst case.

The Generator Load Interface model defines an induction and a PM generator with a third order differential equations generator, consisting of two electromagnetic differential equations, for calculating the electromagnetic torque, and a mechanical differential equation, which is the torque balance equation of the drive train system. The GLI model presents two drivetrain system models, namely one-mass, which considers the consists of one single mass rotating, and two-masses, which takes under consideration the shaft flexibility. Both Induction and PM generators responses under a constant mechanical torque as well as a step of mechanical torque are analyzed. Moreover a network fault simulation for both types of generators is performed. The simulation of the Induction generator are executed with one mass and two mass drive train in order to observe the influence of the drive train system model on the generator response, concluding that two mass drive train model provides a more realistic model that shows the oscillations on the rotor speed and on the electromagnetic torque responses.

The Tower Load Interface models the loads of drivetrain supports coming from the tower vibrations generated by the interaction with wind or also with wave, in case of an off-shore wind turbines. The tower is modeled as a multi-body system designed with the mass lumped-parameters technique. The top of the tower is welded with the bed plate that is connected by a couple of spring and damper with a rigid body which represents drive train and generator combined together. The same model is proposed for off-shore wind turbines, which includes the foundation equally represented as rigid bodies but characterized by different material properties. A simulation of an on-shore tower under constant wind speed condition is presented. Equal wind condition have been used for an off-shore tower simulation with the introduction of a periodic wave loads acting on foundations. The simulation of the on-shore wind turbine tower shows period loads on drivetrain supports with a specific frequency modes. On the contrary

the off-shore tower simulation presents six vibration modes generated by both wave and wind. Although the amplitude of the loads is not comparable to one coming from rotor blades, they should be considered in any case during the design phase in order to improve the durability of the supports.

As conclusion, with this Msc project, a new tool has been developed that can be used for two different tasks. First, the three interface models can provide the input data for dynamic analysis of advanced drive train models in order to evaluate the internal loads as well as the deformations responses of the drivretrain components under different set of operational scenarios. The strength of this tool is possibility of providing input data with a good accuracy, for different operational conditions, in a faster way compared to the commercial codes such as ADAMSWT ®, FAST ®, that require high computational time as well as long time for setting the models.
Second, the data of the models can also be used to design new wind turbines; indeed it possible to estimate the amounts loads under critical operational scenarios, for instance high turbulence condition, that allow to properly design the drivetrain system components (e.g. gears) and possibly guarantee the durability of 20 years [15].

Bibliography

[1] Andreas Heege, Jaume Betran, Elisabet Lens, *Computation of Dynamic Loads in Wind Turbine Power Trains*, DEWI Magazin Nr. 23, 2003.

[2] Brian Petersen , Marty Pollack , Benjamin Connell , David Greeley , Dwight Davis , Charles Slavik , Benjamin Goldman, *Evaluate the effect of turbine period of vibration requirements on structural design parameters: technical reports of findings*, Applied Physical Sciences Corp., September 1, 2010.

[3] J. F. Manwell, J.G.McGowan, A.L. Rogers, *Wind Energy Explained*, John Wiley & Sons, pp.165-195, 2009.

[4] J.Peeters, D. Vandepitte, P. Sas, *Structural analysis of a wind turbine and its drive train using the flexible multibody simulation technique*, proceeding of ISMA 2006.

[5] Det Norske Veritas, Copenhagen, and Wind Energy Department, Risø National Laboratory, *Guidelines for design of wind turbines*, 2nd Edition, Jydsk Centraltrykkeri, Denmark 2002.

[6] Dazhi Wangl, Huaming Wangl, Yupeng Shi, Jun Li, Keling Song, Shengli Liu, Yiqi Li, *Wind Turbine Simulation of Offshore Environmental Conditions,* Second International Conference on Computational Intelligence and Natural Computing (CINC), 2010.

[7] A. Perdana, *Dynamic Models of Wind Turbines*, Chalmers University of Technology, Goteborg, Sweden 2008.

[8] Stefan S. A. Ivanell, *Numerical Computations of Wind Turbine Wakes,*Royal Institute of Technology, Department of Mechanics, Stockholm, January 2009.

[9] Peter Hauge Madsen, Sten Frandsen, William E. Holley and Jens Carsten Hansen, *Dynamics and Fatigue Damage of Wind Turbine Rotors during Steady Operation,* RisØNational Laboratory, DK-4000 Roskilde, Denmark, July 1984.

[10] M.Todorov, I. Dobrev, F. Massouh, *Analysis of Torsional Oscillation of the Drive Train in Horizontal-Axis Wind Turbine,* ELECTROMOTION 2009 EPE Chapter Electric Drives Joint Symposium, 1-3 July 2009.

[11] Thomas P. Fuglseth, *Modelling a 2.5 MW direct driven wind turbine with permanent magnet generator,* Department of Electrical, Power Engineering Norwegian University of Science and Technology, NO-7491 Trondheim, Norway, June 2005

[12] Donghoon Lee, Dewey H. Hodges. and Mayuresh J. Patil, *Multi-flexible-body Dynamic Analysis of Horizontal Axis Wind Turbines,* School of Aerospace Engineering, Georgia Institute of Technology, John Wiley & Sons, August 2002.

[13] Grant Ingram, *Wind Turbine Blade Analysis using the Blade Element Momentum Method,* Grant Ingram, 2011.

[14] Bunlung Neammanee, Somporn Sirisumrannukul, Somchai Chatratana, *Development of a Wind Turbine Simulator for Wind Generator Testing,* B. Neammanee et al. / International Energy Journal 8, 2007.

[15] Anders Ahlstrm, *Simulating Dynamical Behaviour of Wind Power Structures,* Royal Institute of Technology, Department of Mechanics, Stockholm, 2002.

[16] Olimpo Anaya-Lara, Nick Jenkins, Janaka Ekanayake, Phill Cartwright, Michael Hughes, *Wind Energy Generation: Modelling and Control*, John Wiley & Sons, pp.126-132 2009.

[17] Hans Øverseth Røstøen, Tore M. Undeland, Terje Gjengedal, *Doubly Fed Induction Generator in a Wind Turbine,* University of Minnesota, 2002.

[18] Hernan De Battista, Ricardo Julib Mantz, *Sliding Mode Control of Torque Ripple in Wind Energy Conversion Systems with Slip Power Recovery,* Conference of IEEE Industrial Electronics Society, 1998.

[19] Åke Larsson, *Power Quality of Wind Turbine Generating System and their interaction with the Grid,* Chalmers University of Technology, Department of Electrical Power Engineering, Goteborg, Sweden, 2000.

[20] H. Li, Z. Chen, *Overview of different wind generator systems and their comparisons,* ET Renew. Power Gener., vol. 2, no. 2, pp. 123-138, 2008.

[21] Jussi Sopanen, Vesa Ruuskanen, Janne Nerg, Juha Pyrhönen, *Dynamic Torque Analysis of a Wind Turbine Drive Train Including a Direct-Driven Permanent Magnet Generator,* Conference of IEEE Industrial Electronic Society, 2010.

[22] Johan Ribrant, *Reliability performance and maintenance - A survey of failures in wind power systems,* Royal Institute of Technology, School of Electrical Engineering, September 2011.

[23] Johan Ribrant, *10th World Wind Energy Conference and Renewable Energy Exhibition,* Cairo, Egypt 31 October - 2 November 2011.

[24] GE ® Drivetrain Technologies; Available from: http://www.gedrivetrain.com, 2012/03/10.

[25] LORD ®; Available from: www.lord.com, 2012/03/15.

[26] Siemens ® Wind turbine; Available from: http://www.energy.siemens.com/fi/en/power-generation/renewables/wind-power/, 2012/03/23.

[27] Perdana, A., *Dynamics Models of wind Turbines: A Contribution towards the Establishment of Standardized Models of Wind Turbines for Power System Stability Studies,* Chalmers University of Technology, Department of Electrical Power Engineering, Goteborg, Sweden, 2008.

[28] *IEC standard 2005,* Available from: http://www.iec.ch/.

[29] Christian LeBlanc, *Design of Offshore Wind Turbine Support Structures,* M.Sc. (Civil Engineering), Technical University of Denmark, 2004.

[30] Shaolin Li, Xing Zhang, Zhen Xie, Shuying Yang, Chongwei Zhang, Renxian Cao, *A Study on Dynamic Model And Analyse of Wind Turbine Generation System,* Conference of IEEE Industrial Electronic Society, 2010.

[31] Victor Chudnovsky, Arnav Mukherjee, Jeff Wendlandt, and Dallas Kennedy, *Modeling Flexible Bodies in SimMechanics,* August 30, 2006: http://www.mathworks.com.

[32] Alejandro Rolan', Alvaro Luna, Gerardo Vazquez, Daniel Aguilar, *Modeling of a Variable Speed Wind Turbine with a Permanent Magnet Synchronous Generator,*Conference of IEEE Industrial Electronic Society, July 5-8, 2009.

[33] Caiyun Ji, Longbiao Zhu and Zhisong Zhu, *Load Analysis of 2.5MW Offshore Wind Turbine Tower,* Applied Mechanics and Materials Vols. 121-126 pp 206-212, 2012.

[34] Claës Dyrbye, Svend Ole Hansen, *Wind loads on structures,* John Wiley & Sons, pp 75-78,1997.

[35] matworks ®; http://www.mathworks.com/matlabcentral/fileexchange/25752-wind-turbine-model, 15 Apr 2011.

[36] Florin Iov, Anca Daniela Hansen, Poul Srensen, Frede Blaabjerg, *MarchWind Turbine Blockset in Matlab/Simulink,* Risø National Laboratory, March 2004.

[37] matworks ®; http://www.mathworks.com/matlabcentral/fileexchange/11027, 06 October 2009.

[38] http://http://www.chalmers.se/ee/swptc-en, March 2012.

[39] J.Peeters, *Simulation of dynamic drivetrain loads in a wind turbine*, University of Leuven, June 2006.

Appendix A

Wind Turbines parameters and IEC:2005 standard

IEC:2005 standard, wind models

Normal turbulence model

$$\sigma_1 = I_{ref}(0.75V_{average} + 5.6)$$

Extreme wind speed

$$\begin{aligned} V_{50} &= 1.4V_{ref} \\ V_1 &= 0.8V_{50} \\ \sigma_1 &= 0.11V_{average} \end{aligned}$$

Extreme operating gust

$$\begin{aligned} V_{gust} &= Min\left\{1.35\left(1.12V_1 - V_{average}\right); 3.3\left(\frac{\sigma_1}{1+0.1(D/\Lambda_1)}\right)\right\} \\ V &= V_{average} - 0.27V_{gust}sin(3\pi t/T)(1 - cos(2\pi t/T)) \end{aligned}$$

Extreme turbulence model

$$\sigma_1 = cI_{ref}\left(0.072\left(\frac{V_{ave}}{c} + 3\right)\left(\frac{V_{average}}{c} - 4\right) + 10\right)$$

Wind turbine parameters

Parameters	Values	Units
Number of blades	3	-
Blade length	40	m
Blade mass	6600	kg
Blade inertia	$2.764 \cdot 10^4$	kg
Blade profile	NACA 0015	-
Hub mass	8500	kg
Pitch angle	20	deg

Table A.1: *Wind Turbine SWT-2.3-82 parameters [26].*

Parameters	Values	Units
Number of blades	2	-
Blade length	6.75	m
Blade mass	375	kg
Blade inertia	2462	kg
Blade profile	NACA 63-2xx	-
Hub mass	980	kg
Pitch angle	2	deg

Table A.2: *Wind Turbine Hönö parameters [38].*

Generator parameters

Parameters	Values	Units
Rated Power	180	kW
Rated Voltage	415	V
Stator resistance	0.0092	Ω
Stator leakage inductance	0.182	mH
Mutual inductance	6.7	mH
Rotor Resistance	0.0061	Ω
Rotor leakage inductance	0.427	mH
Number of pole pair	3	-
Shaft Stiffness	2700	Nm/rad
Shaft Damper	100	Nm.sec/rad

Table A.3: *180 kW Induction Generator [38].*

Parameters	Values	Units
Rated Power	4.5	MW
Rated Voltage	400	V
Stator resistance	2.34e-3	Ω
Stator leakage inductance	0.182	mH
Mutual inductance	6.7	mH
Rotor Resistance	17.36e-3	Ω
Rotor leakage inductance	0.125	mH
Number of pole pair	60	-
Rotor inertia	10^7	kgm^2
Generator inertia	97030	kgm^2
Shaft stiffness coefficient	$3.67 \cdot 10^8$	Nm.sec/rad
Shaft damping coefficient	$0.2 \cdot 10^8$	Nm/rad

Table A.4: *4.5 MW PM Generator [21].*

On-shore tower parameters

Parameters	**Values**	**Units**
Module mass	100	Kg
Module inertia (I_x)	10^5	kgm^2
Module inertia (I_y)	10^3	kgm^2
Module inertia (I_z)	10^5	kgm^2
Tower height	100	m
Module stiffness property (EI)	$2.3 \cdot 10^{11}$	Nm^2
Module damping coefficient	10^6	Ns/m

Table A.5: *Data of on-shore wind turbine tower [34].*

Parameters	**Values**	**Units**
Nacelle mass	107500	Kg
Nacelle inertia (I_x)	10^3	kgm^2
Nacelle inertia (I_y)	10^1	kgm^2
Nacelle inertia (I_z)	10^3	kgm^2
Generator spring stiffness	$0.3 \cdot 10^6$	Nm
Generator damping coefficient	$0.5 \cdot 10^5$	Ns/m
Drivetrain spring stiffness	10^6	Nm
Drivetrain damping coefficient	10^5	Ns/m

Table A.6: *Data of on-shore wind turbine nacelle.*

Off-shore tower parameters

Parameters	**Values**	**Units**
Module mass	100	Kg
Module inertia (I_x)	10^5	kgm^2
Module inertia (I_y)	10^3	kgm^2
Module inertia (I_z)	10^5	kgm^2
Tower height	65	m
Module stiffness property (EI)	$2.3 \cdot 10^{11}$	Nm^2
Module damping coefficient	10^6	Ns/m

Table A.7: *Data of off-shore wind turbine tower [33].*

Parameters	**Values**	**Units**
Nacelle mass	107500	Kg
Nacelle inertia (I_x)	10^3	kgm^2
Nacelle inertia (I_y)	10^1	kgm^2
Nacelle inertia (I_z)	10^3	kgm^2
Generator spring stiffness	$0.3 \cdot 10^6$	Nm
Generator damping coefficient	$0.5 \cdot 10^5$	Ns/m
Drivetrain spring stiffness	10^6	Nm
Drivetrain damping coefficient	10^5	Ns/m

Table A.8: *Data of off-shore wind turbine nacelle.*

Parameters	**Values**	**Units**
Module mass	250	Kg
Module inertia (I_x)	10^6	kgm^2
Module inertia (I_y)	$1.3{\cdot}10^4$	kgm^2
Module inertia (I_z)	10^6	kgm^2
Foundation height	20	m
Module stiffness property (EI)	$2.75 \cdot 10^{12}$	Nm^2
Module damping coefficient	10^6	Ns/m

Table A.9: *Data of off-shore wind turbine foundation [33].*

Appendix B

Wave Loads Derivation

Hereinafter the proceedings for the derivation of the wave force equation (5.4 formula) used on TLI model is illustrated. The wave force requires the knowledge of water particle velocity and acceleration as function of time; the velocity of a water particle can be evaluated using the following expression

$$u_{wave} = \sum_{i=1}^{N} A_i w_i e^{k_i z} cos(w_i t + \varphi_i) \tag{B.1}$$

the acceleration of a water particle is defined by the formula

$$a_{wave} = \sum_{i=1}^{N} A_i w_i^2 e^{k_i z} sin(w_i t + \varphi_i) \tag{B.2}$$

where A_i represents the wave amplitude, defined as $A_i = \sqrt{2S(w_i)\Delta w}$, while w_i, k_i,φ_i and $S(w_i)$ are respectively: the circular frequency, wave number, random phase angel and wave spectrum. The wave randomness can be defined through the wave spectrum which expresses the energy distribution of a defined marine environment within a specific angular frequency range. The wave spectral density function approximated as

$$S_w = \frac{4\pi^3 h_s^2}{T_0^4 w^5} e^{\left[-\frac{1}{\pi}\left(\frac{2\pi}{wT_0}\right)^4\right]} \tag{B.3}$$

where h_s is the wave height expressed as $h_s = 0.21/gu^2$, T_0 is the cross-zero cycle, $T_0 = 0.81(0.81/g)u$. Using these equations and following the procedure stated in [33] it is possible to obtain the value of the wave force acting on foundation of the tower thanks to the formula 5.4

Appendix C

Simulink models

C.1 MatWorks ® Wind Turbine

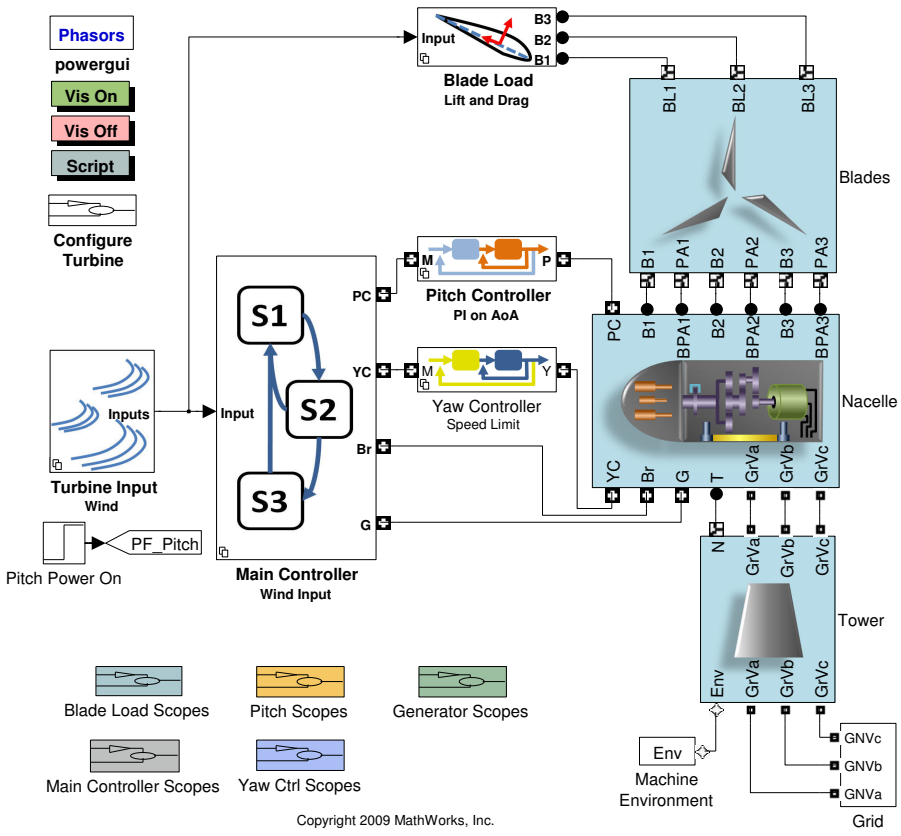

Figure C.1: *MatWorks wind turbine by Steve Miller.*

C.2 MatWorks ® GBE

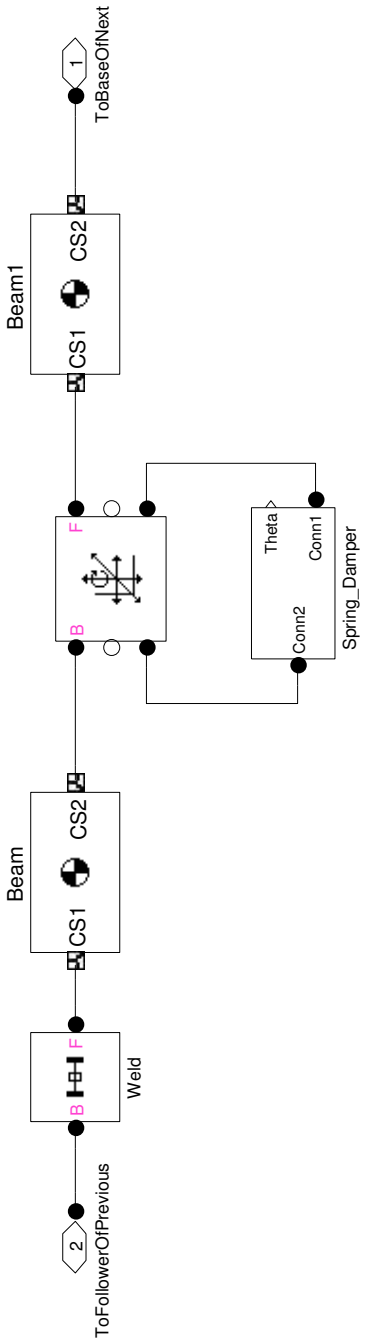

Figure C.2: *MatWorks GBE by Dallas Kennedy.*

Appendix D

List of Symbols and Abbreviations

Symbols

a_{wave}	Acceleration of water particle
c	Friction coefficient
C_D	Drag coefficient
C_{DF}	vibration resistance coefficient
C_{DS}	Steady resistance coefficient
C_L	Lift coefficient
C_M	Wave inertia coefficient
F_D	Drag force
F_L	Lift force
F_N	Thrust force
F_T	Torque force
i_r	Rotor current
i_s	Stator current
I	Inertia
j	Imaginary operator, $\sqrt{-1}$
J_g	Generator inertia
J_r	Rotor inertia
L_m	Mutual inductance
L_r	Rotor inductance

L_s	Stator inductance
R_r	Rotor resistance
R_s	Stator resistance
T_e	Electrical torque
T_m	Mechanical torque
u_{wave}	Velocity of water particle
v_r	Rotor voltage
v_{rel}	Relative speed
v_s	Stator voltage
β	Pitch angle
ω_k	Yaw speed
ω	Rotor speed
ρ_{air}	Air Density
ρ_{sw}	Sea Water Density
ψ_r,ψ_s	Rotor and stator flux

Abbreviations

$DFIG$	Double fed induction generator
DOF	Degree of freedom
$FCWT$	Full converter wind power
FE	Finite element
FMB	Flexible multi body
GBE	Generalized beam elements
GLI	Generator load interface
$HAWT$	Horizontal axis wind turbine
PM	Permanent Magnet
RFD	Real forces distribution
RMB	Rigid multi body
RLI	Rotor load interface
TLI	Tower load interface
UFD	Uniform forces distribution
$VAWT$	Vertical axis wind turbine